Swing-up Control of a power-assisted electrical Wheelchair

Michael Gray

Thèse de doctorat pour obtenir le grade de Docteur de

l'UNIVERSITÉ POLYTECHNIQUE HAUTS-DE-FRANCE

et de l'INSA HAUTS-DE-FRANCE

Automatique, Génie informatique, Traitement du signal et des images

Présentée et soutenue par Michael GRAY

le 02/06/2021, à Valenciennes

Ecole doctorale : Sciences Pour l'Ingénieur (ED SPI 072)
Laboratoire : Laboratoire d'Automatique, de Mécanique et d'Informatique Industrielles et Humaines (LAMIH – UMR 8201)

Swing-up Control of a power-assisted electrical Wheelchair

Commande d'un fauteuil roulant à assistance électrique

Président du jury
- Guy Bouhris, Pr, Université de Lorraine

Rapporteurs
- Eric Monacelli, Pr, UVSQ – Univ. Paris Saclay
- Rodolfo Orjuela, MdC HDR, Univ. Haute-Alsace

Examinateurs
- Marie Babel, MdC HDR IRISA / INRIA – INSA Rennes
- Mohammad, Sami. CEO, Autonomad-Mobility, Valenciennes

Directeur de thèse
- Thierry-Marie Guerra, Pr, Université Polytechnique Hauts-de-France

Co-directeur de thèse :
- Sébastien Delprat, Pr, INSA Hauts-de-France

Abstract

According to the World Health Organization, more than 70 million disabled people in the world need a wheelchair to aid their daily mobility needs. Providing access to low cost wheelchairs that covers the users basic needs is therefore a societal challenge that not only contribute to their well-being but also their dignity. Manual wheelchairs are widespread due to their low cost and high maneuverability. In order to mitigate the physical effects of the repeated efforts on the push rims, the company Autonomad Mobility developed an electrification kit. Among the available features, the so-called gyroscopic mode allows operating the wheelchair in an upright position with the caster wheels lifted off the ground. In this thesis, different control laws are proposed to swing-up the wheelchair from the grounded position to the unstable equilibrium position (gyroscopic mode). The specificity of the control problem is that the user is part of the system to be controlled.

A mathematical model of the wheel chair and the user is built from the mechanical equations motion and its parameters are identified through adequate experiments. The wheelchair swing-up is first casted as a reference tracking problem where the control associated with the trajectory is known. The system is modeled as a continuous Takagi-Sugeno descriptor model and the closed loop Lyapunov stability is formulated as a set on Linear Matrix Inequalities to be solved. The reference control and state trajectories are computed as a solution to an optimal control problem. The tuning of the criterion allows to tune the compromise between the control amplitude and the deviation from the wheelchair target position. Simulation and experimental results are provided and analyzed. Experimental results are globally similar to the simulations, thus demonstrating the validity of the model and the effectiveness of the control approach. Even though the trajectory is actually followed by the wheelchair, the quantification of some sensor readings combined with the numerical implementation of the continuous control law on a discrete system leads to some degradation of the control performances.

To make improvements on the above control strategy, a second control approach, using a discrete time controller, is suggested. The wheelchair dynamics is formulated as an uncertain discrete time Takagi-Sugeno discrete descriptor model that accounts for different users' characteristics. The tracking problem is formulated and again, the control approach consists in tracking a given state trajectory but now it is generated by an a priori chosen model stabilized by an appropriate state feedback. The robust stabilization conditions are provided as a set of Linear Matrix Inequalities. Finally, simulation and experimental results are provided. Videos

of the experiments are provided to illustrate the robustness of the control law to different users and the closed loop behavior when the user voluntary rocks its upper body.

Keywords: Wheelchair, Self-balancing, Takagi-Sugeno models, Lyapunov stability, Linear Matrix Inequalities, Optimal control, Euler-Lagrange, Mean Value Theorem

Résumé

D'après l'Organisation Mondiale de la santé, plus de 70 millions de personnes à mobilité réduite ont besoin d'un fauteuil roulant pour assurer leurs déplacements quotidiens. Garantir l'accès à des fauteuil abordables et capable de couvrir les déplacements de base est un challenge sociétal qui contribue non seulement au bien-être des personnes mais également à leur dignité.

Les fauteuils manuels sont les plus repandus en raison de leur cout modeste et leur grande manœuvrabilité. Pour limiter les troubles musculaires liés aux appuis répétés sur les roues, la société Autonomad Mobility propose un kit d'électrification. Parmi les différentes fonctionnalités proposées, le mode gyroscopique permet à l'utilisateur de se déplacer en équilibre sur deux roues, les petites roues avant étant levées. Dans cette thèse, plusieurs lois de commande sont proposées pour assurer le passage du mode stable (avec les 4 roues posées sur le sol) à la position en équilibre instable du mode gyroscopique. Une des spécificités des lois de commandes proposées, est que l'utilisateur fait partie du système piloté.

Un modèle mathématique du fauteuil et de l'utilisateur est construit en utilisant les lois de la mécanique, et ses paramètres sont identifiés grâce à des expérimentations spécifiques. Le passage à la position d'équilibre instable est formulé comme un problème de suivi de trajectoire où la commande utilisée pour générer la trajectoire est connue. Le système est écrit sous la fomre d'un descripteur flou de type Takagi Sugeno et la stabilité de la boucle fermée, au sens de Lyapunov, est formulée comme un ensemble d'inégalités linéaires matricielles. La trajectoire de référence est calculée comme la solution d'un problème de commande optimale. Les pondérations entre les différents termes du critère permettent de choisir le compromis entre l'amplitude de commande et le déplacement longitudinal du fauteuil. Les résultats de simulation et des expérimentations sont présentés et discutés. Globalement, les résultats expérimentaux sont similaires à ceux obtenus en simulation, démontrant ainsi la validité du modèle et la pertinence de l'approche utilisée. Même si la trajectoire de référence est bien suivie par le fauteuil, la quantification des mesures des capteurs et la mise en œuvre sur un calculateur numérique de la loi de commande formulée en temps continue, amène une dégradation des performances de la loi de commande.

Afin d'améliorer les résultats obtenus, une deuxième approche, formulée en temps discret, est envisagée. La dynamique du fauteuil roulant est tout d'abord écrite sous la forme d'un descripteur flou de type Takagi-Sugeno. Des incertitudes sur les paramètres permettent de

prendre en compte la morphologie de différents utilisateurs. Un problème de suivi de trajectoire est formulée de sorte à suivre une trajectoire d'état donné, mais cette fois ci, la trajectoire est généré en utilisant un modèle fixé a priori et stabilisé via un retour d'état approprié. L'écriture de la stabilisation robuste de la boucle fermée se résume à un ensemble d'inégalité matricielles linéaires. Finalement, des résultats de simulation et expérimentaux sont discutées. Des vidéos des expérimentations sont mises à dispositions. Différents utilisateurs ont testé la loi de commande proposée qui a été en mesure de réguler correctement le fauteuil en équilibre instable en dépit des brusques mouvement volontaires des utilisateurs.

Mots clés: Fauteuil roulant, modèles de type Takagi-Sugeno, stabilité de Lyapunov, inégalités matricielles linéaires, contrôle optimal, Euler-Lagrange, théorème de la valeur moyenne

Table of Contents

List of Figures

List of Tables

Chapter 1 Introduction

1.1 Disability

According to the World Health Organization (WHO) disabilities are classified into three areas: impairments, activity limitations, and participation restrictions. Impairments are problems in body function, activity limitations are difficulties in executing activities, and participation restrictions are problems with involvement in any area of life. Then, the WHO defines a disability as difficulties encountered in any of all three of these areas and estimate that worldwide over 1 billion people are suffering from a disability (World Health Organization 2011).

In the United States it is estimated that over 60 million adults have some type of disability and about 20 million adults under 65 years of age are disabled in their mobility (Okoro, et al. 2018). A disability in mobility includes people that have a hard time walking or climbing stairs. Many people with a disability in mobility need an assistance device for aid, such as a wheelchair, cane, walker, etc. Among this group people that are using wheelchairs and four wheeled electric scooters make up about 1.7 million people (Kaye, Kang and LaPlante 2000).

1.2 Wheelchair

Wheelchairs are used to help disabled people that have difficulties walking move around. Wheelchairs have been around for a longtime and over the years, many advancements have been made. Some believe the first wheelchairs were developed between the 6th and the 4th centuries BCE with the development of wheeled furniture and two-wheeled carts, and the first self-propelled wheelchair is believed to have been developed by German watchmaker Stephan Farfler in 1665 (Watson and Woods 2015).

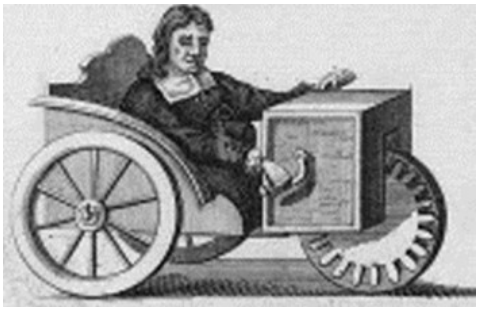

Fig. 1. Sketch of Farfler using the first known self-propelled wheelchair (Wikipedia contributors 2020)

Self-propelled wheelchairs have advanced considerably since the one developed by Stephan Farfler, Fig. 1. Today there are three main classes of wheelchairs: manual, power-assist, and electric. Manual wheelchairs are normally cheaper, lightweight, easy to maneuver, and easy to transport. These wheelchairs consist of two large rear wheels with hand-rims fixed to them which are used to propel the wheelchair Fig. 2.

Fig. 2. Manual wheelchair (left), manual hand-rims (right)

However, the repetitive motion of pushing the hand-rims can cause the user to get fatigued quickly and can lead to long term injuries. The high forces put on the shoulders during this repetitive motion increases the chances the user will develop coracoacromial edema and coracoacromial ligament thickening (Mercer, et al. 2006). The coracoacromial ligament plays an important role in shoulder biomechanics and stability and thickening and stiffening may contribute to rotator cuff tear arthropathy and impingement syndrome (Rothenberg, et al. 2017). While there are many benefits to using a manual wheelchair there are also risks of long-term health problems. In addition, manual wheelchairs have caster wheels in front so the user can turn the wheelchair left and right. However, these caster wheels are small and block the wheelchair from rolling over obstacles (even small obstacles) Fig. 3.

Fig. 3. Small obstacle blocking caster wheel

One of the newer additions to the self-propelled wheelchair market is the power-assisted wheelchair. Power-assist wheelchairs in most cases started as a manual wheelchair that gets converted to a power-assist wheelchair Fig. 4.

Fig. 4. Power-assisted wheelchair (Autonomad-Mobility)

To convert a manual wheelchair to a power-assist wheelchair, motors are embedded in the push-wheels that are powered by a battery. Some wheelchairs come with a control box so the user can read battery health, change power settings, etc. Fig. 5.

Fig. 5. Electric motor embedded in wheel (left), battery (center), control box (right)

In most cases the push-wheels are constructed with a sensor between the wheels and the hand-rims to detect when the user pushes the hand-rim. These wheelchairs have the maneuvering ability of a manual wheelchair and can widely reduce the stress on the shoulders compared to a manual wheelchair. They make it easier for the user to travel long distances with less fatigue. In addition, the power-assisted propulsion can reduce cardiovascular and respiratory strain (Kloosterman, et al. 2012). However, the addition of the electric components add weight to the system, and the small caster wheels continue making obstacles a challenge.

Lastly is the full electric wheelchair where only the electric motors propel the wheelchair. Normally these wheelchairs do not have hand-rims on the rear wheels that the user can push, but instead the user controls the wheelchair with a joystick Fig. 6. Electric wheelchairs give users that are not able to use the hand-rims mobility in their lives. While there are advantages of using a traditional electric wheelchair there are also disadvantages. For example, electric wheelchairs are typically larger and less maneuverable. As a result, users have reported difficulties such as going through doorways, avoiding obstacles, and using streets and sidewalks (Torkia, et al. 2015). In addition, the lack of exercise of electric wheelchair users is an important factor which can lead to secondary health conditions. For example, electric wheelchair users have exercise barriers such as too few places to exercise, and exercise being harder (Barfield et Malone 2013). These barriers can lead to secondary health problems such as obesity.

Fig. 6. Full electric wheelchair

A different option is to combine manual and electrical mode, in a kind of "hybrid" propulsion wheelchair. This solution is available using assistance kits such as the Nomad from Autonomad-Mobility Fig. 7. The Nomad is a kit that converts a manual wheelchair to an electric wheelchair (Mohammad and Guerra 2019). This conversion kit enables the user to choose different levels of electrical assistance from the manual mode (no assistance) to full electric mode where the motors do the work. In addition, the equipped wheelchair can operate in a 2-wheel self-balancing mode (so-called gyroscopic mode) Fig. 7.

Fig. 7. Nomad from Autonomad-Mobility (Gyroscopic Mode).

1.3 Autonomad-Mobility

Autonomad-Mobility (A-M) is a start-up company created by Sami Mohammad located in Famars, France. The company specializes in building kits that convert a manual wheelchair to electric wheelchair. There are companies that built conversion kits before A-M but, the A-M kit is unique because it has an extra operating mode called "Gyroscopic mode" Fig. 7.

The company started as a project at UVHC-CNRS Research lab LAMIH in January of 2013. A-M was such a success that it was considered a top 15 European Biotech Incubator later that year, and in June was granted €35k to help the company creation. The next year (2014) the company was awarded 2 patents, then in 2015 the first prototypes for DUO and NOMAD were built. In June 2015 A-M was the winner of "I-LAB créadev" and Bpifrance granted the company € 200k to support its development. Then, by the end of 2015 the company had started the commercialization of both DUO and the NOMAD, and only a year later had their first sales. In the end of 2017, the company had raised enough money to start to optimize the commercialization of DUO and NOMAD, and in 2018 hired its first employees.

This thesis is part of the investment the company made in 2018 through a CIFRE (**C**onventions **I**ndustrielles de **F**ormation par la **RE**cherche) convention. CIFRE is a grant from the ministry for research with the double objective "*of placing doctoral students in the conditions for scientific employment and encouraging research partnerships between the academic and business spheres*."

http://www.anrt.asso.fr/sites/default/files/cifre_plaquette_2019_eng.pdf

1.4 Thesis outline

The thesis structured with three main chapters.

Chapter 2 starts with a description of the prototype used for testing. Then, the system is modeled using the Euler-Lagrange method. Next, the parameters are identified for the model. Since the system can only operate in an unstable equilibrium point, the parameters are identified in a three steps process. Finally, the model is validated.

Chapter 3 presents a continuous swing-up algorithm design with a two-step procedure. The first part of the chapter recalls some properties of the so-called Takagi-Sugeno models belonging to the quasi-LPV family. As the design uses a wheelchair model written in a descriptor form, some particular results for this kind of systems are also provided. A controller is designed to follow a specified trajectory from the grounded position to the gyroscopic mode. An optimal control problem is solved to compute this trajectory in order to minimize simultaneously the control amplitudes and the overall wheelchair displacement. Simulation and experimental results are discussed.

Chapter 4 proposes to solve the problem of the wheelchair swing-up in a discrete framework in a one-step design, including reference trajectory and robust control. Some fundamentals of discrete descriptors models in the Takagi-Sugeno form are given first. The advantages of the approach are to have all-in-one (no need to have two different control algorithms) and to derive a robust control law that is designed according to uncertainties such as the masses of the wheelchair and user.

Conclusions and some perspectives end the manuscript.

Chapter 2 System & Modeling

2.1 State of the Art

Wheelchairs are great tools to aid disabled people in their mobility. However, a wheelchair still has limitation that impede the mobility of the user. For example, large and heavy wheelchairs are hard to transport (in a vehicle) and are difficult to maneuver in crowds or in tight hallways and doorways.

Manual wheelchairs have small caster wheels in the front of the wheelchair so that it can turn sharply and move in tight places. The problem with caster wheels is that they are small and block the wheelchair from going over small obstacles, but with a manual wheelchair the user can accelerate quickly to lift the caster wheels over the obstacle so the user can still pass over it Fig. 8

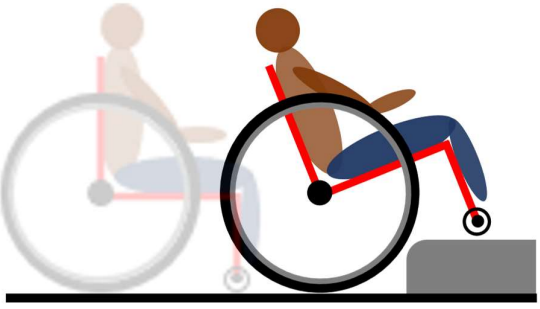

Fig. 8. Manual wheelchair raising front wheels to pass over an obstacle.

Unlike manual wheelchairs electric wheelchairs may or may not have small caster wheels. When an electric wheelchair does not have caster wheels it is more stable going over obstacles, however it is difficult to operate in tight areas because it cannot turn sharply. Then, when an electric wheelchair has caster wheels the user cannot accelerate quick enough to lift the caster wheels to pass over obstacles. A great solution to this problem is to have a wheelchair that can turn sharply like it has caster wheels but still be able to pass over obstacles.

2.1.1 Some solutions on the market

The iBOT is a novel wheelchair that is aimed to overcome some of the limitations brought on by conventional electric and manual wheelchairs. The iBOT is able operate in four different modes: standard mode where two caster wheels and two drive wheels touch the ground,

balancing mode where the wheelchair balances on two wheels drive wheels Fig. 9, 4-wheel mode where four drive wheels touch the ground to climb obstacles, and a stair climbing mode. The iBOT was developed by Dean Kamen in 1990 in partnership between DEKA and Johnson and Johnson's (Wikipedia contributors 2020). This wheelchair has many nice options but the price tag is $30,000 making impossible to own for many users.

Fig. 9. iBOT in balancing mode with creator Dean Kamen and American President Bill Clinton (Wikipedia contributors 2020)

Another option is the Ninebot by Nano Mobility. The Ninebot is another novel mobility device that balances on two wheels (gyroscopic mode), Fig. 10. The user moves the chair forward and backward by leaning his/her upper body forward or backward, and then there is either a joystick or handlebars to turn the wheelchair. One advantage of the ninebot is that it does not have small caster wheels that can prevent it from going over small obstacles. However, if the battery runs out or there is another malfunction, the user will not be able to move. This wheelchair is much cheaper than the iBOT but still has a large price tag.

Fig. 10. Ninebot by Nano Mobility

Then there is the NOMAD by Autonomad-Mobility Fig. 7 which can operate in 3 different modes. First, it can operate in conventional manual mode where the user uses the hand-rims to accelerate the wheelchair. Next, the wheelchair operates in an electric mode with caster wheels. When the wheelchair is in this mode it can maneuver quickly but the caster wheels block it from going over obstacles. Then, there is the gyroscopic mode where the wheelchair balances on its rear two wheels. In this mode the wheelchair can still make sharp turns and in addition it can now pass over obstacles because the caster wheels are raised off the ground.

2.1.2 Existing research

Very few works address such a challenging task. In (Ahmad and Tokhi 2008) the process of transitioning a 4-wheeled wheelchair to add 2-wheeled wheelchair by lifting the wheelchair up (like the iBOT) is proposed in simulation. However, this method adds an extra actuator to the system increasing its complexity and uses Fuzzy Logic Control without any stability and robustness considerations. Similar to the NOMAD in Fig. 7 (Takahashi, Ishikawa and Hagiwara 2003) and (Takahashi et Tsubouchi 2005) discuss the swing up of an electrified manual wheelchair. Their solution consists in using a classical Proportional Integer (PI) controller with the angle of the pendulum as reference to swing-up the wheelchair. Nevertheless, using only the angle of the pendulum as feedback, the displacement of the wheelchair cannot be controlled. Apart from this drawback, the stability issues of the closed-loop and the robustness are not considered.

2.2 Problem Statement

A solution for having a better mobility is to be able to travel on 2 wheels in a so-called gyroscopic mode. The advantages are clear: the wheelchair can turn sharply like in the conventional mode (with the caster wheels on the ground), and it can pass over obstacles, Fig. 7, because the caster wheels are raised off the ground. The gyroscopic mode gives the user many advantages that he/she would not have with a traditional manual/electric wheelchair, however the new functionality comes at a cost.

On an automatic control point of view, it leads to move from a stable open-loop wheelchair (4 wheels) to an unstable one (2 wheels) and thus, safety issues are to be considered. The wheelchair control, which is rather “simple” for the stable 4-wheels mode, has to be thought in terms safety and robustness properties for the 2-wheels or so-called gyroscopic mode.

Robustness must be thought for different aspects. First, as the kit is to be used with any kind of wheelchairs, the control laws must cope with different mechanical characteristics and wheelchair geometries. Second, no extra sensors can be added, not only for costs issues but also because it is unrealistic to measure some parameters like the user's capabilities or the ground adherence for example. Therefore, control law of the unstable equilibrium position has to consider: the unknown parameters such as mass, inertia… for both the wheelchair and the user, ground adherence… Beyond the system safety, the system acceptability by the users is crucial. It includes fearless usage, confidence in the system, easy-to-use, and more generally a "good feeling" about the system. This part, called thereinafter under the word "comfort" should be achieved by control robustness and guaranteed dynamic performances.

Thus, the automatic control problem to solve resumes to:

1. Robust trajectory tracking: minimum displacement to swing up/down
2. Robustness to varying unknown parameters (mass, inertias, etc.)
3. Comfort (dynamic performances, easy-to-use, smoothness)

2.3 System Hardware & Software

The system is a manual wheelchair equipped with an electrical assistance kit developed by Autonomad-Mobility, Fig. 11. This kit consists of electric motors embedded in the push-wheels, a control box, and a socket to connect the battery.

Fig. 11. Electric motor embedded in wheel (left), battery (center), control box (right)

When this project started the Nomad already had a functioning gyroscopic mode, and the kit was being sold on the market. However, the transition from standard mode to gyroscopic mode is done manually with the joystick and new users find it difficult to learn this maneuver, so the objective is to automate this process.

In order to implement new control algorithm, a new control box needs to be installed on the wheel since the commercialized version does not allows easy modification of its source code. There are some popular products on the market today for doing rapid prototyping such as dSpace or SpeedGoat. These companies make systems that can be programmed directly with the C code generated by the Simulink Coder which greatly reduces the time from simulation to real-time experiments. In addition, these products log data and allow for parameter tuning in real-time. The problem with these products is that they are designed for more complicated systems, so they are large and expensive. Since the considered Nomad Kit has relatively few inputs/outputs and large sample time a Launchpad from Texas Instruments was able to be used instead Fig. 12.

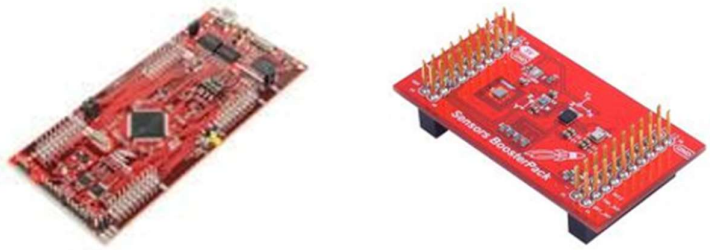

Fig. 12. Texas Instrument LAUNCHXL-F28377S & BOOSTXL-SENSORS

The Launchpad LAUNCHXL-F28377S is a development board based on the TMS320F38377S microprocessor. This microprocessor has a $200\,MHz$ CPU, $1024\,kB$ flash memory, $164\,kB$ RAM, and communications via I2C, CAN, etc. In addition, the card has addon BosterPacks which simply plug onto the top of the card. The BOOSTXL-SENSORS BoosterPack has a Bosch BMI160 IMU, Bosch BMM150 magnetometer, Bosch BME280 environmental sensor, OPT3001 light sensor, and TMP007 temperature sensor. For this system, the CAN bus is needed for communicating with the motor cards and the IMU on the BoosterPack is needed to measure the angle of the wheelchair in gyroscopic mode. In addition, functionalities needed for this system, the Launchpad can also be programmed with the code generated from Simulink Coder, and it can communicate with Simulink in real-time to log data and tune parameters while the card is running.

Fig. 13. Control box design for prototype

Since the Launchpad is needed for the experiments a new control box was designed to fit the card. The Launchpad and a joystick are mounted inside the box, and on the outside of the box is a USB connector for the PC, an 8-pin connector to motor cards, and an emergency on/off switch. The joystick operates at $5V$ but the input for the Launchpad is only $3.3V$ so a conditioning circuit was built to step down the voltage Fig. 14.

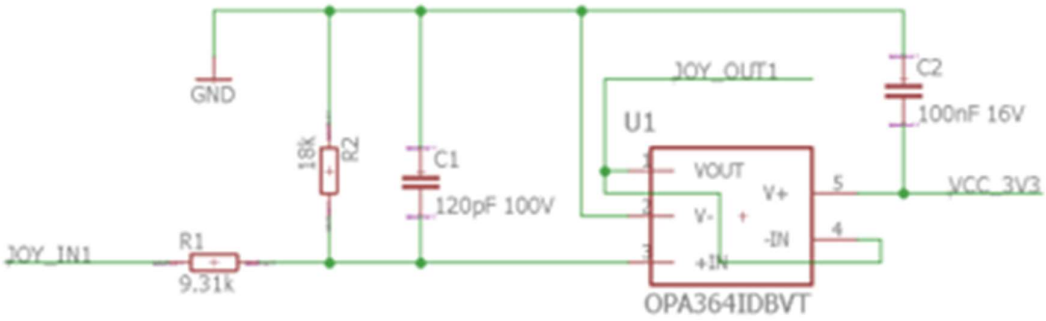

Fig. 14. Conditioning circuit $5V \rightarrow 3.3V$

The motor cards are mounted inside a plastic housing (socket) which is also where the battery is mounted, Fig. 11. The battery can be charged up to a maximum of $40V$ and the input to the motor cards comes from the CAN bus which is connected to the control box. These motor cards can operate in two different modes. The first mode denoted as “Voltage mode” is controlling the motor in open-loop by applying a PWM signal to the driver. As a result, the average motor voltage varies from $[0 \quad 40]V$ according to the PWM duty cycle. The second is the “Current mode” where the current in the motors is regulated by a PI controller running in the motor card.

The motors embedded in the push-wheels are brushless and have a maximum current of $I \approx 40A$ for each motor, and can propel the wheelchair at a maximum speed of $\dot{y} \approx 2.2\, m \cdot s^{-1}$. The motor cards measure the position of the motor by counting the phase changes to turn the brushless motors. These motors have about 785 pulses per revolution of the wheel which leads

to a quantization error $|\theta_{error}| < {}^{2\pi}/_{785}\, rd$. This quantization error combined with the fixed sampling period make the estimation of the velocity a difficult problem, Fig. 15.

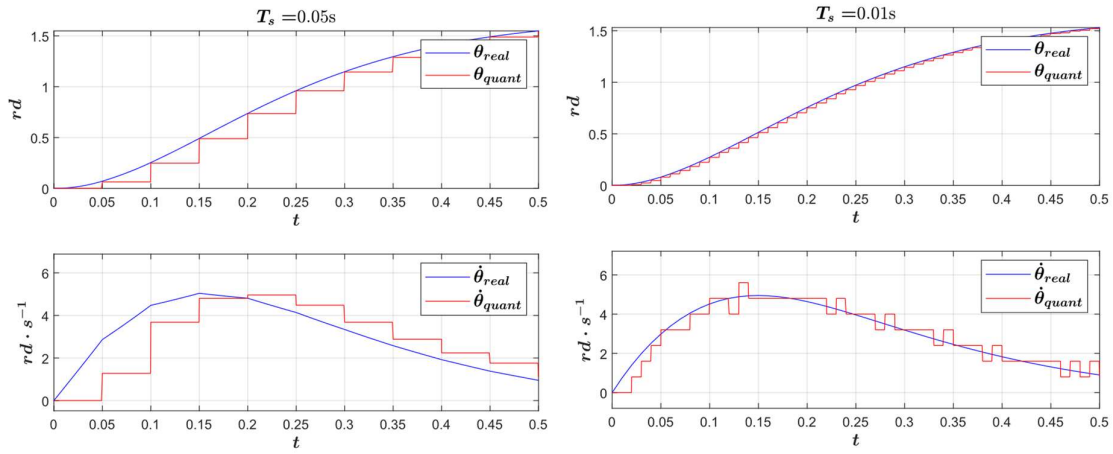

Fig. 15. Estimated motor angular position (top) and velocity (bottom) for different sampling period T_s

As the sampling time decreases, the maximum position error at every sampling instant does not change, however velocity error amplifies. As a result, during the control law synthesis, it will be required to pay attention to the controller gains on the velocity signals such the effect of these errors on the control signal remains small enough.

2.4 Modeling

As stated previously, the objective is to be able for a user to travel in the so-called gyroscopic mode. Therefore, a first step is to automate the "swing-up" of the wheelchair, Fig. 16. During the swing-up, the wheelchair only needs to move forward-n-backward, turning left-n-right is not necessary. As a result, only a longitudinal model is needed to describe the motion of the system for the swing-up.

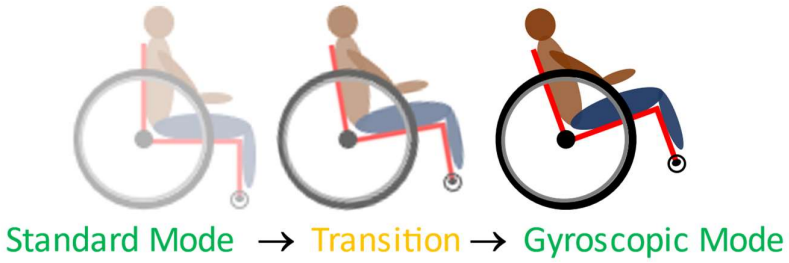

Fig. 16. Swing-up from Standard Mode to Gyroscopic Mode

The equations of motion for the system are derived using the Euler-Lagrange method with the extended Hamilton's principal and the Rayleigh's dissipation function (Cline et Sarkis 2017).

$$\frac{d}{dt}\left(\frac{\partial L}{\partial \dot{q}_k}\right)-\frac{\partial L}{\partial q_k}+\frac{\partial D}{\partial \dot{q}_k}=Q_k \tag{1}$$

Where L is the Lagrange function, D is the Dissipation function, Q_k are the Generalized forces, and q_k are the Generalized coordinates.

Referring to the free-body diagram in Fig. 17, the wheelchair is modeled as if it has only 2 degrees of freedom and is composed of 2 rigid bodies (the base and the pendulum). The two rigid bodies are connected at the pivot of the push-wheel axels. The base of the system is composed of the two push wheels and the electric motor stators where the center of mass coordinates are y_b, z_b. Then, the pendulum is composed of the chassis, human, and the electric motor rotors with center of mass coordinates y_p, z_p.

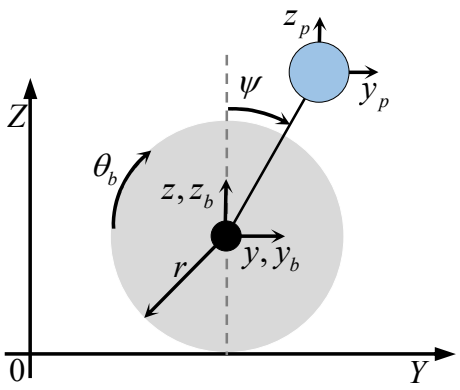

Fig. 17. Free-Body diagram swing-up model

The coordinate frame of the body (x_b, y_b, z_b) is equal to the coordinate frame of the wheelchair (x, y, z), and the coordinate frame (x_p, y_p, z_p) rotates around the origin of the body frame. The two rigid bodies are linked by the following constraints:

$$
\begin{aligned}
y_b &= y, \theta = y_b r^{-1} \\
z_b &= 0 \\
y_p &= y_b + l\sin(\psi) \\
z_p &= z_b + l\cos(\psi)
\end{aligned}
\tag{2}
$$

Where r is the push-wheel radius and l is the distance from the body center of mass to the pendulum center of mass. Table I gives the description of the parameters.

Table I. Model parameter description

Parameter	Description
$M_b\left(kg\right)$	Mass of user, frame, and stator.
$J_b\left(kg\cdot m^2\right)$	Inertia of user, frame, and stator.
$M_w\left(kg\right)$	Mass wheel and rotor.
$J_w\left(kg\cdot m^2\right)$	Inertia wheel and rotor.
$r\left(m\right)$	Push wheel radius.
$g\left(m\cdot s^{-2}\right)$	Acceleration of gravity.
$l\left(m\right)$	Distance from pivot to center mass.
$\mu_m\left(N\cdot m\cdot s\right)$	Viscous friction in the motor.
$\mu_{wg}\left(N\cdot m^{-1}\cdot s\right)$	Viscous friction from wheel and ground.
$K_t\left(N\cdot m\cdot A^{-1}\right)$	Motor torque constant.

On the wheelchair, the two motor drivers control the electric motors current I and motor torque τ_m is proportional to it, i.e. $\tau_m = K_t I$. When the motors generate torque τ_m, an equal and opposite torque is applied to the base (push-wheels) and the pendulum (frame, human) of the wheelchair. As a result, the electric motors generate a force on the base $F_y = \tau_m r^{-1}$ and torque $\tau_\psi = -\tau_m$ on the chassis of the wheelchair.

Using equation (1) the equations of motion are computed. First, the Lagrangian L and the dissipative function D are defined:

$$
L = T - V \tag{3}
$$

$$
D = \tfrac{1}{2}\sum_i d_i \dot{x}_i^2 \tag{4}
$$

Where T is the kinetic energy, U is the potential energy, and d_i are the coefficients of viscous friction of the system. To calculate the equations of motion L, D, Q, and q must be defined for each of the two rigid bodies:

$$\begin{aligned} T_1 &= 2\left(\tfrac{1}{2} M_w \dot{y}_b^2 + \tfrac{1}{2} J_w \dot{\theta}^2\right) \\ V_1 &= 0 \\ D_1 &= 2\left(\tfrac{1}{2} \mu_{wg} \dot{y}_b^2\right) \\ Q_1 &= F_y = \tau_m / r = K_t I / r \\ q_1 &= y \end{aligned} \tag{5}$$

$$\begin{aligned} T_2 &= \tfrac{1}{2} M_b \left(\dot{y}_b^2 + \dot{z}_b^2\right) + \tfrac{1}{2} J_b \dot{\psi}^2 \\ V_2 &= M_b g\, z_p \\ D_2 &= 2\tfrac{1}{2} \mu_m \left(\dot{\theta}^2 - \dot{\psi}^2\right) \\ Q_2 &= \tau_\psi = -\tau_m = -K_t I \\ q_2 &= \psi \end{aligned} \tag{6}$$

Then applying (1), the system of equations for the swing-up is derived:

$$\left(M_b + 2M_w + \frac{2J_w}{r^2}\right)\ddot{y} + M_b l \cos(\psi)\ddot{\psi} + \left(\mu_{\text{wg}} + \frac{2\mu_m}{r^2}\right)\dot{y} - \frac{2\mu_m}{r}\dot{\psi} - M_b l \sin(\psi)\dot{\psi}^2 = \frac{K_t}{r} I \tag{7}$$

$$\left(J_b + M_b l^2\right)\ddot{\psi} + M_b l \cos(\psi)\ddot{y} + 2\mu_m \dot{\psi} - \frac{2\mu_m}{r}\dot{y} - M_b g l \sin(\psi) = -K_t I \tag{8}$$

Let us define the total mass as $M_b = M + M_{b_{Frame}}$ with M the user mass and $M_{b_{Frame}}$ the mass of the wheelchair frame (including all the different accessories and components). $M_{b_{Frame}}$ can be easily measured and M is user dependent. Similarly, the total inertia is defined as $J_b = J + J_{b_{Frame}}$ with J the user's inertia and $J_{b_{Frame}}$ the wheelchair frame inertia.

2.5 Parameter identification

The dynamic model (7)-(8) comprises 6 unknown parameters J_b, J_w, μ_m, μ_{wg}, K_t and l that need to be identified to get an accurate representation of the real system. Of course, the gyroscopic mode corresponds to operating around an unstable equilibrium point. Therefore, the parameters identification cannot be done around this point, excepted if a control law synthesis

has been already realized. Like a pendulum, a 2-wheel stable equilibrium point could be reached if a complete rotation could occur, which obviously, at least with a human, is impossible Fig. 18. However, a 3-step identification procedure has been conducted to identify the wheelchair parameters and is presented thereafter.

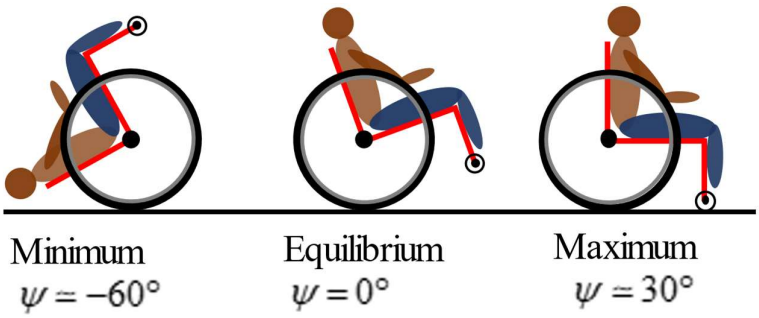

Fig. 18. Operating region in gyroscopic mode

2.5.1 Motor friction μ_m and torque constant K_t

The idea to identify the motor friction μ_m and its torque constant K_t was to consider the system around its 2-wheel stable equilibrium point by raising the wheelchair to allow its complete rotation. Fig. 19 shows the wheelchair tied up and strapped so that the chassis can swing freely.

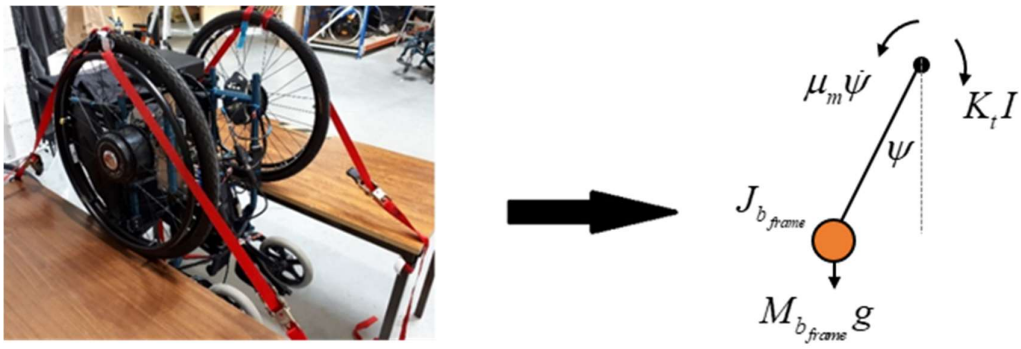

Fig. 19. Identification experiment 1

Of course, the system dynamics around this stable equilibrium position corresponds to a different mathematical model that can be easily derived using Newton's method.

$$\left(M_{b_{frame}} l^2 + J_{b_{frame}}\right)\ddot{\psi} + 2\mu_m\dot{\psi} + M_{b_{frame}} g l_{b_{frame}} \sin\left(\psi\right) = -K_t I \tag{9}$$

As usual, the identification procedure consists in building an excitation signal, logging sensor data while the excitation signal is applied, estimating the parameters values and validating the resulting model. The excitation signal must be sufficiently "rich" to represent the frequency and amplitude ranges useful for the system operation. Therefore, to cover these ranges, a multisine signal has been defined (Schoukens and Ljung 2019).

$$u(t) = \sum_{k=1}^{F} U_k \cos\left(2\pi k f_0 t + \sigma_k\right) \tag{10}$$

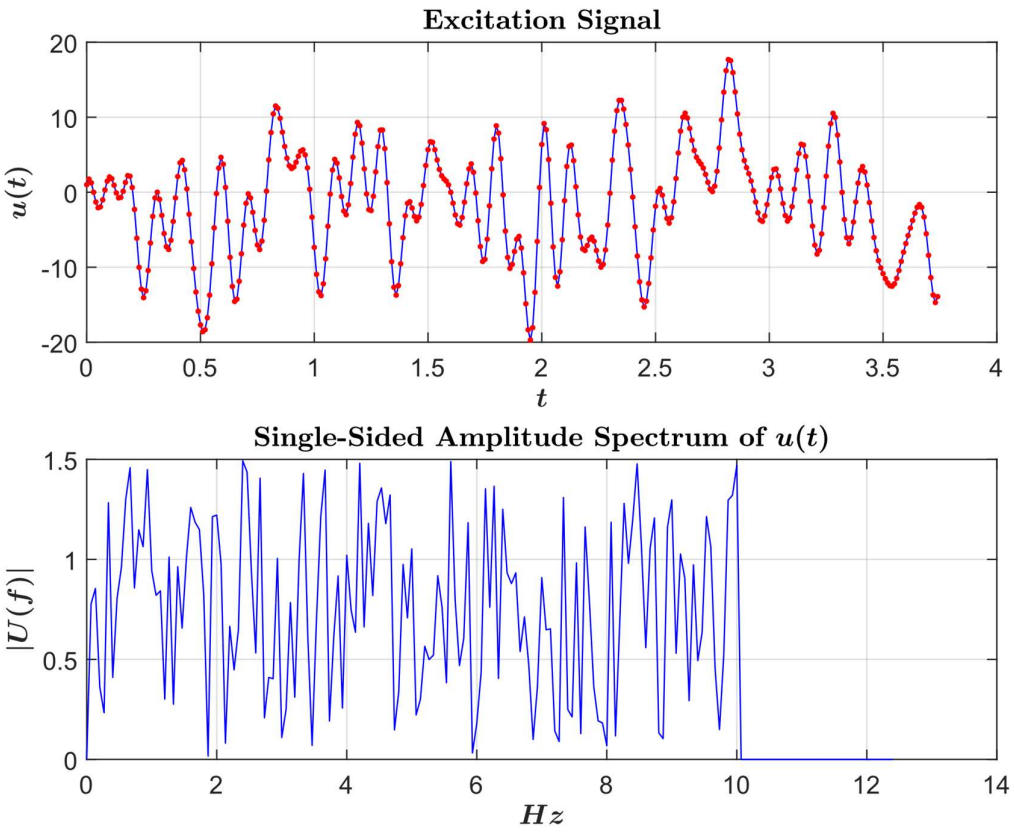

Fig. 20. MultiSine excitation signal

Equation (10) is used to build the signal in Fig. 20, with spectral resolution $f_0 = {}^{f_s}\!/_{N}$, period length N, random amplitude spectrum U_k, random phases σ_k and a length of 3 periods for a total of $45s$.

$$
\begin{aligned}
&T_s = 0.01 \\
&N = {}^{15}\!/_{T_e} \\
&f_0 = {}^{1}\!/_{T_e N} \\
&U_k = \begin{bmatrix} 1.30 & 1.42 & 0.60 & \dots \end{bmatrix} \\
&\sigma_k = \begin{bmatrix} 2.73 & 1.19 & 2.33 & \dots \end{bmatrix}
\end{aligned}
\tag{11}
$$

When collecting data, there are two ways to measure the position and velocity of the frame: using the accelerometer and the gyroscope with the following algorithm (already available by the company):

$$
\psi[z] = \left(\psi\left[z^{-1}\right] + t_s \dot{\psi}_{gyro}[z]\right)(1-\alpha) + \alpha \tan^{-1}\left(\frac{y_{acc}[z]}{\sqrt{x_{acc}^2[z] + z_{acc}^2[z]}}\right)\frac{180}{\pi} \tag{12}
$$

where $\alpha = 0.001$ is referred to as the "accelerometer-gyroscope", or by counting the phase changes in the brushless motors. As discussed in section 2.3 there are large quantization errors when measuring velocity from motor phase changes. Counting the phase changes is analogous counting pulses from an encoder, so for now on counting phase changes will be referred to as an encoder.

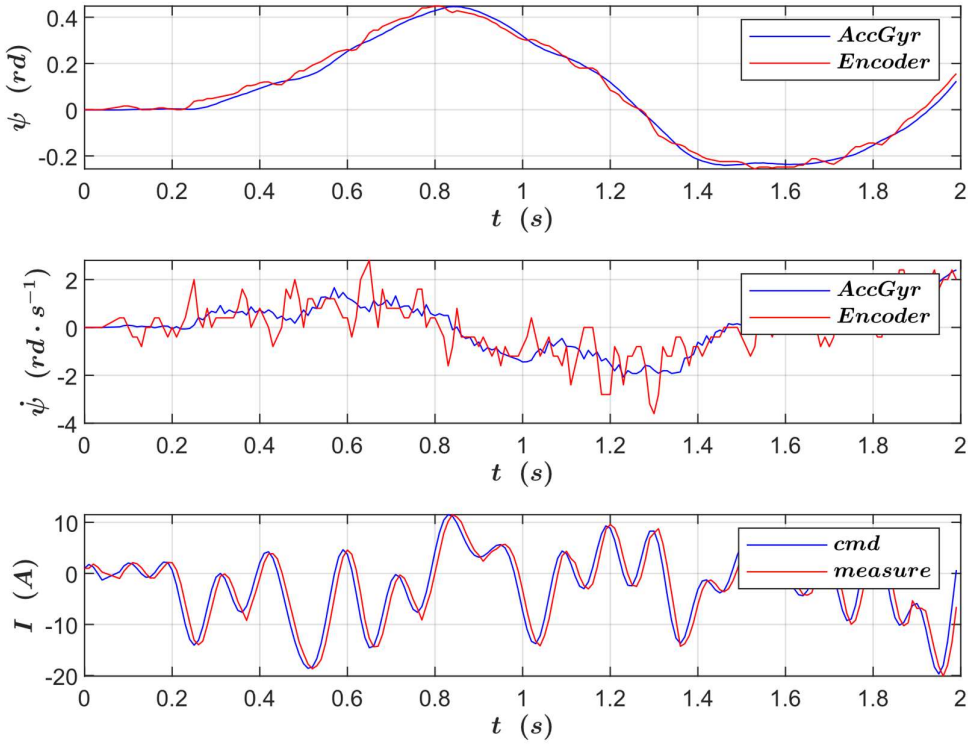

Fig. 21. Encoder, Gyroscope-Accelerometer measurement from pendulum experiment

The accelerometer-gyroscope gives much better measurement of the position and velocity Fig. 21. This is mostly due to non-modeled nonlinearities such as backlash in the motor and quantization effects that heavily affect the encoders readings. As a result, the encoder will not be used for this experiment.

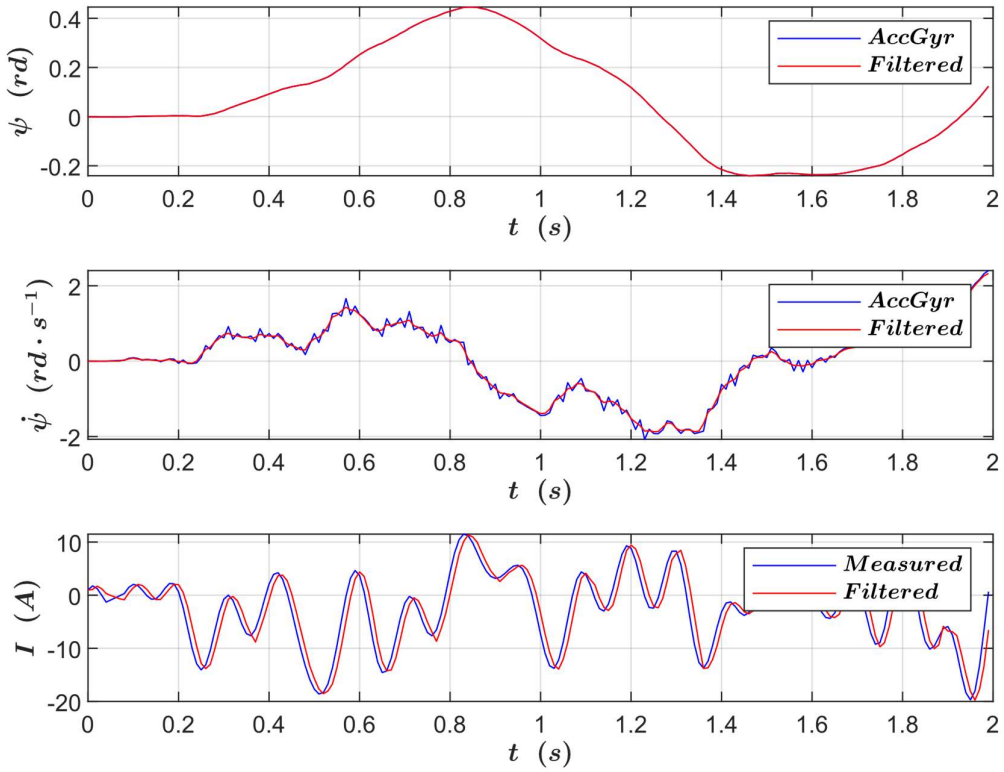

Fig. 22. Filtered accelerometer-gyroscope data

As usual, to eliminate the measurement noise the data was filtered. A zero-phase digital filter (implemented in the Matlab *filfilt* function) with a 40Hz cutoff frequency represents a good trade-off Fig. 22. The filter smooths out the noise in the velocity $\dot{\psi}$ without degrading the signal.

A first set of data, Fig. 23. is used to identify the parameters involved in the model dynamics (9). The identification procedure is provided by the Matlab identification toolbox and is based on a Trust-Region Reflective Newton algorithm to solve the corresponding optimization problem. The obtained parameters values are $M_{b_{frame}} = 17.14\ kg$, $J_{b_{frame}} = 1.44\ kg \cdot m^2$ and $l_{b_{frame}} = 0.29\ m$, and:

$$K_t = 2.22\ Nm \cdot A^{-1} \qquad \mu_m = 0.85\ N \cdot m \cdot s \tag{13}$$

Due to non-modeled nonlinearities (backslash, etc.), the model fit of the data is not perfect. Nevertheless, the results are sufficiently accurate to capture the essential of the signals and, as shown latter on, the robustness of the control laws widely compensate for this imperfection.

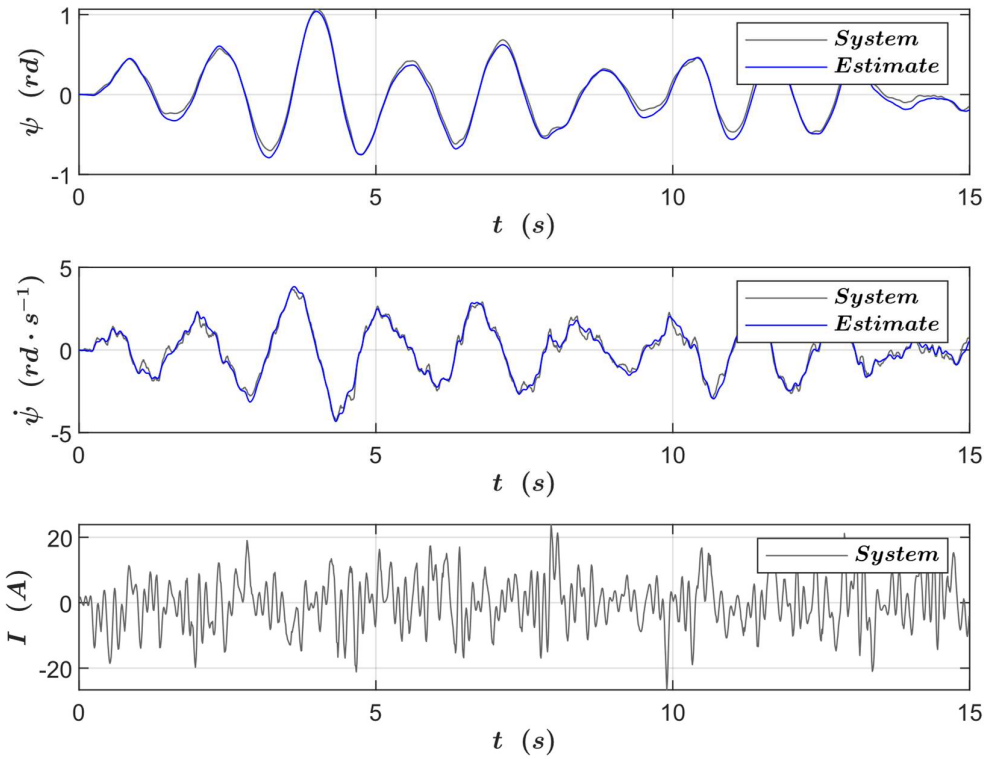

Fig. 23. (Pendulum) identified model and recorded data

The model is further validated on another dataset denoted as *Validation*, Fig. 24. The Normalized Root Mean Squared Error (NRMSE) between simulated and measured signals provides insight on the model accuracy:

$$NRMSE(x,\hat{x}) = \frac{\|x-\hat{x}\|}{\|x-mean(x)\|} \tag{14}$$

The RMS value of the angular position error is 0.1857 and the RMS value of the speed error is 0.2195.

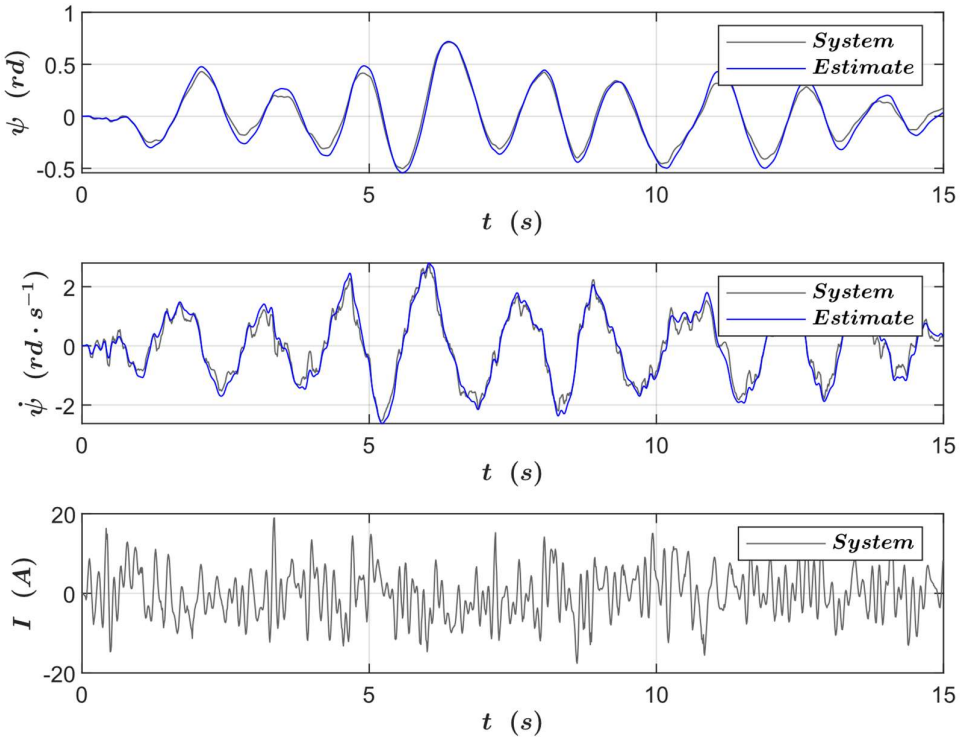

Fig. 24. Comparison of experimental data and simulation results on the *Validation* dataset.

2.5.2 Wheel-ground friction coefficient μ_{wg} and wheel inertia J_w

The second experiment identifies the wheel-ground friction coefficient μ_{wg} and the inertia J_w with the wheelchair in standard mode. The wheel-ground interaction is a complex phenomenon that depends on many unmeasurable or unmeasured parameters such as the tire slip, wear and temperature, the ground micro-surface, etc. The simplified viscous friction model considered in this study is solely used to add a dissipative force in the wheel chair dynamics rather than modeling the tire physics. As a result, a very rough approximation of the wheel-ground friction is expected.

In this experiment the wheelchair just moves forward in a straight line to prevent any disturbance caused by the caster wheels, Fig. 25. Data was collected for 5 different users of different mass.

Fig. 25. Experiment for the 2.5.2 Wheel-ground friction coefficient μ_{wg} and wheel inertia J_w identification

A new model needs to be derived for the straight-line grounded motion of the wheelchair:

$$\left(\mathrm{M_b}r^2 + 2\mathrm{M_w}r^2 + 2\mathrm{J_w}\right)\ddot{y} + \left(2\mu_{\mathrm{m}} + 2\mu_{\mathrm{wg}}r^2\right)\dot{y} = \mathrm{K_t}rI \tag{15}$$

The experiments were done twice for each different user masses $M = [40, 60, 80, 95.5, 115.5]kg$ and equation (15) uses the parameters K_t, μ_m previously identified. Let us recall that the total mass is defined as $M_b = M + M_{b_{Frame}}$ with $M_{b_{Frame}}$ known (measured). For each experiment, the excitation signal has the same shape, Fig. 26, however the amplitudes, according to the mass, needed to be adjusted so that the wheelchair velocity remains in its admissible bounds.

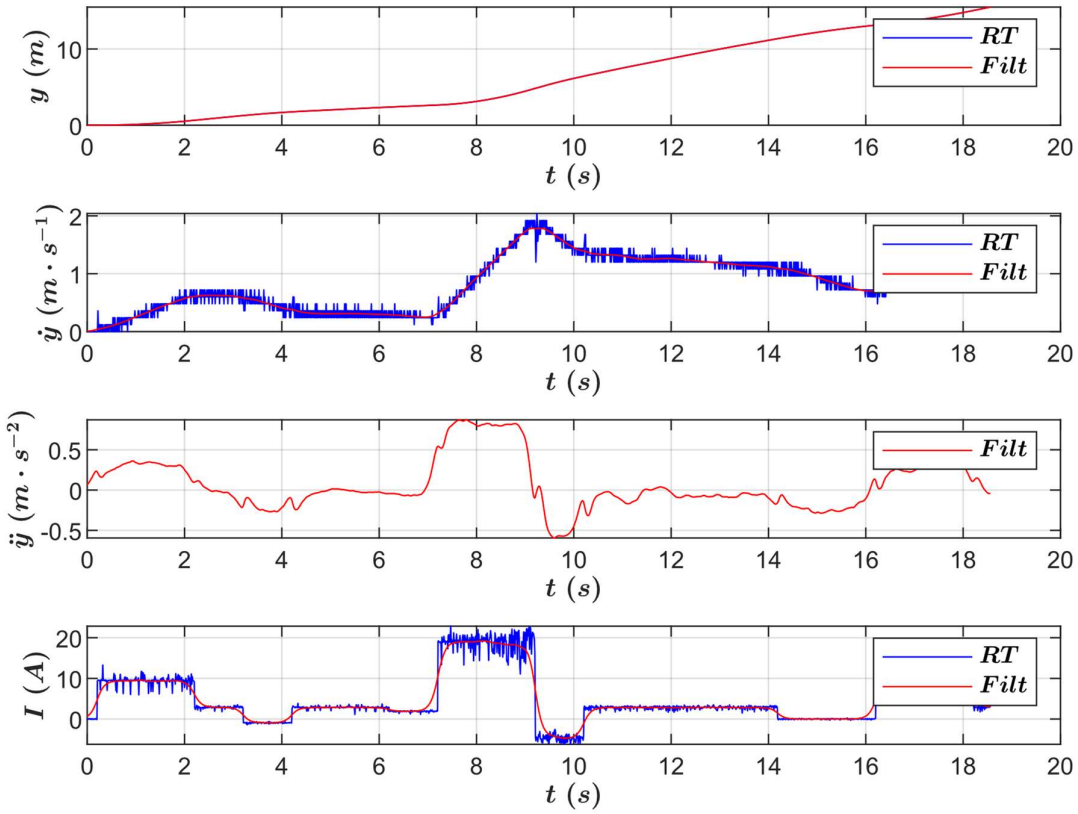

Fig. 26. Recorded (RT) and filtered (Filt) signals

To estimate the speed and acceleration from the quantized encoder readings, the signals are filtered using a second order low pass filter with a 12Hz cutoff frequency. The model dynamics (15) is linear in the parameters, thus a very classical Least Square fitting has been implemented. The Least Square method finds the solution that minimizes the sum of the squares of the errors of an over-determined system of linear equations (Boyd and Vandenberghe 2018).

$$\text{minimize} \left\| Ax - b \right\|^2 \tag{16}$$

where:

$$\left\| Ax - b \right\|^2 = \left(A_{1,m} x - b_1 \right)^2 + \cdots + \left(A_{n,m} x - b_n \right)^2 \tag{17}$$

and m being the number of independent variables and n being the number of linear independent observations. Then, a solution to (16) can be written as:

$$x = \left(A^T A \right)^{-1} A^T b \tag{18}$$

First, the least squares regression is used to identify the wheel inertia J_w. Referring to Fig. 27 the identified parameter $J_w \in [0.2, 0.5] kg \cdot m^2$ for all experiments. The averaged value of J_w is:

$$J_w = 0.36\ kg \cdot m^2 \tag{19}$$

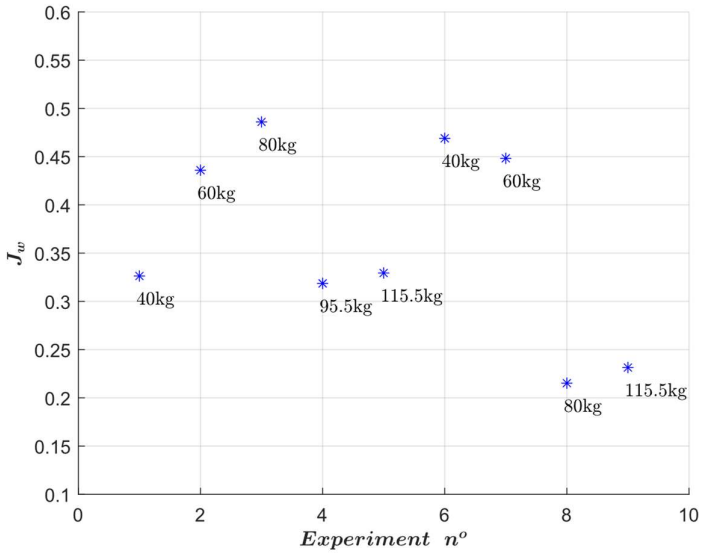

Fig. 27. Identification results for parameter J_w

Next, the parameter μ_{wg} is considered. Since the parameter J_w is already known the linear regression is preformed again on the experiment data with J_w being held constant with the value in (19).

$$\mu_{wg} = 1.79\ N \cdot m^{-1} \cdot s \tag{20}$$

In order to validate the resulting model, real time data and open loop simulation results were done. As an example, we present a result for a person weighting $95.5\ kg$. Therefore, the model will have the resulting parameters: $M_b = 112.64\ kg$, $M_w = 4.68\ kg$, $J_w = 0.36\ kg \cdot m^2$, $\mu_m = 0.85\ kg \cdot s^{-1}$, $\mu_{wg} = 1.79\ N \cdot m^{-1} \cdot s$, $K_t = 2.22\ N \cdot m \cdot A^{-1}$ and $r = 0.3\ m$.

The results of this open-loop validations are depicted in Fig. 28. Despite the simplicity of the considered model, it is sufficiently accurate to capture the essential of the signals and, again, as shown latter on, the robustness of the control laws widely compensate for this imperfection. Then, using (14) the NRMSE for the position y is 0.27, and the NRMSE for the velocity $\dot{y}$ is 0.4007.

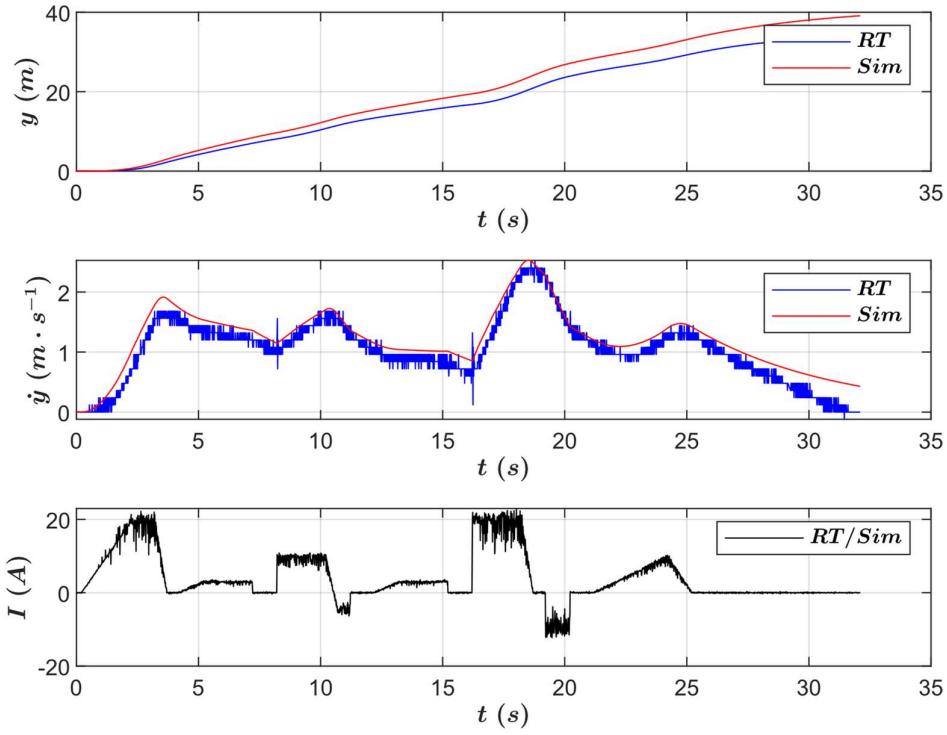

Fig. 28. (Standard) identification open-loop validation

2.5.3 Inertia J_b and length l

Lastly, as the values for M_b, M_w, J_w, μ_m, μ_{wg}, K_t and r have been previously fixed, only the value of J_b and l remains unknown yet.

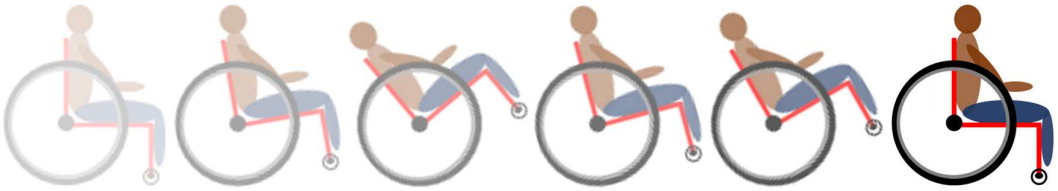

Fig. 29. Identification procedure for parameters J_b & l

In order to tune the parameters J_b and l, a person sat on the wheelchair and operated it in open-loop. The objective was for the person to "ride a wheely" for as long as possible Fig. 29. The model for this experiment is the same as the model for the swing-up (7) and (8).

By comparing the open loop simulation with the recorded data, it becomes possible to adjust the parameters using a direct trial-and-errors procedure.

$$J_b = 11.99\ kg \cdot m^2 \qquad l = 0.295\ m \tag{21}$$

An example of open-loop simulation results and recorded data are plotted in Fig. 30.

In this experiment, the user manually controls the wheelchair using the joystick from the kit. He starts the swing-up sequence by applying a negative current to the motors, thus going backward and increasing the absolute value of the longitudinal speed. At time $t = 1.35\ s$, he estimated that the speed was negative "enough" and applied a positive torque to swing-up the wheel chair. Then, until time $t = 3.8\ s$, he tries to balance the wheel chair by applying appropriate motor current values.

Notice that over $2 \sim 3\ s$ of balancing the errors become important. This is due mainly to the modelling errors accumulation over time. Nevertheless, during the interval $1.35 \le t \le 3.8\ s$ is the most sensitive to the parameters J_b and l, and is used for their estimation. Fig. 30 shows that over this interval the position and angle are subject to integral drifts.

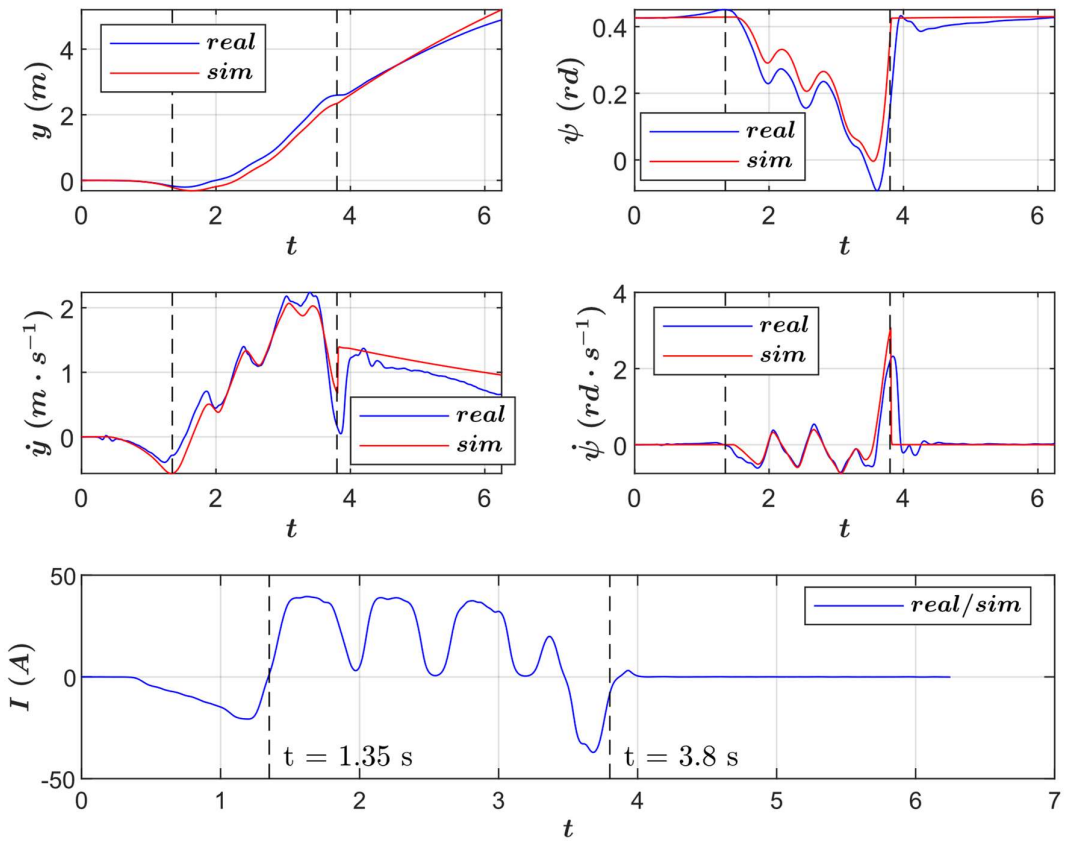

Fig. 30. Comparison of simulated (sim) and recorded (real) signals during manual swing-up

The results of the open-loop validation show that the model closely follows the real system, even though the error accumulates over time. When taking the NRMSE (14) of the simulated model and recorded data in the time range $t \in [0, \ 3.2] s$ the NRMSE for y is 0.2489, $\dot{y}$ is 0.2404, ψ is 0.4833, and $\dot{\psi}$ is 0.3345.

A validation experiment has been performed. Collected data are shown Fig. 33. The obtained results confirm that the model captures the overall system dynamics. The simulated longitudinal and rotational speed globally represents the recorded one even though small offsets are encountered. As a result, a drift in the longitudinal position and rotational angle is experienced. Using (14) the NRMSE for the position y is 0.8141 , and the NRMSE for the velocity $\dot{y}$ is 0.4009, ψ is 0.5976, and $\dot{\psi}$ is 0.3522.

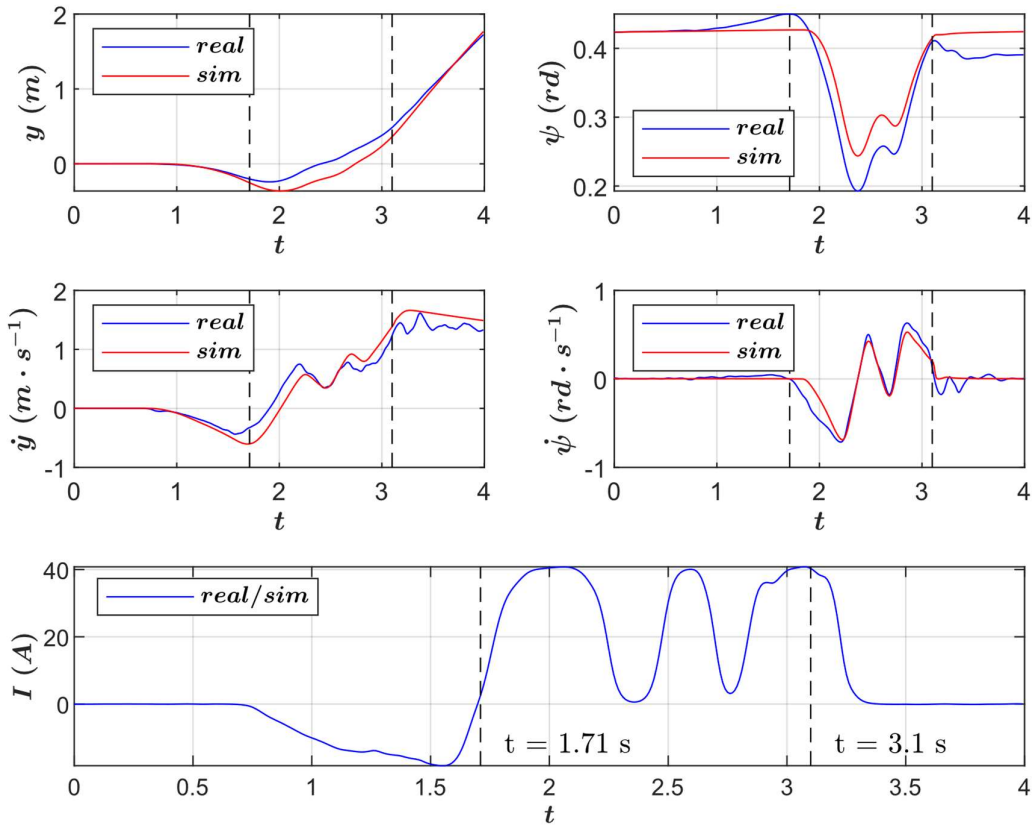

Fig. 31. Validation of parameters J_b, and l

2.6 Conclusion

This chapter introduced the necessary initial works to obtain a "wheelchair + user" model that can be fully exploited for control. Modeling of a wheelchair using Euler-Lagrange method and identification of its parameters were presented. The main parameters that need to be recovered were obtained in three different steps. The overall system validation had to take into account that the system only operates at or close to its unstable equilibrium position. As a result, during open-loop validation, the errors in the model accumulate and the model deviates quickly when near the equilibrium position. However, a sufficiently good validation of the swing-up phase (for example from 0 to $3.2s$, Fig. 30) were obtained. Next chapters will show that the model obtained is sufficiently accurate for deriving robust control laws, that compensate for the relative uncertainties observed.

Chapter 3 Continuous Swing-up Optimal Trajectories

Wheelchairs are used by people that have disabilities in their mobility, and while a wheelchair can be life changing for these people their mobility is still limited. For example, wheelchairs are not able to roll over some common obstacles (street curbs) or maneuver on terrains like grass or stones. An interesting solution that improves the mobility of a wheelchair user is the NOMAD from Autonomad-Mobility Fig. 7. The NOMAD operates in Gyroscopic mode (balancing on its rear two wheels) which allows if to roll over small obstacles and maneuver in rough terrains. However, from a control point-of-view a crucial issue is that neither the ground characteristics nor the Person with Reduced Mobility (PRM) characteristics (height, mass) are known and/or even measured. Then, the swing-up results with the wheelchair being in an unstable equilibrium position with internal and external unknown parameters. As a result, the goal of this chapter is to find a unique solution that will swing-up the wheelchair in a safe, secure manner that can cope system unknowns (user mass, height, and wheelchair geometry). In particular, the solution for the end-user should be smooth, comfortable.

This chapter will start off with Takagi-Sugeno Fuzzy modeling using Sector Nonlinearity Approach. The modeling includes two classical forms, state-space and descriptor continuous models. Then, the stabilization of the state-space and descriptor model is presented. The application of such methodology to the swing-up of a wheelchair is presented. A reference trajectory model in a descriptor form is first defined, whereas the trajectories are performed using optimal control design based on expert admissible trajectories. A robust control based on Lyapunov 2nd method and Linear Matrix Inequalities (LMIs) design (Boyd, et al. 1994) is obtained. Simulations and real-time experiments are provided to show the effectiveness of the proposed approach.

3.1 Takagi-Sugeno Fuzzy Modeling

This part quickly describes the fundamentals of Takagi-Sugeno (Tanaka et Wang 2001) modeling in two cases: classical state-space models and descriptor form models.

3.1.1 "Classical" State-Space Models

Takagi-Sugeno (TS) models are a collection of local linear models blended by nonlinear membership functions (Tanaka et Wang 2001). We restrict our work to the so-called affine-in-control models:

$$\begin{cases} \dot{x}(t) = \sum_{i=1}^{r} h_i\left(z(t)\right)\left(A_i x(t) + B_i u(t)\right) \\ y(t) = \sum_{i=1}^{r} h_i\left(z(t)\right) C_i x(t) \end{cases} \tag{22}$$

where $x(t) \in \mathbb{R}^n$ is the state, $y(t) \in \mathbb{R}^q$ is the output and $u(t) \in \mathbb{R}^p$ is the input that only appears affinely in (22). r is the number of local linear models or vertices, sometimes denoted as number of rules, for historical reasons. $\forall i = 1 \ldots r \quad A_i \in \mathbb{R}^{n \times n}$ are the state matrices of the local linear models, $B_i \in \mathbb{R}^{n \times p}$ the input matrices, $C_i \in \mathbb{R}^{q \times n}$ the output matrices. The nonlinear functions $h_i\left(z(t)\right)$ depend on the so-called premises variables $z(t)$ that can be possibly output, input, state or external parameters dependent. They are subject to a convex sum constraint:

$$\sum_{i=1}^{r} h_i\left(z(t)\right) = 1, \; h_i\left(z(t)\right) \geq 0 \tag{23}$$

Different approaches can be used to design a TS model from an affine-in-control nonlinear model:

$$\begin{cases} \dot{x}(t) = A(\cdot) x(t) + B(\cdot) u(t) \\ y(t) = C(\cdot) x(t) \end{cases} \tag{24}$$

where $A(\cdot) \in \mathbb{R}^{n \times n}$, $B(\cdot)\mathbb{R}^{n \times p}$ and $C(\cdot) \in \mathbb{R}^{q \times n}$ are nonlinear matrices and $(\cdot)$ indicates some output, state or external dependency.

One common approach is to use linearize the nonlinear model (24) around several operating points to derive TS model that approximates the nonlinear dynamics (Johansen, Shorten and Murray-Smith 2000) (Lendek, Guerra, et al. 2010). Another way is the so-called Sector Nonlinearity Approach (SNA) (Ohtake, Tanaka et Wang 2001) which tries to find an **exact** representation of the nonlinear model (24), at least in a compact set of the state variables. However, exactness of the TS model comes at the price of an exponential increase of the number

of vertices; the number of linear systems being related to $2^{n_{NL}}$ with n_{NL} the number of considered nonlinearities in the original nonlinear model. Keeping the number of nonlinearities to be treated using the sector nonlinearity approach low is therefore of particular importance.

Following this classical approach with SNA, a fuzzy model for the wheelchair model in (7) and (8) is constructed (Tanaka et Wang 2001). The goal being to transform each nonlinearity into a defined sector depending on their validity domain. First, in (7) and (8) the nonlinearity $\sin(\psi)$ is substituted with $\frac{\sin(\psi)}{\psi}\psi$ which is equal to $\mathrm{sinc}\left(\frac{\psi}{\pi}\right)\psi$ where $\mathrm{sinc}(\psi)=\frac{\sin(\pi\psi)}{\pi\psi}$. Then, the equations are expanded to first order equations:

$$\begin{aligned}
\dot{x}_1 &= \frac{-a_{x_1}\dot{y}+b_{x_1}\dot{\psi}+c_{x_1}\psi+d_{x_1}I}{M_b\left(M_b l^2r^2+2J_w l^2+J_b r^2+2M_w l^2r^2\right)+2J_b\left(M_w r^2+J_w\right)-M_b{}^2 l^2r^2\cos^2(\psi)} \\
\dot{x}_2 &= \frac{a_{x_2}\dot{y}-b_{x_2}\dot{\psi}-c_{x_2}\psi-d_{x_2}I}{r\left(M_b\left(M_b l^2r^2+2J_w l^2+J_b r^2+2M_w l^2r^2\right)+2J_b\left(M_w r^2+J_w\right)-M_b{}^2 l^2r^2\cos^2(\psi)\right)} \\
\dot{x}_3 &= \dot{\psi}
\end{aligned} \tag{25}$$

where:

$$\begin{aligned}
a_{x_1} &= M_b l^2r^2\mu_{\mathrm{wg}}+2M_b l^2\mu_m+J_b r^2\mu_{\mathrm{wg}}+2J_b\mu_m+2M_b lr\mu_m\cos(\psi) \\
b_{x_1} &= 2\mu_m r\left(M_b l^2+J_b+M_b lr\cos(\psi)\right) \\
c_{x_1} &= \left(M_b lr\left(M_b l^2r+J_b r\right)\dot{\psi}^2-M_b{}^2 gl^2r^2\cos(\psi)\right)\mathrm{sinc}\left(\tfrac{\psi}{\pi}\right) \\
d_{x_1} &= K_t r\left(M_b l^2+J_b+M_b lr\cos(\psi)\right) \\
a_{x_2} &= 4J_w\mu_m+2M_b\mu_m r^2+4M_w\mu_m r^2+2M_b l\mu_m r\cos(\psi)+M_b l\mu_{\mathrm{wg}}r^3\cos(\psi) \\
b_{x_2} &= 2\mu_m r\left(M_b r^2+2M_w r^2+2J_w+M_b lr\cos(\psi)\right) \\
c_{x_2} &= \left(M_b glr\left(M_b r^2+2J_w+2M_w r^2\right)-M_b{}^2 l^2r^3\cos(\psi)\dot{\psi}^2\right)\mathrm{sinc}\left(\tfrac{\psi}{\pi}\right) \\
d_{x_2} &= K_t r\left(M_b r^2+2M_w r^2+2J_w+M_b lr\cos(\psi)\right)
\end{aligned} \tag{26}$$

In (25) there are four nonlinearities that are defined to build the vertices:

$$\begin{aligned}
z_1(t) &= \frac{1}{M_b\left(M_b l^2r^2+2J_w l^2+J_b r^2+2M_w l^2r^2\right)+2J_b\left(M_w r^2+J_w\right)-M_b{}^2 l^2r^2\cos^2(\psi)} \\
z_2(t) &= \cos(\psi) \\
z_3(t) &= \mathrm{sinc}\left(\tfrac{\psi}{\pi}\right) \\
z_4(t) &= \dot{\psi}^2
\end{aligned} \tag{27}$$

Referring to Fig. 18, the wheelchair operating range is restricted to $\psi \in [-60° \quad 30°]$. Next, the bounds for each nonlinearity in (27) are defined.

$$\left[\min\left(z_i(t)\right) \quad \max\left(z_i(t)\right)\right] = \left[m_i \quad M_i\right],\ i \in \{1,2,3,4\} \tag{28}$$

From where the SNA defines the membership functions:

$$w_i^1\left(z_i(t)\right) = \frac{z_i(t) - m_i}{M_i - m_i}, \quad w_i^2\left(z_i(t)\right) = \frac{M_i - z_i(t)}{M_i - m_i} \tag{29}$$

Then, the resulting T-S model will have $2^4 = 16$ vertices. The vertices are the combinations of all $w_i^j(z_i)$, $i \in \{1,2,3,4\}$, $j \in \{1,2\}$:

$$h_k(z) = \prod_{i=1}^{4} w_i^{j_i}(z_i),\ k = \sum_{i=1}^{4} 2^i\left(j_i - 1\right) \tag{30}$$

For example: $9 = 1\times 2^0 + 0\times 2^1 + 0\times 2^2 + 1\times 2^3$ thus: $h_9(z) = w_1^2(z_1)\times w_2^1(z_2)\times w_3^1(z_3)\times w_4^2(z_4)$.

3.1.2 Descriptor state-space Models

Many nonlinear systems, such as mechanical systems, can be naturally written as a descriptor model, (Guelton, Delprat et Guerra 2008), (Lendek, Nagy and Lauber 2018).:

$$\begin{cases} E(x)\dot{x}(t) = A(x)x(t) + B(x)u(t) \\ y(t) = Cx(t) + Du(t) \end{cases} \tag{31}$$

where $E(\cdot) \in \mathbb{R}^{n\times n}$ is the descriptor matrix, and generally for mechanical systems is well-posed, i.e. $E(\cdot)^{-1}$ exists. In this particular case of an invertible $E(\cdot)$ matrix, a state space representation (24) can be derived from (31) by multiplying by the state dynamic by $E(\cdot)^{-1}$. As a consequence, the resulting TS model (obtained using the sector nonlinearity approach) is likely to have a very a number of rules that will be important in the controller design.

Applying the sector nonlinearity approach to the dynamics of (31) a TS descriptor model is derived:

$$\begin{cases} \sum_{k=1}^{r_e} v_k\left(z(t)\right) E_k \dot{x}(t) = \sum_{i=1}^{r} h_i\left(z(t)\right)\left\{A_i x(t) + B_i u(t)\right\} \\ y(t) = \sum_{i=1}^{r} h_i\left(z(t)\right) C_i x(t) \end{cases} \tag{32}$$

With $E_k \;\; k = 1 \cdots r_e$ the local descriptor matrices, v_k are blending functions subject to a convex sum constraint similar to (23):

$$\sum_{k=1}^{r_e} v_k\left(z(t)\right) = 1, \; v_k\left(z(t)\right) \geq 0 \tag{33}$$

The wheelchair model naturally writes as the descriptor model:

$$E(\psi)\dot{x} = A(\psi, \dot{\psi})x + Bu \tag{34}$$

Where:

$$\begin{aligned} E(\psi) &= \begin{pmatrix} M_b + 2M_w + \dfrac{2J_w}{r^2} & M_b l\cos(\psi) & 0 \\ M_b l\cos(\psi) & M_b l^2 + J_b & 0 \\ 0 & 0 & 1 \end{pmatrix} \\ A(\psi, \dot{\psi}) &= \begin{pmatrix} -\mu_{\text{wg}} - \dfrac{2\mu_m}{r^2} & \dfrac{2\mu_m}{r} & M_b l\dot{\psi}^2 \;\text{sinc}\left(\frac{\psi}{\pi}\right) \\ \dfrac{2\mu_m}{r} & -2\mu_m & M_b g l \;\text{sinc}\left(\frac{\psi}{\pi}\right) \\ 0 & 1 & 0 \end{pmatrix} \quad B = \begin{pmatrix} \dfrac{K_t}{r} \\ -K_t \\ 0 \end{pmatrix} \quad x = \begin{pmatrix} \dot{y} \\ \dot{\psi} \\ \psi \end{pmatrix} \end{aligned} \tag{35}$$

Following the same SNA strategy as for the classical case for the wheelchair model, a T-S descriptor model is obtained. First only three nonlinearities are considered, one in $E(\psi)$ and two in $A(\psi, \dot{\psi})$:

$$\begin{aligned} z_1(t) &= \cos(\psi) \\ z_2(t) &= \text{sinc}\left(\tfrac{\psi}{\pi}\right) \\ z_3(t) &= \dot{\psi}^2 \end{aligned} \tag{36}$$

With their bounds

$$\left[\min\left(z_i(t)\right) \quad \max\left(z_i(t)\right)\right] = \left[m_i \quad M_i\right],\ i \in \{1,2,3\} \tag{37}$$

From where the SNA defines the membership functions:

$$w_i^1\left(z_i(t)\right) = \frac{z_i(t) - m_i}{M_i - m_i}, \quad w_i^2\left(z_i(t)\right) = \frac{M_i - z_i(t)}{M_i - m_i} \tag{38}$$

The resulting fuzzy model will have 4 local linear A_i matrices and 2 local linear E_i matrices:

$$\sum_{k=1}^{2} w_k^1(\psi) E_k \dot{x}(t) = \sum_{i=1}^{4} h_i(\psi, \dot{\psi})\left(A_i x(t) + B_i u(t)\right) \tag{39}$$

$$E_1 = \begin{pmatrix} M_b + 2M_w + \frac{2J_w}{r^2} & M_b l m_1 & 0 \\ M_b l m_1 & M_b l^2 + J_b & 0 \\ 0 & 0 & 1 \end{pmatrix} \qquad E_2 = \begin{pmatrix} M_b + 2M_w + \frac{2J_w}{r^2} & M_b l M_1 & 0 \\ M_b l M_1 & M_b l^2 + J_b & 0 \\ 0 & 0 & 1 \end{pmatrix}$$

$$A_1 = \begin{pmatrix} -\mu_{\text{wg}} - \frac{2\mu_m}{r^2} & \frac{2\mu_m}{r} & M_b l m_2 m_3 \\ \frac{2\mu_m}{r} & -2\mu_m & M_b g l m_3 \\ 0 & 1 & 0 \end{pmatrix} \qquad A_2 = \begin{pmatrix} -\mu_{\text{wg}} - \frac{2\mu_m}{r^2} & \frac{2\mu_m}{r} & M_b l M_2 m_3 \\ \frac{2\mu_m}{r} & -2\mu_m & M_b g l m_3 \\ 0 & 1 & 0 \end{pmatrix}$$

$$A_3 = \begin{pmatrix} -\mu_{\text{wg}} - \frac{2\mu_m}{r^2} & \frac{2\mu_m}{r} & M_b l m_2 M_3 \\ \frac{2\mu_m}{r} & -2\mu_m & M_b g l M_3 \\ 0 & 1 & 0 \end{pmatrix} \qquad A_4 = \begin{pmatrix} -\mu_{\text{wg}} - \frac{2\mu_m}{r^2} & \frac{2\mu_m}{r} & M_b l M_2 M_3 \\ \frac{2\mu_m}{r} & -2\mu_m & M_b g l M_3 \\ 0 & 1 & 0 \end{pmatrix}$$

$$B = \begin{pmatrix} \frac{K_t}{r} \\ -K_t \\ 0 \end{pmatrix}$$

Using a descriptor form is common for mechanical systems; specifically, because it is a natural way to write equations derived from the Euler-Lagrange method (Guelton, Delprat et Guerra 2008), (Lendek, Nagy and Lauber 2018). Generally, in this form the matrix $E(x)$ ends-up being regular, in particular this is the case for the wheelchair making discussions about the singular case such as in (Zhang, Xia et She 2008) useless. As $E^{-1}(x)$ exists, a classical state

space representation can also be derived from the descriptor model (31). Nevertheless, a first key point to reduce conservatism (in term of LMI complexity) is to keep a constant B matrix (Bouarar, Guelton et Manamanni 2010). A second point is that for many problems coming from mechanical descriptions, the descriptor formulation (32) have been shown to reduce the conservatism of the solutions, i.e. to enlarge the set of feasible solutions (Estrada-Manzo, et al. 2015), (Lendek, Nagy and Lauber 2018), and (Chadli and Darouach 2012). Therefore, the descriptor form (39) of the wheelchair will be kept in the manuscript.

3.2 Stabilization of T-S models

Some useful notations that will be used in the following section are defined.

3.2.1 Notations and useful technical lemmas

In order to shorten the expressions, the following notation are introduced for single or multiple sums:

(40)

And extended for multiple sums: $A_{hh} = \sum_{i=1}^{r}\sum_{i=1}^{r} h_i(z) h_i(z) A_{ij}$ or $K_{hv} = \sum_{k=1}^{r_e}\sum_{i=1}^{r} h_i(z) v_k(z) K_{ki}$, Υ_{hhv} and so on.

The TS descriptor model (32) can be written as:

$$\begin{cases} E_v \dot{x}(t) = A_h x(t) + B_h u(t) \\ y(t) = C_h x(t) \end{cases}$$

$$E_v = \sum_{k=1}^{r_e} v_k\left(z(t)\right) E_k,\ A_h = \sum_{i=1}^{r} h_i\left(z(t)\right) A_i,\ X_h^{-1} = \left(\sum_{i=1}^{r} h_i\left(z(t)\right) E_i\right)^{-1} \quad (41)$$

For a matrix X, X^T denotes its transpose, $X = X^T \succ 0$ stands for a symmetric definite positive matrix. In a matrix and/or in an expression $(*)$ stands for the term deduced by

symmetry, for example $\begin{bmatrix} A & (*) \\ B & C \end{bmatrix} = \begin{bmatrix} A & B^T \\ B & C \end{bmatrix}$ or $PA + (*) = PA + A^T P$, and different possible combinations such as: $\begin{bmatrix} A + (*) + Q & (*) \\ B & C \end{bmatrix} = \begin{bmatrix} A + A^T + Q & B^T \\ B & C \end{bmatrix}$.

Often LMI constraints problems can include multiple sums. For double sums it can be necessary to check if $\sum_{i=1}^{r}\sum_{j=1}^{r} h_i(z) h_j(z) \Upsilon_{ij} < 0$, or in a compact form $\Upsilon_{hh} < 0$. A trivial solution is $\Upsilon_{ij} < 0 \;\; i, j \in \{1, \ldots r\}$ that ends with conservative results as it does not exploit the fact that $h_i(z) h_j(z) = h_j(z) h_i(z)$. Exploiting this kind of property is known as relaxation schemes. The one used thereinafter is due to (Tuan, et al. 2001).

Sufficient conditions to ensure $\sum_{i=1}^{r}\sum_{j=1}^{r} h_i(z) h_j(z) \Upsilon_{ij} < 0$ are:

$$\Upsilon_{ii} < 0 \tag{42}$$

$$\frac{2}{r-1}\Upsilon_{ii} + \Upsilon_{ij} + \Upsilon_{ji} < 0 \qquad i \neq j,\ i, j \in \{1, \ldots r\} \tag{43}$$

Next, two technical inequalities lemmas are often necessary (Boyd, et al. 1994).

Lemma 1 (completion of squares): Consider X, Y two matrices of appropriate dimension, a scalar $\varepsilon > 0$ and a positive definite matrix $Q = Q^T > 0$, the following statements hold:

$$X^T Y + Y^T X \leq \varepsilon X^T X + \varepsilon^{-1} Y^T Y \tag{44}$$

$$X^T Y + Y^T X \leq X^T Q X + Y^T Q^{-1} Y \tag{45}$$

These results are direct from the inequality $(QX - Y)^T Q^{-1} (QX - Y) \geq 0$.

Lemma 1 (Schur's complement): let $P \in \mathbb{R}^{n \times n}$ be a positive definite matrix $P = P^T > 0$ and $Q \in \mathbb{R}^{m \times n}$ the following statements are equivalent:

$$Q - X^T P^{-1} X > 0 \tag{46}$$

$$\begin{bmatrix} Q & X^T \\ X & P \end{bmatrix} > 0 \tag{47}$$

3.2.2 Stabilization of TS models

State-space stabilization of TS models is done generally via Lyapunov functions and so-called Parallel Distributed Compensation (PDC) schemes (Tanaka et Wang 2001). For example, with (24) in a TS form (22), a quadratic Lyapunov function generally applies:

$$V(t) = x^T(t) P x(t),\ P = P^T > 0 \tag{48}$$

Together with the PDC that shares the same SNA as the model:

$$u(t) = F_h P^{-1} x(t) \tag{49}$$

It renders the state close-loop model:

$$\dot{x}(t) = \left(A_h + B_h F_h P^{-1}\right) x(t) \tag{50}$$

And after some classical manipulation, the derivative of (48) along the trajectories of the closed-loop (50) is negative if: $A_h P + B_h F_h P^{-1} + (*) < 0$ or equivalently using the sums:

$$\sum_{i=1}^{r}\sum_{j=1}^{r} h_i(z) h_j(z) \Upsilon_{ij} < 0,\ \Upsilon_{ij} = A_i P + B_i F_j + \left(A_i P + B_i F_j\right)^T = A_i P + B_i F_j + (*) \tag{51}$$

Thus a LMI constraints problem can be proposed:

LMI T-S Stabilization Problem: $\Upsilon_{ij} = A_i P + B_i F_j + (*)$

Find $P = P^T > 0$ and F_i, $i \in \{1, \ldots r\}$ such that conditions (42) and (43) hold. (52)

3.2.3 Stabilization of TS descriptor models

Now, consider the descriptor model (41) written in its compact form:

$$\begin{aligned} E_v \dot{x}(t) &= A_h x(t) + B_h u(t) \\ y(t) &= C_h x(t) \end{aligned} \tag{53}$$

The usual way to cope with such descriptor form is to introduce an extended vector $\hat{x} = \begin{pmatrix} x \\ \dot{x} \end{pmatrix}$ (Taniguchi, Tanaka and Wang 2000). It allows to rewrite (53) as:

$$\begin{aligned} \hat{E}\dot{\hat{x}}(t) &= \hat{A}_{hv}\hat{x}(t) + \hat{B}_h u(t) \\ \hat{y}(t) &= \hat{C}_h \hat{x}(t) \end{aligned} \tag{54}$$

where: $\hat{A}_{hv} = \sum_{i=1}^{r}\sum_{k=1}^{r_e} h_i(z(t)) v_k(z(t)) \hat{A}_{ik}$, $\hat{B}_h = \sum_{i=1}^{r} h_i(z(t))\hat{B}_i$, $\hat{C}_h = \sum_{i=1}^{r} h_i(z(t))\hat{C}_i$ and: $\hat{E} = \begin{pmatrix} I & 0 \\ 0 & 0 \end{pmatrix}$, $\hat{A}_{hv} = \begin{pmatrix} 0 & I \\ A_h & -E_v \end{pmatrix}$, $\hat{B}_h = \begin{pmatrix} 0 \\ B_h \end{pmatrix}$.

The quadratic Lyapunov function used writes:

$$V(x) = \hat{x}^T(t)\hat{E}X\hat{x}(t) \tag{55}$$

As $V(x)$ is definite positive, we need symmetry: $\hat{E}X = X^T\hat{E}$ and $V(x) > 0$, $x \neq 0$, thus the form of X is (Taniguchi, Tanaka and Wang, Fuzzy descriptor systems and nonlinear model following control 2000):

$$X = \begin{pmatrix} X_1 & 0 \\ X_3 & X_4 \end{pmatrix}, \; X_1 = X_1^T > 0 \tag{56}$$

Then the following control law, corresponding to an extended PDC scheme can be used with $P_1^{-1} = X_1$:

$$u(t) = F_{hv}P_1^{-1}x(t) \tag{57}$$

The descriptor closed-loop writes:

$$E_v\dot{x}(t) = \left(A_h + B_h F_{hv} P_1^{-1}\right)x(t) \tag{58}$$

And in its extended form:

$$\hat{E}\dot{\hat{x}}(t) = \begin{pmatrix} 0 & I \\ A_h + B_h F_{hv} P_1^{-1} & -E_v \end{pmatrix}\hat{x}(t) \tag{59}$$

Now, considering the derivative of the Lyapunov function $\dot{V}(x) = 2\hat{x}^T(t) X^T \hat{E}\ \dot{\hat{x}}(t)$ along the trajectories leads to:

$$\begin{pmatrix} P_1^{-1} & 0 \\ X_3 & X_4 \end{pmatrix}^T \begin{pmatrix} 0 & I \\ A_h + B_h F_{hv} \left(P^1\right)^{-1} & -E_v \end{pmatrix} + (*) < 0 \tag{60}$$

And multiplying right with: $P = \begin{pmatrix} P_1 & 0 \\ P_3 & P_4 \end{pmatrix}$ and left P^T, such that $XP = P^T X^T = I$ gives:

$$\begin{pmatrix} 0 & I \\ A_h + B_h F_{hv} P_1^{-1} & -E_v \end{pmatrix} \begin{pmatrix} P_1 & 0 \\ P_3 & P_4 \end{pmatrix} + (*) < 0 \tag{61}$$

Or equivalently (Taniguchi, Tanaka and Wang 2000):

$$\begin{pmatrix} P_3 + P_3^T & (*) \\ A_h P_1 + B_h F_{hv} - E_v P_3 + P_4^T & -E_v P_4 + P_4^T E_v^T \end{pmatrix} < 0 \tag{62}$$

A refinement is possible with extra slack variables introducing P_{3h} and P_{4h} in place of P_3 and P_4 to get (Guerra, Bernal and Kruszewski, et al. 2007):

$$\begin{pmatrix} P_{3h} + P_{3h}^T & (*) \\ A_h P_1 + B_h F_{hv} - E_v P_{3h} + P_{4h}^T & -E_v P_{4h} + P_{4h}^T E_v^T \end{pmatrix} < 0 \tag{63}$$

From (63), a LMI constraint problem can be derived via the relaxation (43):

LMI Descriptor T-S Stabilization Problem: $\Upsilon_{ij}^k = \begin{pmatrix} P_{3j} + P_{3j}^T & (*) \\ A_i P_1 + B_i F_{jk} - E_i P_{3j} + P_{4j}^T & -E_i P_{4j} + P_{4j}^T E_i^T \end{pmatrix}$

Find $P_1 = P_1^T > 0$, P_{3j}, P_{4j}, and F_{jk} $i, j \in \{1, \ldots r\}$, $k \in \{1, \ldots r_e\}$ such that:

$$\begin{aligned} &\Upsilon_{ii}^k < 0 && k \in \{1, \ldots r_e\} \\ &\frac{2}{r-1} \Upsilon_{ii}^k + \Upsilon_{ij}^k + \Upsilon_{ji}^k < 0 && i, j \in \{1, \ldots r\}\ i \neq j, k \in \{1, \ldots r_e\} \end{aligned} \tag{64}$$

With these "basic" results being recalled, the application to the wheelchair is presented.

3.3 Application

The objective is to bring the wheelchair form the grounded standard-position (SP) where $\psi = \psi_g$ to the self-balancing mode (SBM) where $\psi = 0\,rd$ with the following constraints: smoothness, safety when transitioning from SP to SBM and minimum displacement. To achieve this goal, a controller is designed to follow predefined reference trajectories. The predefined trajectories are computed using the optimal control framework.

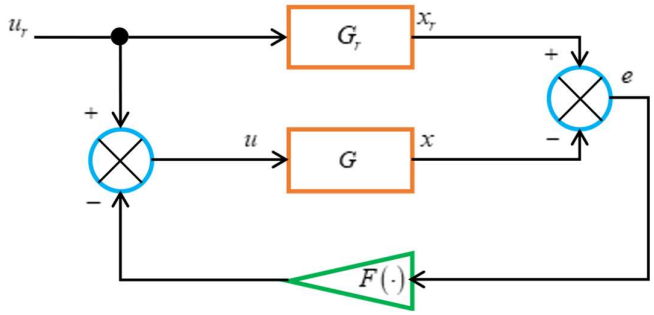

Fig. 32. Tracking feedback loop (continuous control)

Fig. 32 shows a diagram of the control strategy. The reference state x_r is an optimal trajectory computed off-line using the plant G_r and the (optimal) reference input u_r .Therefore, the control u has to minimize the effect of the error between the reference state x_r and x the state vector corresponding to the real plant G . The synthesis and the expression of the feedback part $F(\cdot)$ is presented subsection 3.3.3. With $e(t) = x_r(t) - x(t)$, the resulting diagram leads to the control law:

$$u(t) = u_r(t) - F(\cdot)e(t) \tag{65}$$

3.3.1 Reference Tracking Model

The model (34), $E(\psi)\dot{x} = A(\psi,\dot{\psi})x + Bu$, presents several nonlinearities depending on ψ and $\dot{\psi}$. There are many possibilities to take them into account such as (39), the choice adopted consists in isolating the nonlinearities of $A(\psi,\dot{\psi})$ in a vector $\Upsilon(\psi,\dot{\psi})$. This way is interesting because it prevents the use of classical Lipschitz conditions that ends with convergence in a ball (Ichalal and Mammar 2015), (Zemouche, Mohamed and Bara 2008). Therein, using this vector

allows with the help of the Mean Value Theorem (MVT) to prove an asymptotic convergence property (Ichalal and Guerra 2019). Therefore, (34) is written as:

$$E(\psi)\dot{x} = \tilde{A}x + \Upsilon(\psi,\dot{\psi}) + Bu \tag{66}$$

where

$$\tilde{A} = \begin{pmatrix} -\mu_{\text{wg}} - \dfrac{2\mu_m}{r^2} & \dfrac{2\mu_m}{r} & 0 \\ \dfrac{2\mu_m}{r} & -2\mu_m & 0 \\ 0 & 1 & 0 \end{pmatrix}, \Upsilon(\psi,\dot{\psi}) = \begin{pmatrix} M_b l\dot{\psi}^2 \sin(\psi) \\ M_b g l \sin(\psi) \\ 0 \end{pmatrix} \tag{67}$$

Thus, (66) is the generic model used to derive the control law and the reference model following the same principle (with similar matrices as (67)) writes:

$$E(\psi_r)\dot{x}_r = \tilde{A}x_r + \Upsilon(\psi_r,\dot{\psi}_r) + Bu_r \tag{68}$$

Now, considering that $E(\psi)$, equation (35), is well-defined, i.e. invertible for every ψ, proving the convergence of $E(\psi)\dot{e} \to 0$ ensures the convergence of the error $\dot{e} \to 0$. Therefore, let us write:

$$E(\psi)\dot{e} = E(\psi)(\dot{x}_r - \dot{x}) \tag{69}$$

which can be expanded to:

$$E(\psi)\dot{e} = E(\psi_r)\dot{x}_r - E(\psi)\dot{x} + \left[E(\psi) - E(\psi_r)\right]\dot{x}_r \tag{70}$$

Then substituting (66) and (68) into (70):

$$E(\psi)\dot{e} = \tilde{A}e + B(u_r - u) + \Delta\Upsilon(\cdot) + \left[E(\psi) - E(\psi_r)\right]\dot{x}_r \tag{71}$$

where

$$\Delta\Upsilon(\cdot) = \Upsilon(\psi_r,\dot{\psi}_r) - \Upsilon(\psi,\dot{\psi}) = \begin{pmatrix} M_b l\left[\dot{\psi}_r^2 \sin(\psi_r) - \dot{\psi}^2 \sin(\psi)\right] \\ M_b g l\left[\sin(\psi_r) - \sin(\psi)\right] \\ 0 \end{pmatrix} \tag{72}$$

And introducing the vector:

$$\Omega(\cdot)=\left[E(\psi)-E(\psi_r)\right]\dot{x}_r=\begin{pmatrix} M_b l\left[\cos(\psi)-\cos(\psi_r)\right]\ddot{\psi}_r \\ M_b l\left[\cos(\psi)-\cos(\psi_r)\right]\ddot{y}_r \\ 0 \end{pmatrix} \tag{73}$$

The equation (70) is equivalent to:

$$E(\psi)\dot{e}=\tilde{A}e+B(u_r-u)+\Delta\Upsilon(\cdot)+\Omega(\cdot). \tag{74}$$

In (74), if $\Delta\Upsilon(\cdot)$ and $\Omega(\cdot)$ are treated via Lipschitz conditions (Ichalal and Mammar 2015), (Zemouche, Mohamed and Bara 2008), the convergence can be only ensured inside a ball whose radius depends directly on the Lipschitz constants. Another way ensuring the convergence to the equilibrium point is to take profit of the Differential Mean Value Theorem (DMVT) (Zill and Write 2011), (Guerra, Márquez, et al. 2018).

Lemma 3: (Zill and Write 2011) Differential Mean Value Theorem: Let $f(x):\mathbb{R}^n\to\mathbb{R}$ and $a,b\in\mathbb{R}^n$. If $f(x)$ is a differentiable function on $[a,b]$, then, there exists a vector $c\in\mathbb{R}^n$ with $c_i\in\,]a_i,b_i[$, $i\in\{1,\ldots,n\}$ such that

$$f(b)=f(a)+\nabla f(c)(b-a) \tag{75}$$

where $\nabla f(c)=\dfrac{\partial f(c)}{\partial x}$ and $]a_i,b_i[$ means the open interval between a_i and b_i.

DMVT can be applied to equations (72) and (73) using the intermediate variables $\varsigma_0,\varsigma_2,\varsigma_3\in\,]\min(\psi_r,\psi),\max(\psi_r,\psi)[$ and $\varsigma_1\in\,]\min(\dot{\psi}_r,\dot{\psi}),\max(\dot{\psi}_r,\dot{\psi})[$. For (72)

$$\sin(\psi_r)=\sin(\psi)+\cos(\varsigma_0)(\psi_r-\psi) \tag{76}$$

$$\dot{\psi}_r{}^2\sin(\psi_r)=\dot{\psi}^2\sin(\psi)+\begin{bmatrix}\varsigma_1^2\cos(\varsigma_2) & 2\varsigma_1\sin(\varsigma_2)\end{bmatrix}\begin{bmatrix}\psi_r-\psi \\ \dot{\psi}_r-\dot{\psi}\end{bmatrix} \tag{77}$$

which leads to

$$\Delta\Upsilon(\cdot)=\Delta\Upsilon^{*}(\cdot)e=M_b l\begin{pmatrix}0 & 2\varsigma_1\sin(\varsigma_2) & \varsigma_1^2\cos(\varsigma_2)\\ 0 & 0 & g\cos(\varsigma_0)\\ 0 & 0 & 0\end{pmatrix}e \tag{78}$$

For (73):

$$\cos(\psi)-\cos(\psi_r)=-\sin(\varsigma_3)(\psi_r-\psi) \tag{79}$$

which leads to

$$\Omega(\cdot)=\Omega^{*}(\cdot)e=\begin{pmatrix}0 & 0 & -M_b l\sin(\varsigma_3)\ddot{\psi}_r\\ 0 & 0 & -M_b l\sin(\varsigma_3)\ddot{y}_r\\ 0 & 0 & 0\end{pmatrix}e \tag{80}$$

Now defining $A^{*}(\varsigma_0,\varsigma_1,\varsigma_2,\varsigma_3,\ddot{\psi}_r,\ddot{y}_r)=\tilde{A}+\Delta\Upsilon^{*}(\cdot)+\Delta\Omega^{*}(\cdot)$, the estimation error dynamic (74) becomes:

$$E(\psi)\dot{e}=A^{*}(\varsigma_0,\varsigma_1,\varsigma_2,\varsigma_3,\ddot{\psi}_r,\ddot{y}_r)e+B(u_r-u) \tag{81}$$

with

$$A^{*}(\cdot)=\begin{pmatrix}-\mu_{\text{wg}}-\dfrac{2\mu_m}{r^2} & \dfrac{2\mu_m}{r}+2M_b l\varsigma_1\sin(\varsigma_2) & M_b l\left[\varsigma_1^2\cos(\varsigma_2)-\sin(\varsigma_3)\ddot{\psi}_r\right]\\ \dfrac{2\mu_m}{r} & -2\mu_m & M_b l\left[g\cos(\varsigma_0)-\sin(\varsigma_3)\ddot{y}_r\right]\\ 0 & 1 & 0\end{pmatrix} \tag{82}$$

Then applying the control law (65):

$$E(\psi)\dot{e}=\left(A^{*}(\varsigma_0,\varsigma_1,\varsigma_2,\varsigma_3,\ddot{\psi}_r,\ddot{y}_r)+BF(\cdot)\right)e \tag{83}$$

However, before describing the procedure to find $F(\cdot)$ that ensures the convergence of (83) reference trajectories are to be defined, in order to ensure not only stability but also comfort.

3.3.2 Reference Trajectories

To analyze the way a swing-up is managed, a manual reference swing-up is presented Fig. 33; it has been performed by an expert at the company Autonomad-Mobility using the hand-

rims. The strategy is decomposed in 2 moves; first, a move in the reverse direction then a forward acceleration that swings up the wheelchair. This strategy backward-forward helps to reduce the displacement of the wheelchair needed for the swing-up. The black dashed line in Fig. 33 show the start of the transition from reverse velocity to forward velocity which is when the swing-up starts.

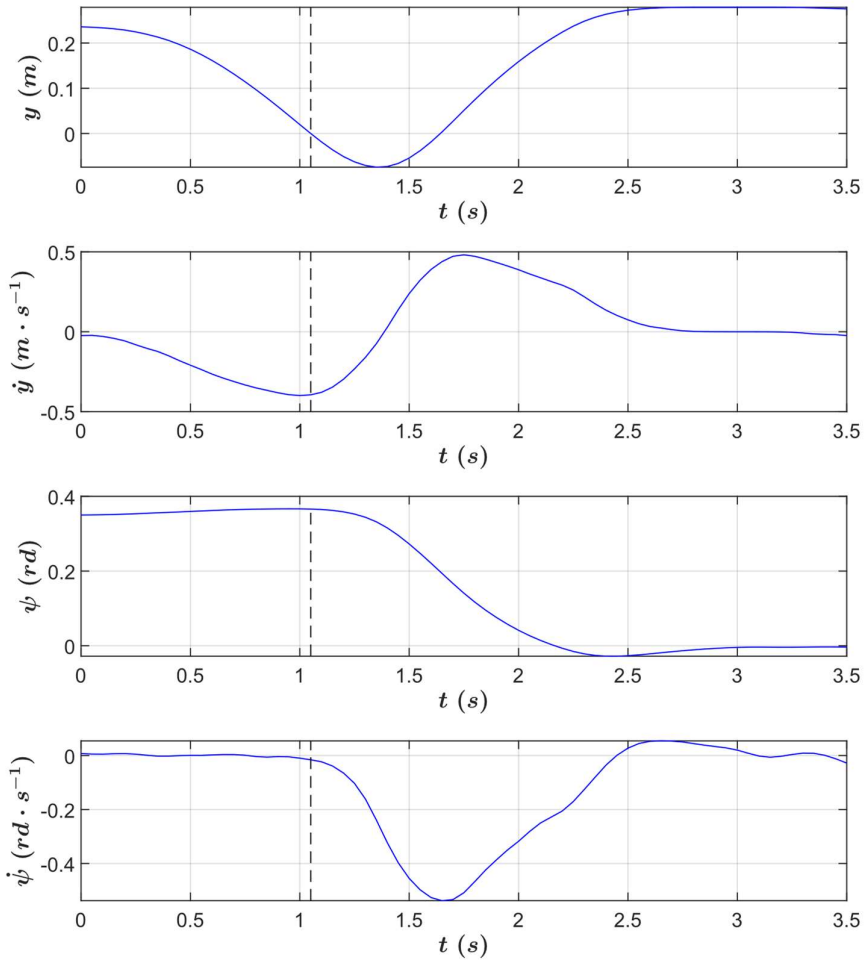

Fig. 33. Manual swing-up trajectories

The reference trajectory starts with the wheelchair grounded $\psi_r(0) = \psi_g$, an initial negative velocity to be determined, and ends when the wheelchair is in the upright position $\psi_r(t_f) = 0$. With t_f the free final time, the criterion to be minimized is:

$$\min_{u_r} J(u_r) = \int_0^{t_f} l(u_r(\tau), y_r(\tau)) d\tau \tag{84}$$

with $l(u_r, y_r) = \frac{1}{2}{u_r}^2 + q_0\left(y_r - y_{\text{target}}\right)^2$. The first term in l allows limiting the control amplitude while the second terms allows simultaneously reducing the swing-up time and enforcing a final position $y_r\left(t_f\right)$ near to y_{target}; $q_0 > 0$ is a weighting factor.

Then, writing the model equations from (7) and (8) as a set of first order equations, the state dynamics can be written as:

$$\dot{x}_r(t) = f\left(x_r(t)\right) + B_r\left(x_r(t)\right)u_r(t) \tag{85}$$

Where

$$\dot{x}_r(t) = \left[\ddot{y}_r(t) \quad \ddot{\psi}_r(t) \quad \dot{y}_r(t) \quad \dot{\psi}_r(t)\right]^T$$

$$f\left(x_r(t)\right) = \begin{pmatrix} \dfrac{-a_1\dot{y}_r + b_1\dot{\psi}_r + c_1\psi_r}{M_b\left(M_b l^2 r^2 + 2J_w l^2 + J_b r^2 + 2M_w l^2 r^2\right) + 2J_b\left(M_w r^2 + J_w\right) - {M_b}^2 l^2 r^2 \cos^2\left(\psi_r\right)} \\ \dfrac{a_2\dot{y}_r - b_2\dot{\psi}_r - c_2\psi_r}{r\left(M_b\left(M_b l^2 r^2 + 2J_w l^2 + J_b r^2 + 2M_w l^2 r^2\right) + 2J_b\left(M_w r^2 + J_w\right) - {M_b}^2 l^2 r^2 \cos^2\left(\psi_r\right)\right)} \\ \dot{y}_r \\ \dot{\psi}_r \end{pmatrix}$$

$$B_r\left(x_r(t)\right) = \begin{pmatrix} \dfrac{d_1}{M_b\left(M_b l^2 r^2 + 2J_w l^2 + J_b r^2 + 2M_w l^2 r^2\right) + 2J_b\left(M_w r^2 + J_w\right) - {M_b}^2 l^2 r^2 \cos^2\left(\psi_r\right)} \\ \dfrac{-d_2}{r\left(M_b\left(M_b l^2 r^2 + 2J_w l^2 + J_b r^2 + 2M_w l^2 r^2\right) + 2J_b\left(M_w r^2 + J_w\right) - {M_b}^2 l^2 r^2 \cos^2\left(\psi_r\right)\right)} \\ 0 \\ 0 \end{pmatrix}$$

With

$$a_1 = M_b l^2 r^2 \mu_{\text{wg}} + 2M_b l^2 \mu_m + J_b r^2 \mu_{\text{wg}} + 2J_b \mu_m + 2M_b lr\mu_m \cos\left(\psi_r\right)$$

$$b_1 = 2\mu_m r\left(M_b l^2 + J_b + M_b lr\cos\left(\psi_r\right)\right)$$

$$c_1 = \left(M_b lr \left(M_b l^2 r + J_b r \right) \dot{\psi}_r^2 - {M_b}^2 g l^2 r^2 \cos\left(\psi_r\right) \right) \operatorname{sinc}\left(\tfrac{\psi_r}{\pi}\right)$$

$$d_1 = K_t r \left(M_b l^2 + J_b + M_b lr \cos\left(\psi_r\right) \right)$$

$$a_2 = 4 J_w \mu_m + 2 M_b \mu_m r^2 + 4 M_w \mu_m r^2 + 2 M_b l \mu_m r \cos\left(\psi_r\right) + M_b l \mu_{\mathrm{wg}} r^3 \cos\left(\psi_r\right)$$

$$b_2 = 2 \mu_m r \left(M_b r^2 + 2 M_w r^2 + 2 J_w + M_b lr \cos\left(\psi_r\right) \right)$$

$$c_2 = \left(M_b glr \left(M_b r^2 + 2 J_w + 2 M_w r^2 \right) - {M_b}^2 l^2 r^3 \cos\left(\psi_r\right) \dot{\psi}_r^2 \right) \operatorname{sinc}\left(\tfrac{\psi_r}{\pi}\right)$$

$$d_2 = K_t r \left(M_b r^2 + 2 M_w r^2 + 2 J_w + M_b lr \cos\left(\psi_r\right) \right)$$

The control saturation is:

$$-\overline{u_r} < u_r(t) < \overline{u_r} \tag{86}$$

The initial condition corresponds to a longitudinal position arbitrarily fixed to 0 with a free initial velocity and a grounded wheel chair, so $\psi_r(0) = \psi_g$. The final condition corresponds to a free longitudinal position, with null longitudinal and angular speeds.

Hence, the boundary conditions are:

$$\psi_r(0) = \psi_g,\ y_r(0) = \dot{\psi}(0) = \dot{y}_r(t_f) = \psi_r(t_f) = \dot{\psi}(t_f) = 0 \tag{87}$$

$$y_r(t_f) = \dot{y}_r(0) = free \tag{88}$$

To facilitate the numerical implementation and to cope with the free final time, the following change of variable is considered:

$$z = \frac{t}{t_f} \in [0,1] \tag{89}$$

z now being the independent variable, and the optimal control to be solved is:

$$\min_{u_r} J(u_r) = \int_0^1 l\left(u_r(z), y_r(z)\right) dz \tag{90}$$

$$\frac{dx_r(z)}{dz} = \left(f\left(x_r(z)\right) + B_r\left(x_r(z)\right)u_r(z)\right)\cdot t_f \tag{91}$$

$$-\overline{u_r} < u_r(t) < \overline{u_r} \tag{92}$$

$$\psi_r(0) = \psi_g,\ y_r(0) = \dot{y}_r(1) = \psi_r(1) = \dot{\psi}(0) = \dot{\psi}(1) = 0 \tag{93}$$

$$y_r(t_f) = \dot{y}_r(0) = free \tag{94}$$

In order to derive optimality conditions using Pontryagin's Minimum Principle (PMP) (Naidu 2003), (Kirk 2004), let us first define the Hamiltonian associated with the optimal control problem:

$$H(x_r, u_r, \lambda) = l(y_r, u_r) + \lambda^T\left(f(x_r) + B_r(x_r)u_r\right)t_f \tag{95}$$

with $\lambda(z) = \left[\lambda_{dy}(z), \lambda_{d\psi},(z), \lambda_y(z), \lambda_\psi(z)\right]^T \in \mathbb{R}^4$ the co-state vector. PMP provides optimality conditions along an optimal trajectory. The optimal co-state dynamics are:

$$\frac{\partial H(x_r, u_r, \lambda_r)}{\partial x} = -\frac{d\lambda}{dz} \tag{96}$$

The optimal control minimizes the Hamiltonian:

$$u_r(t) = \underset{-\overline{u_r} < v < \overline{u_r}}{\arg\min}\, H(x_r, v, \lambda) \tag{97}$$

The Hamiltonian is a second order of the control u_r:

$$H(x_r, u_r, \lambda) = a_0 + a_1 u_r + \frac{1}{2}{u_r}^2 \tag{98}$$

with $a_0 = q_0\left(y_r - y_{\text{target}}\right)^2 + \lambda^T f(x_r)t_f$ $a_1 = \lambda^T B_r(x_r)t_f$.

The Hamiltonian being convex with respect to the scalar control u_r, its unconstrained minimum is :

$$u_r^{uc} = -\lambda^T B_r(x_r) \tag{99}$$

The optimality control policy $u_r = \Pi(x_r, \lambda)$, solution of (97), is obtained by considering the control saturation (86):

$$\Pi(x_r, \lambda) = \max\left(\underline{u_r}, \min\left(\overline{u_r}, u_r^{uc}\right)\right) \tag{100}$$

For each free initial or final state in (94), the corresponding co-state value is null:

$$\lambda_y(1) = \lambda_{dy}(0) = 0 \tag{101}$$

The final time t_f being free, the final Hamiltonian value is null (Geering 2007).

$$H(x_r(1), u_r(1), \lambda_r(1)) = 0 \tag{102}$$

The final time being a constant, the following dynamics is considered:

$$\frac{dt_f(z)}{dz} = 0 \tag{103}$$

Let us denote $Y_r = \left[x^T, \lambda^T, t_f\right]^T$. The optimal control problem is thus reduced to the following boundary value problem:

$$\begin{cases} \dfrac{dY_r}{dt} = F(Y_r) \\ G(Y_r(0), Y_r(1)) = 0 \end{cases} \tag{104}$$

With $F(Y_r) = \begin{pmatrix} f(x_r(t)) + B(x_r(t))\Pi(x_r, \lambda) \\ -\dfrac{\partial H(x_r, u_r, \lambda_r)}{\partial x}\Big|_{u_r = \Pi(x_r, \lambda)} \\ 0 \end{pmatrix}$

and $G=(G_i)$, $G\left(Y_r(0),Y_r(t_f)\right)=\begin{pmatrix}\lambda_{dy_r}(0)\\ \dot{\psi}_r(0)\\ y_r(0)\\ \psi_r(0)-\psi_g\\ \dot{y}_r(1)\\ \dot{\psi}_r(1)\\ \lambda_{y_r}(1)\\ \psi_r(1)\\ H\left(x_r(1),u_r(1),\lambda_r(1)\right)\end{pmatrix}$.

The boundary value problem (104) can be solved using colocation approach, for instance using the bvp4c solver (Kierzenka and Shampine 2001). To compute a solution, two parameters needs to be fixed : q_0 and y_{target} used in the criterion (84). According to the swing-up experiments performed in manual mode, Fig. 33, the target position y_{target} has been set to $0.34\,m$ and only q_0 remains unfixed. To illustrate its effect on the optimal solutions, two of them are computed for $q_0=100$ and $q_0=2000$, and depicted in Fig. 34. Two signals are of particular interest: the longitudinal position y and the wheel chair angle ψ. Small q_0 values generate solutions that take longer and have no position overshoot. Large q_0 values lead to more dynamic solutions with overshoots on position, angle and control signals. These solutions have also smaller t_f values.

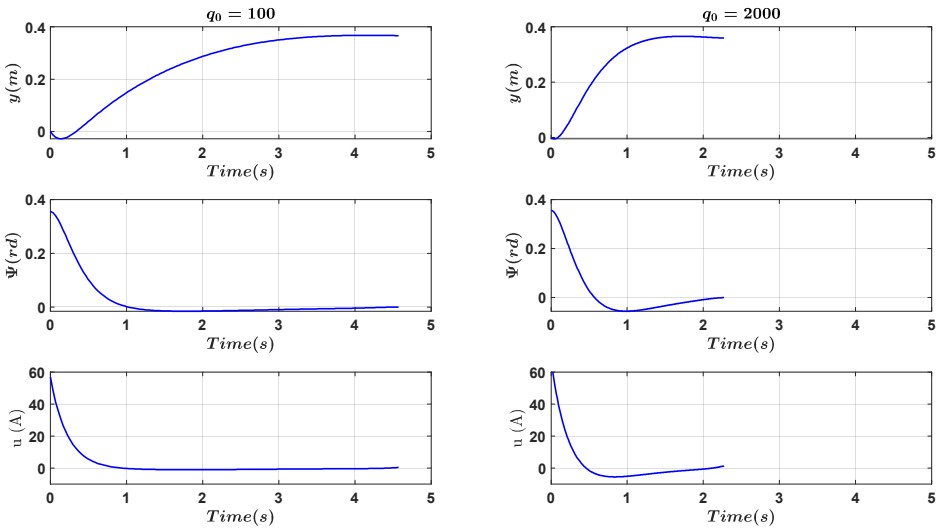

Fig. 34 : Comparison of optimal solutions for two q_0 values

In order to generate safe and comfortable trajectories, the value of q_0 is chosen such that the generated reference trajectories are close enough to the one recorded during swing-up performed by an expert. Let us denote with subscript m the data recorded during the manual operation and let J_y be the normalized root mean squared deviation between the optimized trajectory position y_r and y_m. Similarly, criterions J_ψ, J_{dy}, $J_{d\psi}$ are also defined for the angular position, the longitudinal velocity and the angular speed. Fig. 35 summarizes the obtained values as a function of q_0.

The generated longitudinal motion $(y_r, \dot{y}_r)$ are closer to the recorded one for q_0 between 700 and 800. The generated angle and angular speed are closer to the recorded one for small values. As a result, a compromise, $q_0 = 405$ has to be found between the longitudinal and rotational behavior.

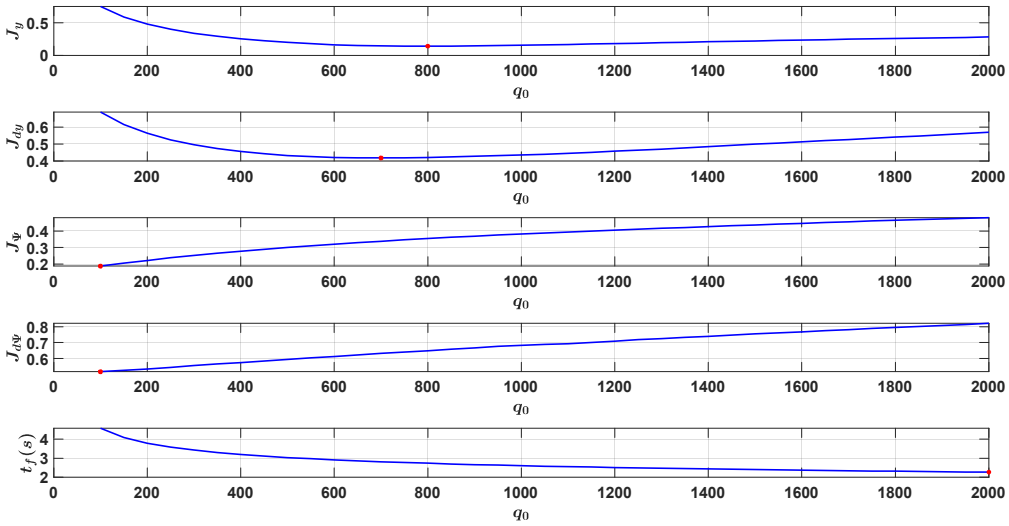

Fig. 35 : Considered criterions as a function of q_0. The red stars depict the best values.

The optimal solution obtained for the chosen q_0 value is depicted in Fig. 36 along with the signals recorded during manual operation. The global behavior of the manual operation is well captured, the shape of the different signals being overall similar. The amplitudes of the signals are in the same range, even when looking carefully, the optimal solution has a slightly lower longitudinal speed and slightly higher angular speed. The obtained final time $t_f = 4.61s$ is much longer than the manual swing-up duration which is approximately $2.25\,s$. In the vicinity of the target position, the optimal trajectory converges very slowly and at $t = 2.25\,s$, the wheelchair is almost at steady state. In practice, the encountered difference is not noticeable.

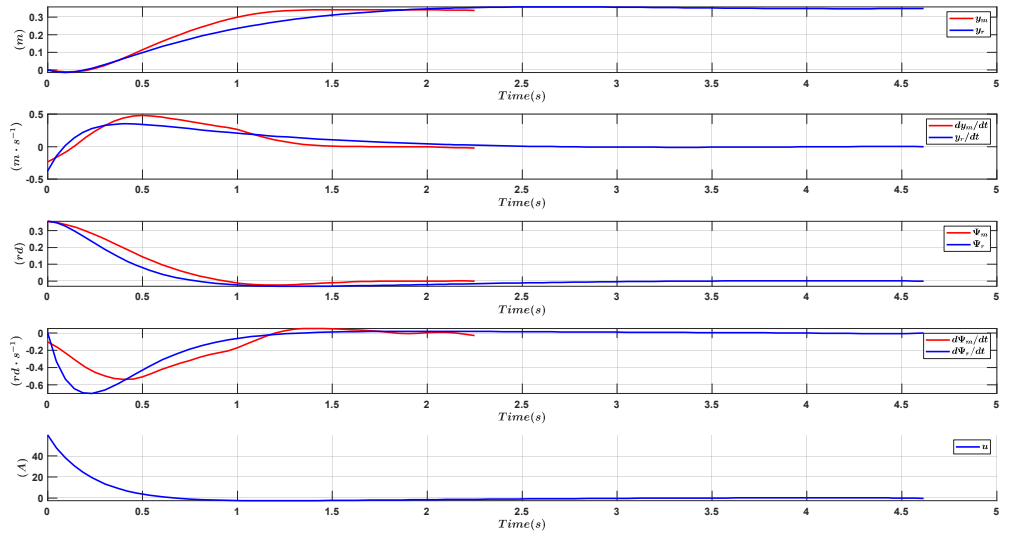

Fig. 36. Comparison between manual operations (red) and optimal solutions (blue)

3.3.3 Reference Tracking Controller Design

With the optimal trajectories being defined, a stable controller (65) is synthesized using the quasi-LPV framework (Tanaka et Wang 2001) and Linear Matrix Inequalities (LMIs) constraints (Boyd, et al. 1994). Since the model of the tracking error is in a descriptor form (83) we will consider as a basis the *LMI Descriptor T-S Stabilization Problem* (64) and extend it for robustness issues. Following the same path as for (64), the extended form of (83) is.

$$\begin{gathered}\hat{E}\dot{\hat{x}} = \hat{A}(\cdot)\hat{x} + \hat{B}\hat{u} \\ \hat{E} = \begin{pmatrix} I & 0 \\ 0 & 0 \end{pmatrix}, \hat{A}(\cdot) = \begin{pmatrix} 0 & I \\ A^*(\cdot) & -E(\psi) \end{pmatrix}, \hat{B} = \begin{pmatrix} 0 \\ B \end{pmatrix}\end{gathered} \tag{105}$$

The goal is now to write (105) as an uncertain T-S model. Considering the definition of $A^*(\cdot)$ in (82) and remembering that the intermediate variables ς_i, $i \in \{0,1,2,3\}$ are bounded but unknown, we will use their bounds to define an uncertain description. Considering:

$$\begin{gathered}\varsigma_0, \varsigma_2, \varsigma_3 \in \left]\min(\psi_r, \psi), \max(\psi_r, \psi)\right[\\ \varsigma_1 \in \left]\min(\dot{\psi}_r, \dot{\psi}), \max(\dot{\psi}_r, \dot{\psi})\right[\end{gathered}, \tag{106}$$

it is possible to find the centers and radii for the uncertainties. For the parameters ς_0, ς_2 and ς_3, the validity domains are direct from the wheelchair mechanical restrictions due to the caster wheels and the anti-tippers. Validity domain of ς_1 is related to safety and comfort of the swing-up and results from real time experiments and company experts' experience. Thus, the minimum and maximum bounds for the uncertainties result in the worst-case combinations of the validity domains that correspond to:

$$2M_b l\varsigma_1 \sin(\varsigma_2) \in \left[\underline{\Gamma}_0 \quad \overline{\Gamma}_0\right] = 2M_b l\left[\min_{\varsigma_1,\varsigma_2}\left(\varsigma_1 \sin(\varsigma_2)\right) \quad \max_{\varsigma_1,\varsigma_2}\left(\varsigma_1 \sin(\varsigma_2)\right)\right] \tag{107}$$

$$\begin{aligned}&M_b l\left(\varsigma_1^2 \cos(\varsigma_2) - \sin(\varsigma_3)\ddot{\psi}_r\right) \in \left[\underline{\Gamma}_1 \quad \underline{\Gamma}_1\right] \\ &= M_b l\left[\min_{\varsigma_1,\varsigma_2,\varsigma_3,\ddot{\psi}_r}\left(\varsigma_1^2 \cos(\varsigma_2) - \sin(\varsigma_3)\ddot{\psi}_r\right) \quad \max_{\varsigma_1,\varsigma_2,\varsigma_3,\ddot{\psi}_r}\left(\varsigma_1^2 \cos(\varsigma_2) - \sin(\varsigma_3)\ddot{\psi}_r\right)\right]\end{aligned} \tag{108}$$

$$\begin{aligned}&M_b l\left(g\cos(\varsigma_0) - \sin(\varsigma_3)\ddot{y}_r\right) \in \left[\underline{\Gamma}_2 \quad \overline{\Gamma}_2\right] \\ &= M_b l\left[\min_{\varsigma_0,\varsigma_3,\ddot{y}_r}\left(g\cos(\varsigma_0) - \sin(\varsigma_3)\ddot{y}_r\right) \quad \max_{\varsigma_0,\varsigma_3,\ddot{y}_r}\left(g\cos(\varsigma_0) - \sin(\varsigma_3)\ddot{y}_r\right)\right]\end{aligned} \tag{109}$$

Therefore, trivially we can define the centers: $c_i = \tfrac{1}{2}\left(\overline{\Gamma}_i + \underline{\Gamma}_i\right)$ and the radii $r_i = \tfrac{1}{2}\left(\overline{\Gamma}_i - \underline{\Gamma}_i\right)$ $i \in \{1,2,3\}$. Now the expression of $A^*(\cdot)$ (82) in (105) can be written as:

$$A^*(\cdot) = \overline{A} + H\Delta(t)J \tag{110}$$

with: $\Delta(t) = \begin{pmatrix} \Delta_0(t) & 0 & 0 \\ 0 & \Delta_1(t) & 0 \\ 0 & 0 & \Delta_2(t) \end{pmatrix}$, $\|\Delta_i(t)\| \le 1$, $i \in \{1,2,3\}$ and:

$$\overline{A} = \begin{pmatrix} -\mu_{\text{wg}} - \dfrac{2\mu_m}{r^2} & \dfrac{2\mu_m}{r} + c_0 & c_1 \\ \dfrac{2\mu_m}{r} & -2\mu_m & c_2 \\ 0 & 1 & 0 \end{pmatrix}, H = \begin{pmatrix} r_0 & r_1 & 0 \\ 0 & 0 & r_2 \\ 0 & 0 & 0 \end{pmatrix}, J = \begin{pmatrix} 0 & 1 & 0 \\ 0 & 0 & 1 \\ 0 & 0 & 1 \end{pmatrix} \tag{111}$$

And for (105)

$$\hat{A}(\cdot) = \begin{pmatrix} 0 & I \\ \overline{A} + H\Delta(t)J & -E(\psi) \end{pmatrix} \tag{112}$$

As ψ is measured, we can consider a quasi-LPV description of (112) via a decomposition of $E(\psi)$ in the validity domain of $\psi \in \left[-\psi_g, \psi_g\right]$ for the nonlinearity $\cos(\psi) \in \left[\cos(\psi_g), 1\right]$. This so-called Sector Nonlinearity Approach (Tanaka et Wang 2001), corresponds to:

$$\cos(\psi) = \cos(\psi_g) \times v_1(\psi) + 1 \times v_2(\psi) \tag{113}$$

Where $v_1(\psi) = \dfrac{\cos(\psi) - \cos(\psi_g)}{1 - \cos(\psi_g)}$, $v_2(\psi) = 1 - v_1(\psi)$

Thus, we define:

$$E_v = v_1(\psi) \times E(\psi_g) + v_2(\psi) \times E(1) \tag{114}$$

E_v represents a polytope with two vertices $E(\psi_g)$ and $E(1)$, and perfectly coincides with $E(\psi)$ when $\psi \in \left[-\psi_g, \psi_g\right]$. Following classical PDC scheme (49), the control writes:

$$F(\cdot) = F_v P_1^{-1} = \left(v_1(\psi) \times F(\psi_g) + v_2(\psi) \times F(1)\right) P_1^{-1} \tag{115}$$

Therefore, we have a quasi-LPV extended description with uncertainties of (83) as:

$$\hat{E}\dot{\hat{e}} = \begin{pmatrix} 0 & I \\ \overline{A} + H\Delta(t)J + BF_v P_1^{-1} & -E_v \end{pmatrix} \hat{e} \tag{116}$$

Then, using the Lyapunov function candidate (55), $V(e^*) = e^{*T}(t) E^* X e^*(t)$, where: $X = \begin{pmatrix} X_1 & 0 \\ X_3 & X_4 \end{pmatrix}$, $X_1 = X_1^T > 0$, and following the same path transforms directly expression (62) into:

$$\begin{pmatrix} P_3 + P_3^T & (*) \\ \overline{A}P_1 + BF_v - E_v P_3 + P_4^T & -E_v P_4 - P_4^T E_v^T \end{pmatrix} + \begin{pmatrix} 0 & \left(H\Delta(t)JP_1\right)^T \\ H\Delta(t)JP_1 & 0 \end{pmatrix} \leq 0 \tag{117}$$

Considering the 2nd term in (117), the sum $\mu_v > 0$, with $\mu_1, \mu_2 \in \mathbb{R}$ and the classical completion of square property (44) (Boyd, et al. 1994):

$$\begin{pmatrix} 0 \\ H \end{pmatrix} \Delta(t) \begin{pmatrix} JP_1 & 0 \end{pmatrix} + (*) \leq \mu_v \begin{pmatrix} 0 \\ H \end{pmatrix} \Delta(t) \Delta^T(t) \begin{pmatrix} 0 \\ H \end{pmatrix}^T + \mu_v^{-1} \begin{pmatrix} P_1 J^T \\ 0 \end{pmatrix} \begin{pmatrix} P_1 J^T \\ 0 \end{pmatrix}^T \tag{118}$$

And since $\left\|\Delta_i(t)\right\| \leq 1$, $i \in \{1,2,3\}$:

$$\begin{pmatrix} P_3 + P_3^T + \mu_v^{-1} P_1 J^T (JP_1) & (*) \\ \overline{A}P_1 + BF_v - E_v P_3 + P_4^T & \mu_v HH^T - E_v P_4 - P_4^T E_v^T \end{pmatrix} \leq 0 \tag{119}$$

Then applying a Schur's complement (47) on the first entry of (119) gives:

$$\begin{pmatrix} -\mu_v I & JP_1 & 0 \\ P_1 J^T & P_3 + P_3^T & (*) \\ 0 & \overline{A}P_1 + BF_v - E_v P_3 + P_4^T & \mu_v HH^T - E_v P_4 - P_4^T E_v^T \end{pmatrix} \leq 0 \tag{120}$$

Therefore, the LMI constraints problem corresponds to:

LMI Descriptor T-S Robust Stabilization Problem:

Find $P_1 = P_1^T > 0$, P_3, P_4 and F_v $v \in \{1,2\}$, $\mu_1, \mu_2 \in \mathbb{R}^+$ such that:

$$\Upsilon_i = \begin{pmatrix} -\mu_v I & JP_1 & 0 \\ P_1 J^T & P_3 + P_3^T & (*) \\ 0 & \bar{A}P_1 + BF_v - E_v P_3 + P_4^T & \mu_v HH^T - E_v P_4 - P_4^T E_v^T \end{pmatrix} < 0, \; v \in \{1,2\} \qquad (121)$$

Then, since the initial conditions are known we can enforce a constraint on the command $\|u(t)\|_2 \le \mu$ for all $t \ge 0$ (Tanaka et Wang 2001) if the LMIs hold:

$$\begin{pmatrix} 1 & x(0)^T \\ x(0) & P^1 \end{pmatrix} \ge 0 \qquad \begin{pmatrix} P^1 & M_v^T \\ M_v & \mu^2 I \end{pmatrix} \ge 0 \qquad (122)$$

3.3.4 Reference Tracking Simulation

The set of parameters identified in chapter 2 are used to design the controller for the simulations with the following values $M_b = M + M_{b_{frame}} = 95.5 + 17.14 = 112.64\ kg$, $J_b = 11.99\ kg \cdot m^2$, $M_w = 4.68\ kg$, $J_w = 0.36\ kg \cdot m^2$, $r = 0.3\ m$, $g = 9.81\ kg/m^2$, $l = 0.295\ m$, $\mu_m = 0.85\ kg/s$, $\mu_{wg} = 1.79\ kg/s$, $K_t = 2.22\ Nm/A$.

The resulting optimal reference trajectories are depicted in Fig. 37, Fig. 38. With $\min(\ddot{y}) = -0.181$, $\max(\ddot{y}) = 4.96$, $\min(\ddot{\psi}) = -7.04$, and $\max(\ddot{\psi}) = 1.03$; following (107), (108), and (109) the bounds are: $\underline{\Gamma}_0 = -52$, $\overline{\Gamma}_0 = 52$, $\underline{\Gamma}_1 = -92$, $\overline{\Gamma}_1 = 214$, $\underline{\Gamma}_2 = 235$ and $\overline{\Gamma}_2 = 365$; that results to the centers $c_0 = 0$, $c_1 = 61$, $c_2 = 300$ and radii $r_0 = 52$, $r_1 = 153$, $r_2 = 65$. Then, for input constraints $x(0) = [-0.45, 0, 0.34]^T$ and $\mu = 80$.

Thus, the matrices involved in the LMI constraints problem (121) are:

$$E_1 = \begin{pmatrix} 130.05 & 33.22 & 0 \\ 33.22 & 21.79 & 0 \\ 0 & 0 & 1 \end{pmatrix}, \; E_2 = \begin{pmatrix} 130.05 & 30.60 & 0 \\ 30.60 & 21.79 & 0 \\ 0 & 0 & 1 \end{pmatrix}$$

$$\tilde{A} = \begin{pmatrix} -20.73 & 5.68 & 61.0 \\ 5.68 & -1.70 & 300.0 \\ 0 & 1 & 0 \end{pmatrix} \text{ and } B = \begin{pmatrix} 7.39 \\ -2.22 \\ 0 \end{pmatrix}.$$

In the top of Fig. 37 is the lateral position of the base of the wheelchair and the curve below is the velocity. The maximum displacement of y is about $0.32\,m$ which is one of the goals of the swing-up. Then, the top 2 curves in Fig. 38 are the angular position and angular velocity of the pendulum. The angular position ψ starts at $0.35\,rd$ and ends at $0\,rd$ in about 1s which is comparable to the manual swing up in Fig. 33. In both Fig. 37, Fig. 38 the optimal reference command is given in the bottom. Also, these trajectories were calculated with $q_0 = 405$.

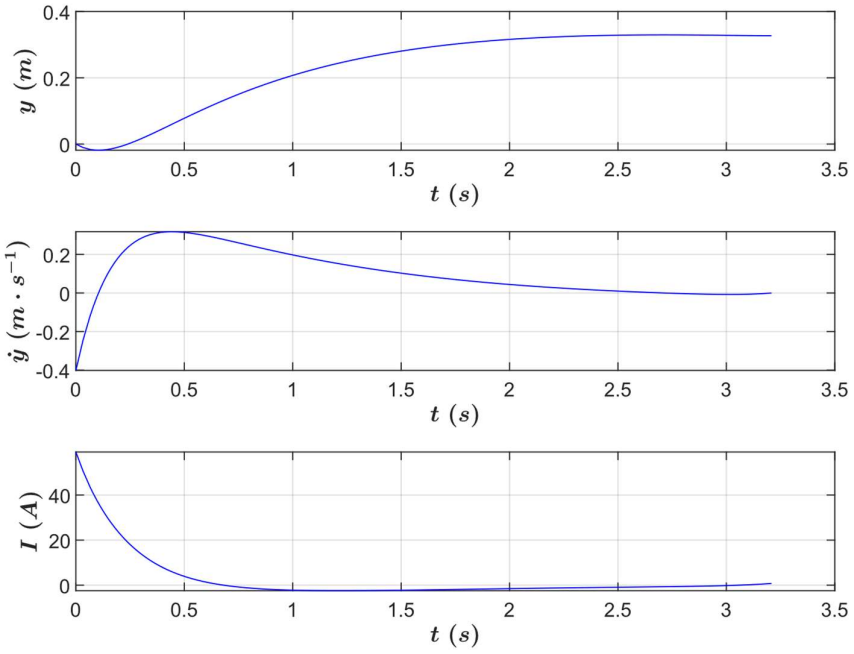

Fig. 37. Optimal swing-up trajectories $y, \dot{y}$

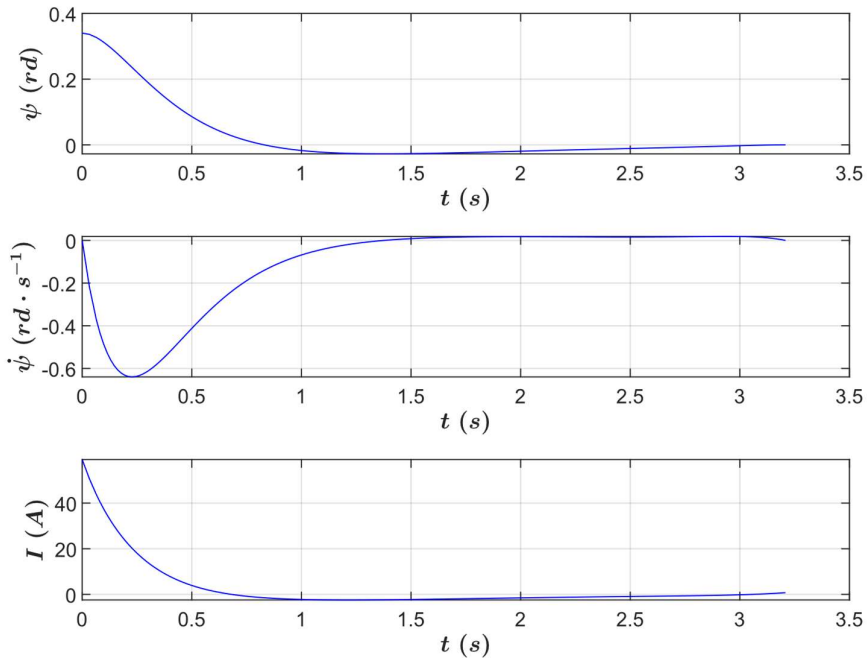

Fig. 38. Optimal swing-up trajectories $\psi, \dot{\psi}$

Solving *LMI Descriptor T-S Robust Stabilization Problem* (121) using YALMIP (Lofberg 2004) gives the following result:

$$P_1 = \begin{pmatrix} 220.83 & -4.44 & -2.51 \\ -4.44 & 7.79 & -1.20 \\ -2.51 & -1.20 & 0.56 \end{pmatrix}, \begin{pmatrix} \mu_1 \\ \mu_2 \end{pmatrix} = \begin{pmatrix} 1.13 \\ 1.07 \end{pmatrix}$$

$$F_1 = \begin{pmatrix} 3.32 & 29.29 & 113.23 \end{pmatrix},\ F_2 = \begin{pmatrix} 3.24 & 29.69 & 111.54 \end{pmatrix}$$

Then, the control law (65) is tested in simulations, and the results of the simulation can be seen in Fig. 39, Fig. 40. The simulations were carried out with one control algorithm for 2 different masses $M = \{80,100\}\, kg$ or $M_b = \{97.14,117.14\}\, kg$. There is no simulation for the nominal mass $M = 95.5\, kg$ because the curves will exactly match the reference line since the reference trajectories and controller were designed from the same nonlinear model.

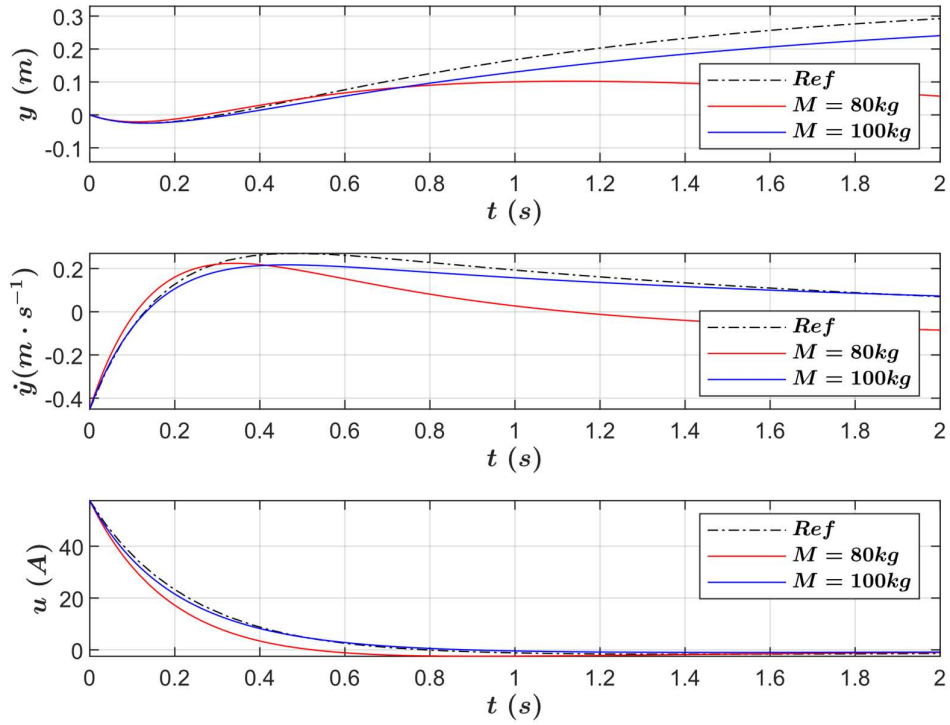

Fig. 39. Simulation continuous swing-up trajectories $y, \dot{y}$

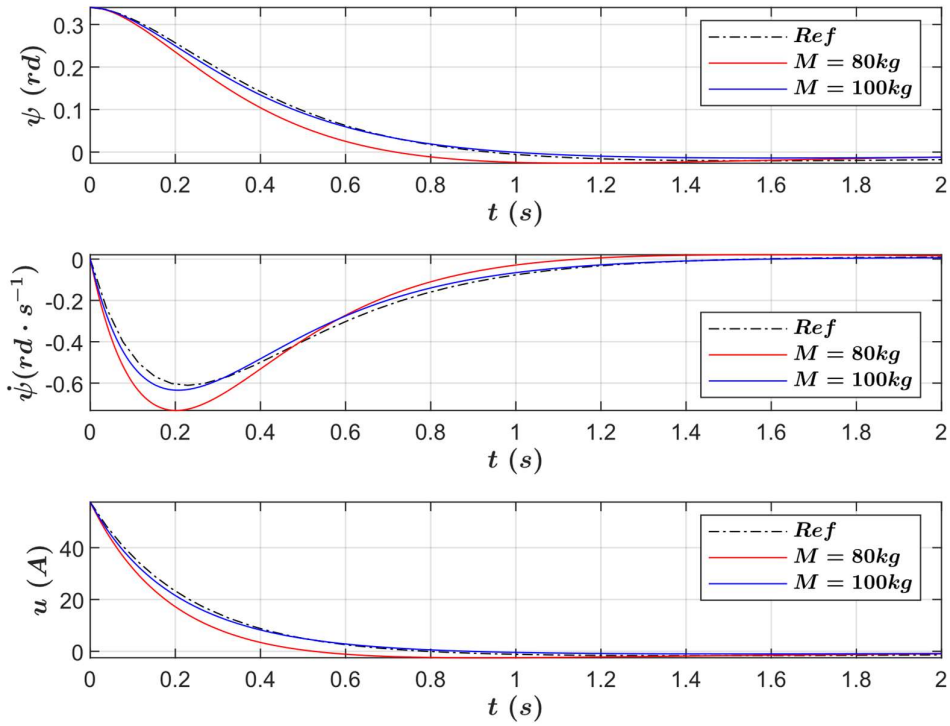

Fig. 40. Simulation continuous swing-up trajectories

In the top of Fig. 39 are the trajectories for $y, \dot{y}$, the position and velocity of the base of the wheelchair, and in Fig. 40 are the trajectories for the angular position and velocity for the pendulum of the wheelchair. Even though the trajectories deviate from the reference trajectories the control law can still swing-up and stabilize the wheelchair.

Fig. 39, Fig. 40, presented the "nice" nominal results in the sense that compared to the real-time system there is no noise, no uncertainties, no quantization issues. Therefore, in order to validate the controller, conditions that are closer to "reality" are considered in the next simulation tests, Fig. 41, Fig. 42: noise and quantization errors are added to the feedback signals as well as a zero-order hold.

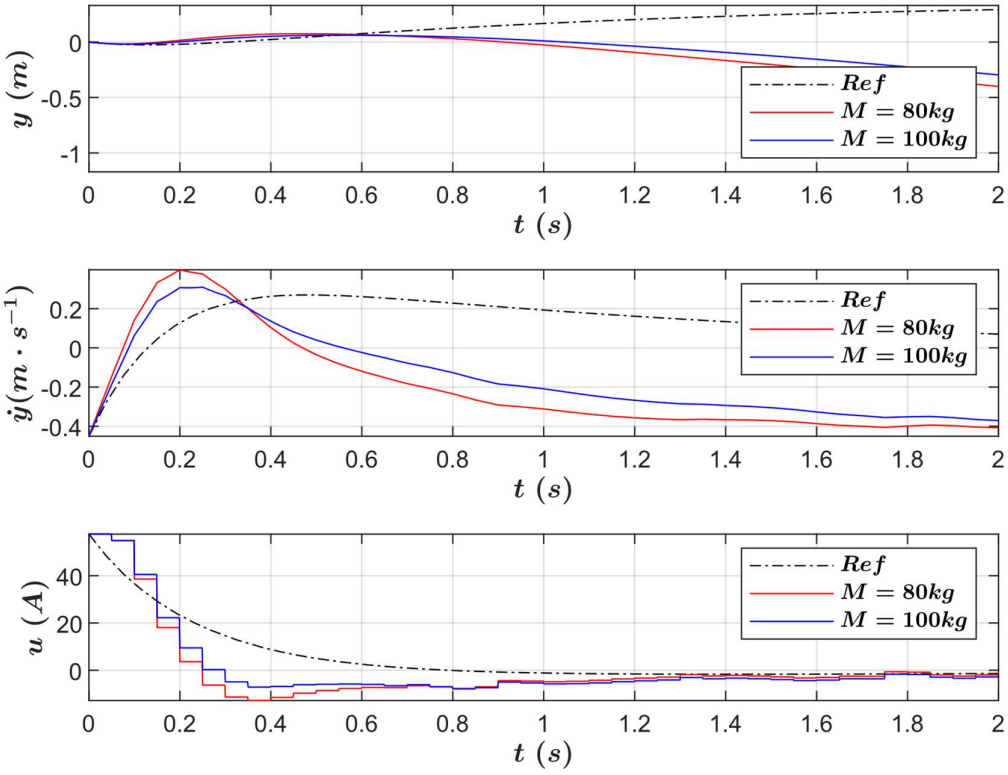

Fig. 41. Simulation continuous swing-up with noise trajectories $y, \dot{y}$

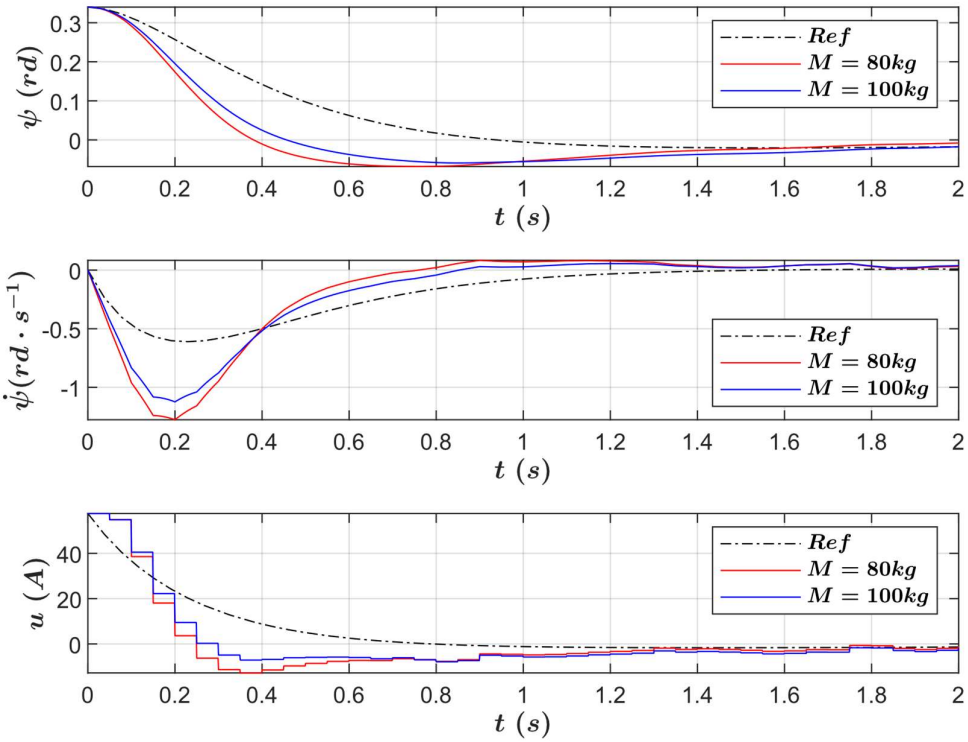

Fig. 42. Simulation continuous swing-up with noise trajectories $\psi, \dot{\psi}$

The red curve $M_b = 100\,kg$ is the nominal mass and should have followed closely the reference but the non-modelled conditions make the trajectories differ from the reference. Referring to the trajectory ψ in Fig. 42 we see that the simulation trajectories reach $0\,rd$ faster than the reference trajectory which we see the same effect on the real-time results. With that being said, the robustness of the controller is still able so swing-up the wheelchair with mass variations of $\pm 20\,kg$ form the nominal mass.

3.3.5 Reference Tracking Real-Time Test

The real-time controller design followed the two-step strategy presented above. A video is also available at the following address https://pod.uphf.fr/video/2758-chapter-3-continuous-swing-up-optimal-trajectories/. Frame captures of the video are provided in Fig. 43.

Fig. 45 and Fig. 44 presents the real-time results of one of the experiments, where the black dashed lines are the reference trajectories, and the blue and red solid lines are the real-time data. The vertical green lines represent time instants *a* to *d* of Fig. 43. Between instant *a* and *b*, a reverse movement (Fig. 43.a) is done. The initial speed is reached at instant *b* and the control law (65) activated. Reference trajectory is depicted with dashed-black curves (Fig. 43.b-e).

A positive motor torque is applied. As a consequence, the wheelchair swings-up with little forward speed until instant c. Then, to increase the wheelchair angle closer to the equilibrium position, the wheelchair speed $\dot{y}$ is increased until the equilibrium is reached at instant d and rests almost standstill (only counteracting the human movements). At the instant d when the wheelchair is balancing at equilibrium is the end of the swing-up, at this point the control unit switches to a different algorithm that allows the user to drive the wheelchair (with joystick) in self-balancing mode.

The most important signal for the swinging-up phase is the wheelchair angle ψ. As depicted in the upper graph of Fig. 44, the system reaches self-balancing position in less than 2 seconds. Even though ψ and $\dot{\psi}$ show oscillations between b and d the algorithm still provides a smooth operation for the user. Overall, the ψ and $\dot{\psi}$ signals are similar to the one obtained in simulation with sensor noise, Fig. 42.

Then, in Fig. 45 we see that the swinging up operation is performed over 45 cm of longitudinal motion, which allows to perform the swing-up in small areas.

Fig. 43. Real-time snapshots continuous controller no obstacle.

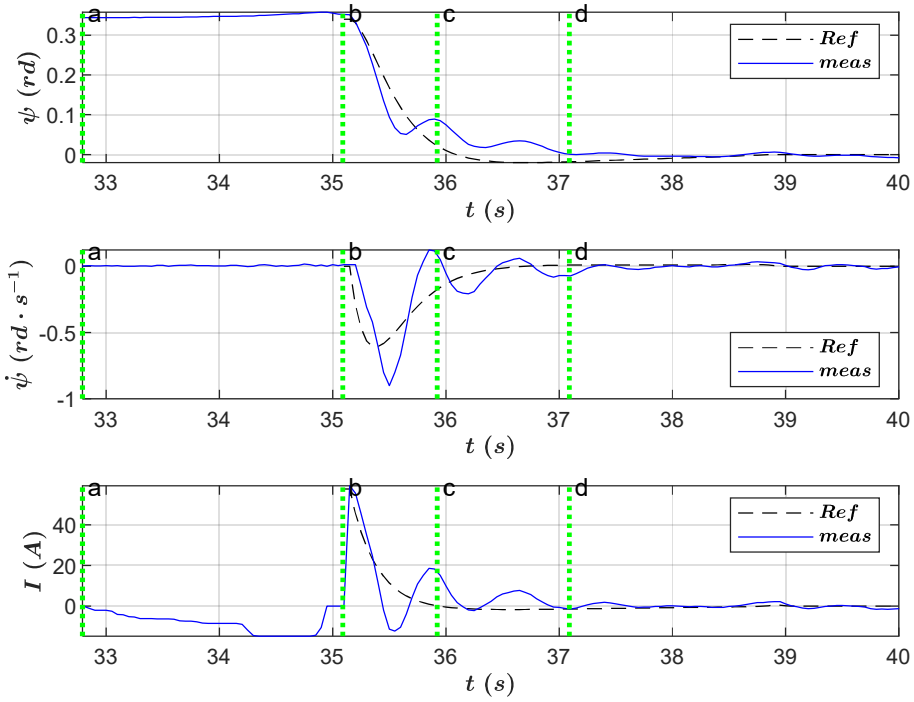

Fig. 44. Continuous swing-up real-time results trajectories $\psi, \dot{\psi}$. The green vertical lines correspond to the video snapshots in Fig. 43

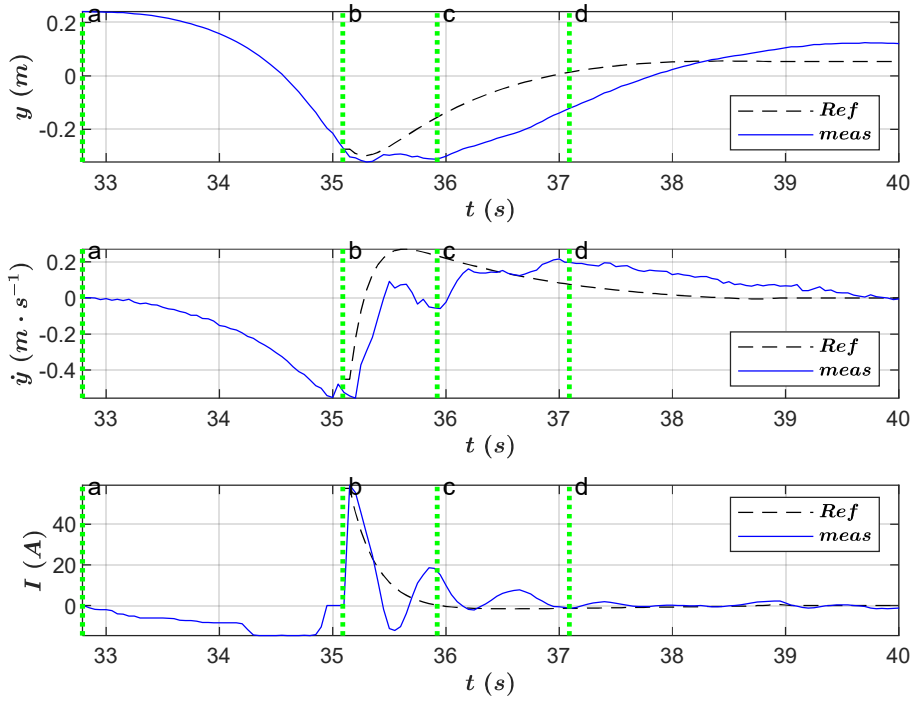

Fig. 45. Continuous swing-up real-time results trajectories $y, \dot{y}$. The green vertical lines correspond to the video snapshots in Fig. 43

Next, a swing-up experiment over an obstacle has been performed, Fig. 46. The wheelchair is initially standing on a wood plank and a swing-up maneuver is performed. Investigating the control law behavior in such situations is important because, in practice, the user may operate the wheelchair on various uneven grounds. This experiment corresponds to the second part of the video is available here: https://pod.uphf.fr/video/2758-chapter-3-continuous-swing-up-optimal-trajectories/

Fig. 46. Real-time snapshots continuous controller obstacle.

The collected data are depicted in Fig. 44 and Fig. 48. Again, the user operated the wheelchair manually to reach the requested initial speed. At time *b*, this initial speed is reached while the wheelchair fall of the obstacle, inducing some disturbances on the angle signal ψ, Fig. 44. As the wheel was touching the obstacle, the wheel chair lifting required more active control to lift the wheel chair between instant *b* and *c*. Finally, in order to reach the equilibrium point at time $t = 13s$ while crossing the obstacle, the wheelchair speed increased significantly. The whole maneuver required approximatively $1.5\,m$.

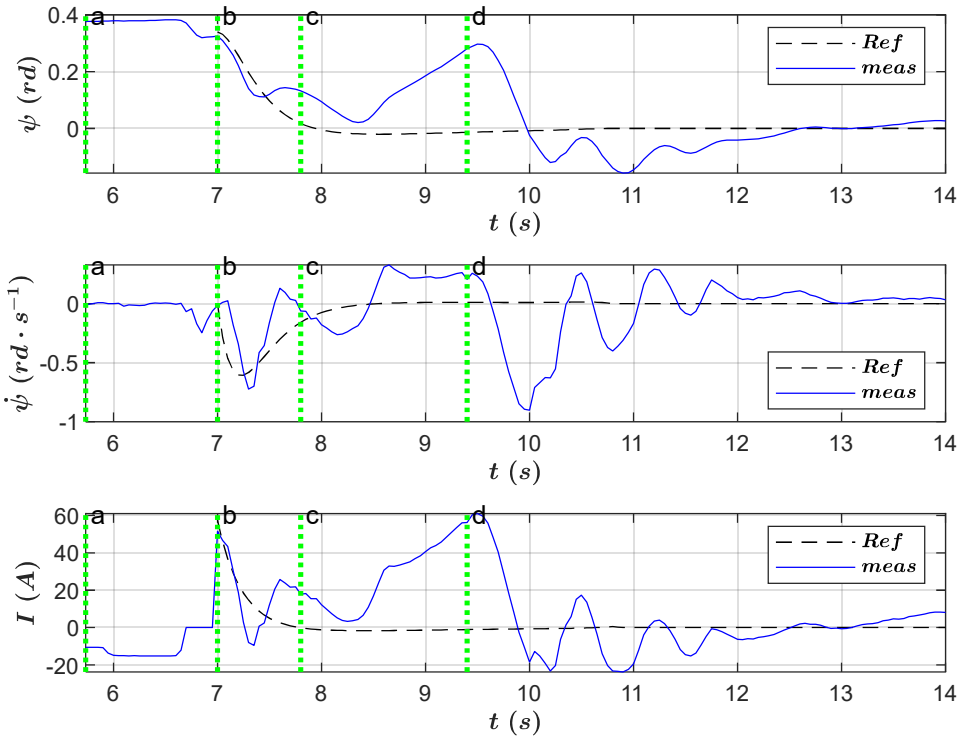

Fig. 47. Continuous swing-up real-time results trajectories $\psi, \dot{\psi}$. The green vertical lines correspond to the video snapshots in Fig. 46.

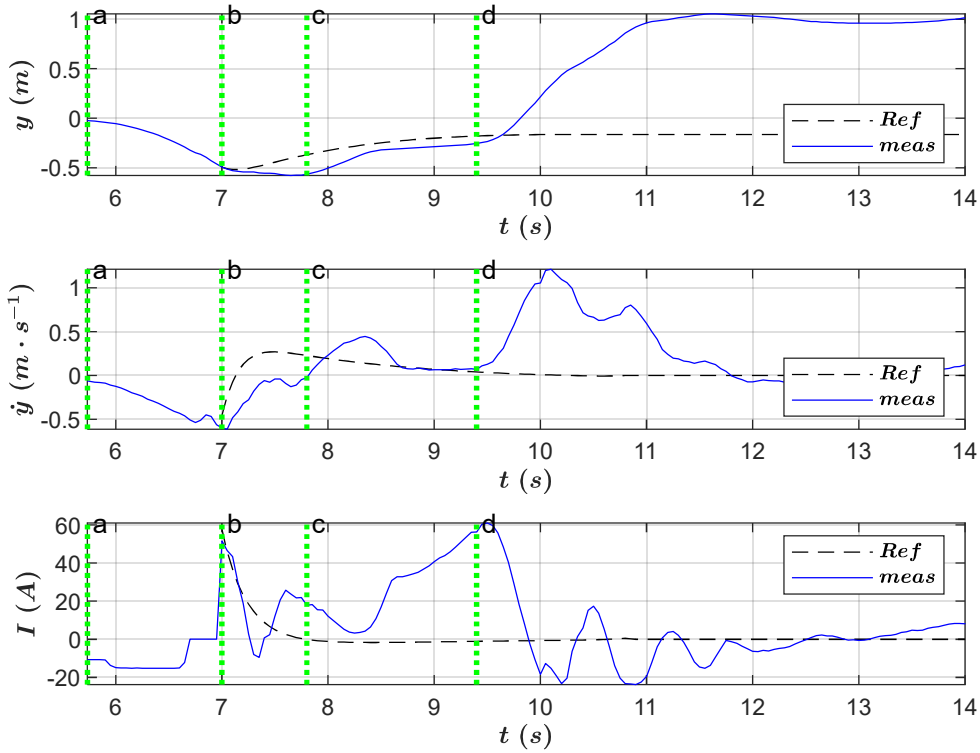

Fig. 48. Continuous swing-up real-time results trajectories $y, \dot{y}$. The green vertical lines correspond to the video snapshots in Fig. 46.

Finally, robustness tests are performed by comparing the closed loop behavior when two different users operate the wheelchair. Results are depicted in Fig. 49 and Fig. 50. The two users have different morphologies: height: 2 m vs 1.65m, weight: 80 kg vs 100kg. The control law parameters were kept to the nominal values for both users.

Overall, it can be seen that the control law behavior remains quite similar therefore demonstrating the robustness of the control law to the user's parameters.

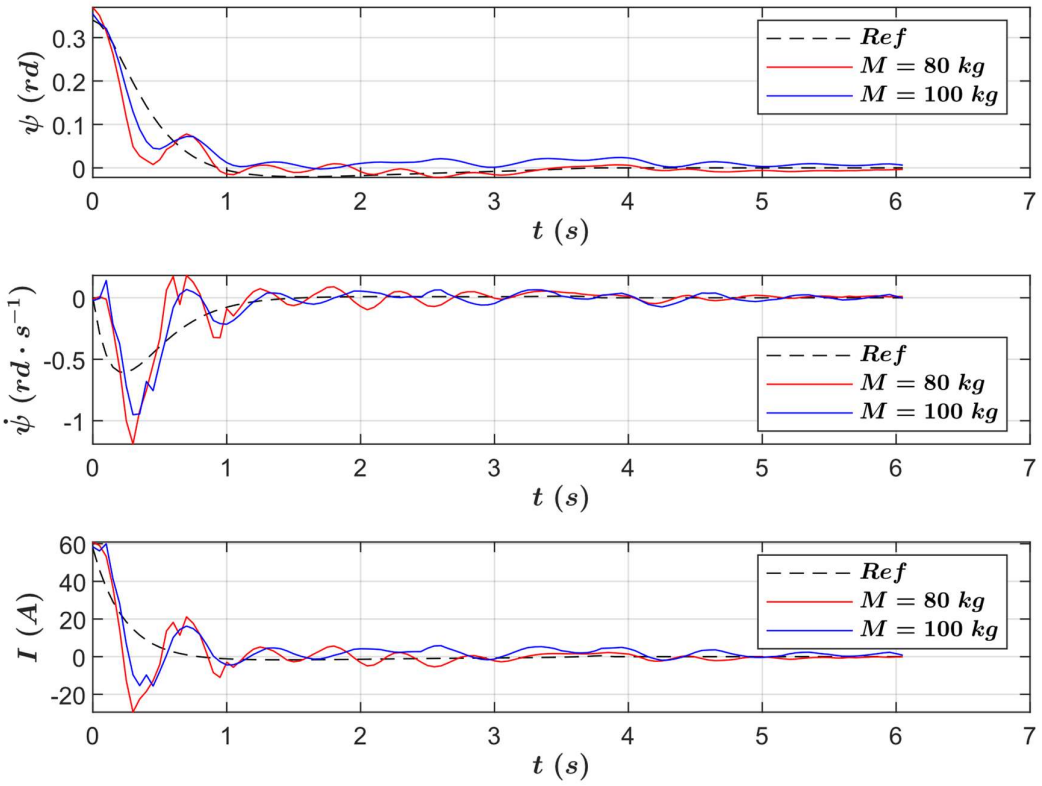

Fig. 49. Continuous swing-up real-time results trajectories $\psi, \dot{\psi}$.: robustness experiment

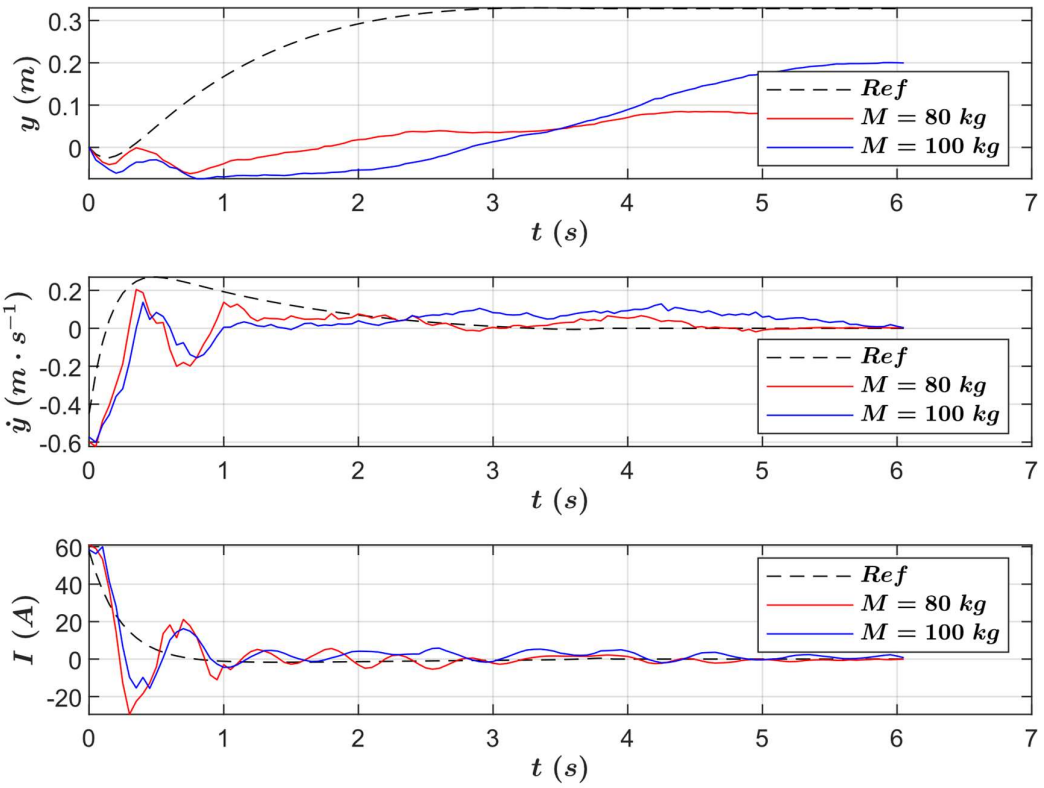

Fig. 50. Continuous swing-up real-time results trajectories $y, \dot{y}$: robustness experiment

3.4 Conclusion

First, the wheelchair dynamics has been formulated using a TS-descriptor model. A control law has been proposed to track a state reference in the particular case of a known reference input. A two steps controller synthesis was suggested.

First, the state and input trajectories have been computed as a solution to an optimal control problem in order to ensure a swing-up with a small wheelchair displacement while minimizing the control amplitude. The compromise between these two criteria has been tuned in such a way that the generated trajectories mimic the one performed by a professional user.

Second, the control law was designed to ensure global stability of the system in a secure way to follow the optimal trajectories. The stability of the closed-loop system was ensured by classical Lyapunov method and Differential Mean Value theorem to write the solution as a LMI constraints problem.

Lastly, the controller was tested in simulation and real-time to show the controller effectiveness. The real-time experiments demonstrated the control law capability to deal with

small grounded obstacles. The control law robustness was tested by different users and similar results were obtained, demonstrating the good sensitivity of the closed loop to user's parameters.

Chapter 4 Discrete Robust Swing-up

The previous chapter proposed a continuous framework mixing optimal control strategy and T-S control synthesis using LMI constraints problems, this chapter focuses on discrete robust control including mass uncertainties. The goal is to propose a solution that is fully using a quasi-LPV formulation both for the trajectories and the robust control.

The discrete framework has been chosen in this part, it is closer to an application level for embedded systems and it presents some advantages for the controller design methodology such as more degrees of freedom for the Lyapunov functions. The descriptor discrete model is first presented as well as its exact T-S form. Some basis of the LMI constraints design for descriptor models is recalled after. Then, a robust control law is designed to swing-up and stabilize the system. To generate a problem that includes the trajectories, they are designed using a discrete linearized model of the system. The idea is that the trajectories delivered will be admissible by the nonlinear system. As they are computed together with the control, stability and performances will be guaranteed. In addition, the system will be written considering the non-measured uncertainty due to the mass M_b (both user and wheelchair) and a robust control law capable to swing-up for an important variation of M_b will be designed. Lastly, the controller has been tested extensively in both simulation and real-time experiments and some of the results are presented to show the effectiveness of the approach. Some limitations conclude the chapter.

4.1 Discrete Modeling

The interest of working using discrete model and discrete control synthesis is to have a controller directly compatible with the embedded system. Of course, the first step is to derive a discrete model of the wheelchair that is representative of the continuous one (34) in the adequate bandwidth. Several ways of discretization are possible, we took the classical forward Euler method $\dot{x}(t) \approx \frac{x_{k+1} - x_k}{s}$. The interest is to keep the continuous model structure and the state space vector signification.

Notations: for the matrices and vectors expressions the subscript d stands for "discrete", k is the sample number, s the sampling period, $x_k = x(k \cdot s)$ and $x_{k+1} = x((k+1) \cdot s)$. When there

is no ambiguity, the subscript k is omitted to lighten the expressions, for example the angle $\psi_k = \psi(k \cdot s) \to \psi$. Moreover, to simplify the expressions and make them readable, the arguments are omitted and replaced with $(\cdot)$, i.e. $A_c(\psi, \dot{\psi}) = A_c(\cdot)$. For Takagi-Sugeno models we recall the corresponding classical notations: $X_h = \sum_{i=1}^{r} h_i(z) X_i$, with $X_i \quad i \in \{1, \ldots, r\}$ matrices of appropriate dimensions, z the so-called premise vector and the nonlinear functions $h_i(z) \geq 0$ sharing the convex sum property: $\sum_{i=1}^{r} h_i(z) = 1$; and $X_h^{-1} = \left(\sum_{i=1}^{r} h_i(z) X_i \right)^{-1}$. Finally, when the sample $k-1$ is necessary, a minus subscript can be used in some place to simplify the expression, for example: $X_{hh-} = X_{h(k)h(k-1)} = \sum_{i=1}^{r} h_i(z(k)) h_i(z(k-1)) X_i$.

The continuous descriptor model (34) is written in a quasi-LPV (Ohtake, Tanaka et Wang 2001) form under the compact set:

$$\Omega_x = \left\{ (\psi_k, \dot{\psi}_k) \in \mathbb{R}^2, |\psi_k| \leq \bar{\psi}, |\dot{\psi}_k| \leq \bar{\dot{\psi}} \right\} \tag{123}$$

with $\bar{\psi} = 0.4 rd$ and $\bar{\dot{\psi}} = 4\, rd/s$. Each nonlinear term of (34) is therefore transformed via the so-called Sector Nonlinearity approach (SNA) (Ohtake, Tanaka et Wang 2001). (34) with 3 nonlinearities will correspond to an exact LPV model in Ω_x with $2^3 = 8$ vertices. This number can be reduced to 4 considering that the functions $\cos(\psi_k)$ and $\mathrm{sinc}(\psi_k / \pi)$ nearly coincide in $[-0.4, 0.4]$ since $|\mathrm{sinc}(\psi_k / \pi) - \cos(\psi_k)| < 3.8\%$ (Guerra, Bernal et Blandeau 2018). Over the considered compact set Ω_x, the two remaining nonlinearities can be exactly rewritten using the membership functions v_0, v_1, w_0 and w_1:

$$\cos(\psi) = v_0(\psi) \cos(\bar{\psi}) + v_1(\psi) \times 1 \tag{124}$$

$$\dot{\psi}^2 = w_0(\dot{\psi}) \times 0 + w_1(\dot{\psi}) \bar{\dot{\psi}}^2 \tag{125}$$

With $v_0(\psi) = \dfrac{1 - \cos(\psi)}{1 - \cos(\bar{\psi})} \in [0,1]$, $w_0(\dot{\psi}) = 1 - \dfrac{\dot{\psi}^2}{\bar{\dot{\psi}}^2} \in [0,1]$, $v_1(\psi) = 1 - v_0(\psi)$ and $w_1(\dot{\psi}) = 1 - w_0(\dot{\psi})$. The resulting quasi-LPV model is:

$$\sum_{i=0}^{1} v_i(\psi) E_{ci} \dot{x}(t) = \sum_{i=0}^{1}\sum_{j=0}^{1} v_i(\psi) w_j(\dot{\psi}) A_{cij} x(t) + Bu(t) \tag{126}$$

Where: $E_{c0} = E_c(\bar{\psi})$, $E_{c1} = E_c(0)$, $A_{c00} = A_c(\bar{\psi}, 0)$, $A_{c10} = A_c(0,0)$, $A_{c01} = A_c(\bar{\psi}, \dot{\bar{\psi}})$ $A_{c11} = A_c(0, \dot{\bar{\psi}})$, $B = B_c$ And:

$$E_{c0} = \begin{pmatrix} M_b + 2M_w + \frac{2J_w}{r^2} & M_b l\cos(\bar{\psi}) & 0 \\ M_b l\cos(\bar{\psi}) & M_b l^2 + J_b & 0 \\ 0 & 0 & 1 \end{pmatrix} \qquad E_{c1} = \begin{pmatrix} M_b + 2M_w + \frac{2J_w}{r^2} & M_b l & 0 \\ M_b l & M_b l^2 + J_b & 0 \\ 0 & 0 & 1 \end{pmatrix}$$

$$A_{c00} = \begin{pmatrix} -\left(\mu_{\text{wg}} + \frac{2\mu_m}{r^2}\right) & \frac{2\mu_m}{r} & 0 \\ \frac{2\mu_m}{r} & 2\mu_m & M_b l\,\text{g}\cos(\bar{\psi}) \\ 0 & 1 & 0 \end{pmatrix} \qquad A_{c10} = \begin{pmatrix} -\left(\mu_{\text{wg}} + \frac{2\mu_m}{r^2}\right) & \frac{2\mu_m}{r} & 0 \\ \frac{2\mu_m}{r} & 2\mu_m & M_b l\,\text{g} \\ 0 & 1 & 0 \end{pmatrix}$$

$$A_{c01} = \begin{pmatrix} -\left(\mu_{\text{wg}} + \frac{2\mu_m}{r^2}\right) & \frac{2\mu_m}{r} & M_b l\dot{\bar{\psi}}\cos(\bar{\psi}) \\ \frac{2\mu_m}{r} & 2\mu_m & M_b l\,\text{g}\cos(\bar{\psi}) \\ 0 & 1 & 0 \end{pmatrix} \qquad A_{c11} = \begin{pmatrix} -\left(\mu_{\text{wg}} + \frac{2\mu_m}{r^2}\right) & \frac{2\mu_m}{r} & M_b l\dot{\bar{\psi}} \\ \frac{2\mu_m}{r} & 2\mu_m & M_b l\,\text{g} \\ 0 & 1 & 0 \end{pmatrix}$$

Thus with the Euler's discretization $\dot{x}(t) \approx \frac{x_{k+1} - x_k}{s}$ and with: $E_d = E_c$, $A_d = sA_c + E_c$, and $B_d = sB_c$, the resulting model is a discrete representation of the continuous model. Then, (126) discretized becomes:

$$\sum_{i=0}^{1} v_i(\psi_k) E_{ci} x_{k+1} = \sum_{i=0}^{1}\sum_{j=0}^{1} v_i(\psi_k)\left(w_j(\dot{\psi}_k) sA_{cij} + E_{ci}\right)x_k + sB_c u_k \tag{127}$$

then with the compact notation:

$$E_v x_{k+1} = A_{vw} x_k + Bu_k \tag{128}$$

Where $E_v = \sum_{i=0}^{1} v_i(\psi_k) E_{ci}$, $A_{vw} = \sum_{i=0}^{1}\sum_{j=0}^{1} v_i(\psi_k)\left(w_j(\dot{\psi}_k) sA_{cij} + E_{ci}\right)$, and $B = sB_c$.

4.2 Descriptor T-S stabilization

Before starting, let us recall some useful properties.

Property 1: let $Q = Q^T \succ 0$ and R be matrices of appropriate dimensions. The following expression holds:

$$\left(R-Q\right)^T Q^{-1}\left(R-Q\right) \geq 0 \Leftrightarrow R^T Q^{-1} R \geq R + R^T - Q \tag{129}$$

Property 2 (Finsler's lemma (Skelton, Iwasaki et Grigoriadis 1998)): let $x \in \mathbb{R}^n$, $Q = Q^T \in \mathbb{R}^{n\times n}$ and $R \in \mathbb{R}^{m\times n}$ such that $rank\left(R\right) < n$; the following expressions are equivalent:

$$x^T Q x < 0\,,\ \forall x \in \left\{x \in \mathbb{R}^n : x \neq 0,\, Rx = 0\right\}$$

$$\exists M \in \mathbb{R}^{n\times m}\,,\ Q + MR + R^T M^T < 0 \tag{130}$$

Considering that the descriptor we are interested in has the property of having an input matrix B constant, we will restrict the results to this case.

$$E_v x_{k+1} = A_{vw} x_k + B u_k \tag{131}$$

This part proposes the basis for the control of such models following the work of (Estrada-Manzo, et al. 2015). Extensions to robustness are provided in the next section. To begin with, let us consider a general control law, with $F_{(\cdot)}$ and $H_{(\cdot)}$ to be defined further on:

$$u_k = F_{(\cdot)} H_{(\cdot)}^{-1} x_k \tag{132}$$

The subscripts $(\cdot)$ are voluntarily kept, as the dependence of the different variables is related to the degree of freedom set by the designer and coming from the LMI constraints problems to solve (see expressions (139) and (140)). Therefore, the closed-loop, control law (132) applied to (131) writes:

$$E_v x_{k+1} = \left(A_{vw} + B F_{(\cdot)} H_{(\cdot)}^{-1}\right) x_k \Leftrightarrow \begin{bmatrix} A_{vw} + B F_{(\cdot)} H_{(\cdot)}^{-1} & -E_v \end{bmatrix} \begin{bmatrix} x_k \\ x_{k+1} \end{bmatrix} = 0 \tag{133}$$

Considering a Lyapunov function $V(x_k) = x_k^T P_{(\cdot)-}^{-1} x_k$, $P_{(\cdot)-} = P_{(\cdot)-}^T > 0$, again $(\cdot)$ depends on the LMI design; its variation writes:

$$\Delta V(x_k) = \begin{bmatrix} x_k \\ x_{k+} \end{bmatrix}^T \begin{bmatrix} -P_{(\cdot)-}^{-1} & 0 \\ 0 & P_{(\cdot)}^{-1} \end{bmatrix} \begin{bmatrix} x_k \\ x_{k+} \end{bmatrix} < 0 \tag{134}$$

Using the Finsler's lemma, Property 2 (Skelton, Iwasaki et Grigoriadis 1998), (134) under equality constraint (133) is equivalent to:

$$\begin{bmatrix} -P_{(\cdot)-}^{-1} & 0 \\ 0 & P_{(\cdot)}^{-1} \end{bmatrix} + \begin{bmatrix} M_{(\cdot)} \\ N_{(\cdot)} \end{bmatrix} \begin{bmatrix} A_{vw} + BF_{(\cdot)} H_{(\cdot)}^{-1} & -E_v \end{bmatrix} + (*) < 0 \tag{135}$$

Setting the free matrix $\begin{bmatrix} M_{(\cdot)} \\ N_{(\cdot)} \end{bmatrix} = \begin{bmatrix} 0 \\ J_{(\cdot)}^{-1} \end{bmatrix}$ (Estrada-Manzo, et al. 2015) and using the property of congruence with the block-diagonal matrix $\begin{bmatrix} H_{(\cdot)} & 0 \\ 0 & J_{(\cdot)} \end{bmatrix}$, (135) is satisfied if:

$$\begin{bmatrix} -H_{(\cdot)}^T P_{(\cdot)-}^{-1} H_{(\cdot)} & 0 \\ 0 & J_{(\cdot)}^T P_{(\cdot)}^{-1} J_{(\cdot)} \end{bmatrix} + \begin{bmatrix} 0 \\ I \end{bmatrix} \begin{bmatrix} A_{vw} H_{(\cdot)} + BF_{(\cdot)} & -E_v J_{(\cdot)} \end{bmatrix} + (*) < 0 \tag{136}$$

Using Property 1 on the first entry of (136) $-H_{(\cdot)}^T P_{(\cdot)-}^{-1} H_{(\cdot)}$ renders a sufficient condition for (135) to hold:

$$\begin{bmatrix} -H_{(\cdot)} - H_{(\cdot)}^T + P_{(\cdot)-} & (*) \\ A_{vw} H_{(\cdot)} + BF_{(\cdot)} & J_{(\cdot)}^T P_{(\cdot)}^{-1} J_{(\cdot)} - E_v J_{(\cdot)} - J_{(\cdot)}^T E_v^T \end{bmatrix} < 0 \tag{137}$$

At last, a Schur's complement (47) is applied to transform $J_{(\cdot)}^T P_{(\cdot)}^{-1} J_{(\cdot)}$, as $P_{(\cdot)}^{-1} \succ 0$ to give the final result:

$$\begin{bmatrix} -H_{(\cdot)} - H_{(\cdot)}^T + P_{(\cdot)-} & (*) & 0 \\ A_{vw} H_{(\cdot)} + BF_{(\cdot)} & -E_v J_{(\cdot)} - J_{(\cdot)}^T E_v^T & (*) \\ 0 & J_{(\cdot)} & -P_{(\cdot)} \end{bmatrix} < 0 \tag{138}$$

To determine the dependence of the variables $(\cdot)$, a goal is to derive conditions with the "less" LMI constraints according to the problem we are faced to. Especially, as the input matrix is constant, we can avoid the cross terms (using twice the same premise by multiplication, the choice H_{vw} for example will imply $A_{vw}H_{vw}$) and the associated relaxations (Sala et Arino 2007) (see discussions in (Estrada-Manzo, et al. 2015)). For our work, we can distinguish 2 cases.

1st case: quadratic stability: $P_{(\cdot)} = P$, therefore, a good choice for the variables is: $F_{(\cdot)} = F_{vw}$, $J_{(\cdot)} = J_w$ and $H_{(\cdot)} = H$ to get a double-sum LMI conditions:

$$\begin{bmatrix} -H - H^T + P & (*) & 0 \\ A_{vw}H + BF_{vw} & -E_v J_w - J_w^T E_v^T & (*) \\ 0 & J_w & -P \end{bmatrix} < 0 \tag{139}$$

and the control writes: $u_k = F_{vw}H^{-1}x_k$.

2nd case: non quadratic stability using for example: $P_{(\cdot)} = P_{vw}$, therefore, a good choice for the variables is: $F_{(\cdot)} = F_{vwv^-w^-}$, $J_{(\cdot)} = J_{wv^-w^-}$ and $H_{(\cdot)} = H_{v^-w^-}$ to get a 4-sum LMI conditions:

$$\begin{bmatrix} -H_{v^-w^-} - H_{v^-w^-}^T + P_{v^-w^-} & (*) & 0 \\ A_{vw}H_{v^-w^-} + BF_{vwv^-w^-} & -E_v J_{wv^-w^-} - (*) & (*) \\ 0 & J_{wv^-w^-} & -P_{vw} \end{bmatrix} < 0 \tag{140}$$

and the control writes: $u_k = F_{vwv^-w^-}H_{v^-w^-}^{-1}x_k$.

4.3 Application

While the wheelchair is in self-balancing mode, it can overcome obstacles and navigates in rough terrain e.g. grass, stony ground, sand. However, the switching between the standard mode to the self-balancing mode safely and smoothly is a challenge. The objective of this section is to design a discrete robust controller that can swing-up the wheelchair from standard mode to self-balancing mode.

4.3.1 Discrete Robust Tracking Method

Fig. 51 exhibits the overall strategy. A predefined tracking reference x_{rk} is generated via a simplified model T_r of the wheelchair. The idea is to generate potentially feasible trajectories in the state space. From these trajectories, a robust controller, implemented in blocks F and G, ensures the stability of the nonlinear model, the robustness to the mass variation and smoothness of the trajectories.

In this chapter, the reference trajectories are defined using a linear descriptor model whose matrices, state and input vectors are denoted with a subscript r:

$$E_r x_{rk+1} = A_r x_{rk} + B u_{rk} \tag{141}$$

where the matrix E_r is nonsingular. The reference input is computed using a state feedback:

$$u_{rk} = F_r x_{rk} \tag{142}$$

The descriptor (141) and control (142) being linear, F_r can be obtained using any appropriate method. Either a descriptor form (141) can be used or a classical linear model using the well-defined E_r^{-1}, $x_{rk+1} = E_r^{-1} A_r x_{rk} + E_r^{-1} B u_{rk}$. Synthesis can come at hand with for example pole placement, Linear Quadratic design or LMI constraints problem such as (139) in its linear form. With F_r derived to ensure the desired trajectory performances the reference closed-loop is written as:

$$E_r x_{rk+1} = \left(A_r + BF_r\right) x_{rk} = A_{rBF} x_{rk} \tag{143}$$

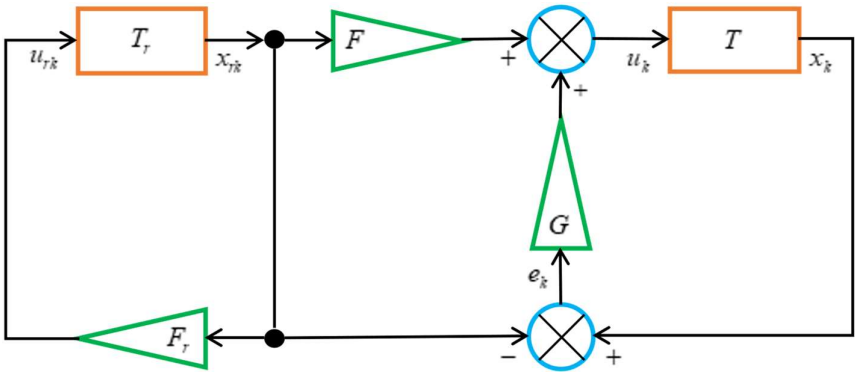

Fig. 51. Robust tracking control law diagram

Combining (128) and (143) allows the tracking error $e_k = x_k - x_{rk}$ to be written as:

$$x_{k+1} - x_{rk+1} = E_v^{-1}\left(A_{vw}x_k + Bu_k\right) - E_r^{-1}A_{rBF}x_{rk} \tag{144}$$

And using $x_k = x_{rk} + e_k$ (144) is transformed as:

$$E_v e_{k+1} = A_{vw}e_k + \left(A_{vw} - E_v E_r^{-1}A_{rBF}\right)x_{rk} + Bu_k \tag{145}$$

Combining (143) and (145) allows writing an extended problem taking into account both the reference tracking and the control law to design:

$$\begin{bmatrix} E_r & 0 \\ 0 & E_v \end{bmatrix}\begin{bmatrix} x_{rk+1} \\ e_{k+1} \end{bmatrix} = \begin{bmatrix} A_{rBF} & 0 \\ A_{vw} - E_v E_r^{-1}A_{rBF} & A_{vw} \end{bmatrix}\begin{bmatrix} x_{rk} \\ e_k \end{bmatrix} + \begin{bmatrix} 0 \\ B \end{bmatrix}u_k \tag{146}$$

Let us now introduce the following control:

$$u_k = \begin{bmatrix} F(\cdot) & G(\cdot) \end{bmatrix} H_{(\cdot)}^{-1}\begin{bmatrix} x_{rk} \\ e_k \end{bmatrix} \tag{147}$$

As previously, matrices $F(\cdot)$, $G(\cdot)$ and $H_{(\cdot)}$ will be defined later on as well as their arguments $(\cdot)$. Regularity of $H_{(\cdot)}$ will also be discussed. Thus, the reference and system in closed-loop writes as:

$$\overline{E}_v \overline{x}_{k+1} = \left(\overline{A}_{vw} + \overline{B}\overline{F}(\cdot)\right)\overline{x}_k \tag{148}$$

With: : $\overline{E}_v = \begin{bmatrix} E_r & 0 \\ 0 & E_v \end{bmatrix}$, $\overline{A}_{vw} = \begin{bmatrix} A_{rBF} & 0 \\ A_{vw} - E_v E_r^{-1}A_{rBF} & A_{vw} \end{bmatrix}$, $\overline{B} = \begin{bmatrix} 0 \\ B \end{bmatrix}$, $\overline{F}(\cdot) = \begin{bmatrix} F(\cdot) & G(\cdot) \end{bmatrix} H_{(\cdot)}^{-1}$ and $\overline{x}_k = \begin{bmatrix} x_{rk} \\ e_k \end{bmatrix}$.

Using conditions (139) or (140) together with matrices defined in (148) allows formulating directly an LMI constraints problem for the nominal case.

Nevertheless, in order to derive generic control laws, the uncertainty on the mass is a crucial issue that must be considered in the control synthesis. This mass uncertainty is related both to the users that may use an identical wheelchair and to the different sorts of wheelchairs that could possibly be equipped with the kit. Thus, we introduce the mass uncertainty in the definition of the matrices in (127) as:

$$\tilde{E}_c(\psi) = E_c(\psi) + \Delta M_b \begin{bmatrix} 1 & l\cos(\psi) & 0 \\ l\cos(\psi) & l^2 & 0 \\ 0 & 0 & 0 \end{bmatrix} \tag{149}$$

$$\tilde{A}_c(\psi,\dot{\psi}) = A_c(\psi,\dot{\psi}) + \Delta M_b \begin{bmatrix} 0 & 0 & l\dot{\psi}^2\ \mathrm{sinc}\left(\frac{\psi}{\pi}\right) \\ 0 & 0 & gl\ \mathrm{sinc}\left(\frac{\psi}{\pi}\right) \\ 0 & 0 & 0 \end{bmatrix} \tag{150}$$

Similarly, the quasi-LPV form in (145) is updated using:

$$\tilde{E}_v = E_v + \Delta E_v,\ \Delta E_v = \Delta M_b \begin{bmatrix} 1 & 0 \\ 0 & 1 \\ 0 & 0 \end{bmatrix} \Upsilon_v \tag{151}$$

with: $\Upsilon_v = \begin{bmatrix} 1 & l\cos(\psi_k) & 0 \\ l\cos(\psi_k) & l^2 & 0 \end{bmatrix} = v_0(\psi_k)\Upsilon_0 + (1 - v_0(\psi_k))\Upsilon_1$

$$\tilde{A}_{vw} = A_{vw} + \Delta A_{vw},\ \Delta A_{vw} = \Delta M_b \begin{bmatrix} 1 & 0 \\ 0 & 1 \\ 0 & 0 \end{bmatrix} \Omega_{vw} \tag{152}$$

$$\Omega_{vw} = \begin{bmatrix} 1 & l\cos(\psi) & sl\dot{\psi}^2\ \mathrm{sinc}\left(\frac{\psi}{\pi}\right) \\ l\cos(\psi) & l^2 & sgl\ \mathrm{sinc}\left(\frac{\psi}{\pi}\right) \end{bmatrix} = \sum_{i=0}^{1}\sum_{j=0}^{1} v_i(\psi_k) w_j(\dot{\psi}_k) \Omega_{ij}$$

Using the quasi-LPV model definition in (126) with the definition of uncertainties (151) and (152), the extra term $\Xi(\cdot)$ has to be added to the nominal problem (138) written with extended model (148):

$$\begin{bmatrix} -H_{(\cdot)} - H_{(\cdot)}^T + P_{(\cdot)-} & (*) & 0 \\ \overline{A}_{vw} H_{(\cdot)} + \overline{B}\overline{F}_{(\cdot)} & -\overline{E}_v J_{(\cdot)} - J_{(\cdot)}^T \overline{E}_v^T & (*) \\ 0 & J_{(\cdot)} & -P_{(\cdot)} \end{bmatrix} + \Xi(\cdot) < 0$$

With:

$$\Xi(\cdot)=\begin{bmatrix} 0 & (*) & 0 \\ \begin{bmatrix} 0 & 0 \\ \Delta A_{vw}-\Delta E_v E_r^{-1} A_{rBF} & \Delta A_{vw} \end{bmatrix} H_{(\cdot)} & -\begin{bmatrix} 0 & 0 \\ 0 & \Delta E_v \end{bmatrix} J_{(\cdot)}-(*) & 0 \\ 0 & 0 & 0 \end{bmatrix} \tag{153}$$

Now considering the classical decomposition of uncertainties, we can write:

$$\begin{bmatrix} 0 & 0 \\ \Delta A_{vw}-\Delta E_v E_r^{-1} A_{rBF} & \Delta A_{vw} \end{bmatrix} H_{(\cdot)} = \begin{bmatrix} 0_{3\times 2} \\ \begin{bmatrix} 1 & 0 \\ 0 & 1 \\ 0 & 0 \end{bmatrix} \end{bmatrix} \Delta M_b \begin{bmatrix} \Omega_{vw}-\Upsilon_v E_r^{-1} A_{rBF} & \Omega_{vw} \end{bmatrix}_{2\times 6} H_{(\cdot)}$$

And: $\begin{bmatrix} 0 & 0 \\ 0 & \Delta E_v \end{bmatrix} J_{(\cdot)}+(*) = \Delta M_b \begin{bmatrix} 0_{3\times 2} \\ \begin{bmatrix} 1 & 0 \\ 0 & 1 \\ 0 & 0 \end{bmatrix} \end{bmatrix} \begin{bmatrix} 0 & \Upsilon_v \end{bmatrix}_{2\times 6} J_{(\cdot)}+(*)$

And it is direct to write (153) as:

$$\Xi(\cdot)=\Delta M_b \begin{bmatrix} 0_{6\times 2} \\ \begin{bmatrix} 0_{3\times 2} \\ I_2 \\ 0_{1\times 2} \end{bmatrix} \\ 0_{6\times 2} \end{bmatrix} \begin{bmatrix} \begin{bmatrix} \Omega_{vw}-\Upsilon_v E_r^{-1} A_{rBF} & \Omega_{vw} \end{bmatrix} H_{(\cdot)} & -\begin{bmatrix} 0 & \Upsilon_v \end{bmatrix}_{2\times 6} J_{(\cdot)} & 0_{2\times 6} \end{bmatrix}+(*) \tag{154}$$

Let us define the maximum of the mass variation as $m=\max(\Delta M_b)$ and introduce a slack matrix $S_{2\times 2}\succ 0$. Thus, applying the completion of square property (45), equation (154) is bounded by:

$$\Xi(\cdot)\le m^2 \begin{bmatrix} 0_{6\times 2} \\ \begin{bmatrix} 0_{3\times 2} \\ I_2 \\ 0_{1\times 2} \end{bmatrix} \\ 0_{6\times 2} \end{bmatrix} S(*)+(*)S^1 \begin{bmatrix} \begin{bmatrix} \Omega_{vw}-\Upsilon_v E_r^{-1} A_{rBF} & \Omega_{vw} \end{bmatrix} H_{(\cdot)} & -\begin{bmatrix} 0 & \Upsilon_v \end{bmatrix}_{2\times 6} J_{(\cdot)} & 0_{2\times 6} \end{bmatrix}$$

(155)

At the end, using a Schur's complement (47) on (155) renders a polytopic form that linearly depends on the variables to search (156):

$$\begin{bmatrix} -H_{(\cdot)} - H_{(\cdot)}^T + P_{(\cdot)-} & (*) & 0 & (*) \\ \mathrm{T}_1(\cdot) & \mathrm{T}_2(\cdot) & (*) & (*) \\ 0 & J_{(\cdot)} & -P_{(\cdot)} & 0 \\ \begin{bmatrix} \Omega_{vw} - \Upsilon_v E_r^{-1} A_{rBF} & \Omega_{vw} \end{bmatrix} H_{(\cdot)} & -\begin{bmatrix} 0 & \Upsilon_v \end{bmatrix} J_{(\cdot)} & 0 & -S \end{bmatrix} \prec 0$$

$$\mathrm{T}_1(\cdot) = \begin{bmatrix} A_{rBF} & 0 \\ A_{vw} - E_v E_r^{-1} A_{rBF} & A_{vw} \end{bmatrix} H_{(\cdot)} + \begin{bmatrix} 0 \\ B \end{bmatrix} \begin{bmatrix} F(\cdot) & G(\cdot) \end{bmatrix} \tag{156}$$

$$\mathrm{T}_2(\cdot) = -\begin{bmatrix} E_r & 0 \\ 0 & E_v \end{bmatrix} J_{(\cdot)} - (*) + \begin{bmatrix} 0 & 0 & 0 \\ 0 & m^2 S & 0 \\ 0 & 0 & 0 \end{bmatrix}$$

From the first entry of (156), if the condition is satisfied then $H_{(\cdot)} + H_{(\cdot)}^T \succ P_{(\cdot)-}$. Thus $H_{(\cdot)}^{-1}$ always exists and the control (147) is well-defined. The choices of the subscripts $(\cdot)$ follow exactly the ones described previously to get the LMI constraints problem using a quadratic Lyapunov function (139) or a NQ one (140).

Moreover, it is important to introduce some elements of performances. For example, it is interesting to have the possibility to act on the norm of the gains in order to be able to increase or to smooth the signals. This is done via a design parameter and using classical tools (Boyd, et al. 1994).

Considering that $H_{(\cdot)} + H_{(\cdot)}^T \succ P_{(\cdot)-}$, fixing a minimum bound on $P_{(\cdot)-}$ will directly act on $H_{(\cdot)}$ and we can work on $\begin{bmatrix} F(\cdot) & G(\cdot) \end{bmatrix} P_{(\cdot)-}^{-1}$ instead of $\begin{bmatrix} F(\cdot) & G(\cdot) \end{bmatrix} H_{(\cdot)-}^{-1}$ to get a LMI constraint formulation. Thus, we can impose: $\begin{bmatrix} F(\cdot) & G(\cdot) \end{bmatrix} P_{(\cdot)-}^{-1} \begin{bmatrix} F^T(\cdot) \\ G^T(\cdot) \end{bmatrix} \leq \lambda I$ and $\lambda P \succ I$, and the parameter $\lambda > 0$ will directly be a parameter that acts on the norm of the gains. Thus, 2 LMI constraints are added, the first one obtained using a Schur's complement (47):

$$\begin{bmatrix} -\lambda I & \begin{bmatrix} F(\cdot) & G(\cdot) \end{bmatrix} \\ \begin{bmatrix} F^T(\cdot) \\ G^T(\cdot) \end{bmatrix} & -P_{(\cdot)-} \end{bmatrix} \prec 0, \quad \lambda P \succ I \tag{157}$$

We can now write the LMI constraints problem. For the Quadratic case (139), case 1, we set $P_{(\cdot)} = P$, $F_{(\cdot)} = F_{vw}$, $J_{(\cdot)} = J_w$ and $H_{(\cdot)} = H$ to get:

LMI Quadratic Discrete Descriptor T-S Robust Stabilization Problem:

Chose $\lambda > 0$; and find symmetric matrices $P = P^T$, $S_{ij} = S_{ij}^T$ and matrices H, J_j, F_{ij} and G_{ij} $i, j \in \{1,2\}$, such that:

$$\begin{aligned} &\lambda P \succ I \\ &\begin{bmatrix} -\lambda I & \begin{bmatrix} F_{ij} & G_{ij} \end{bmatrix} \\ (*) & -P \end{bmatrix} \prec 0, \; i, j \in \{1,2\} \\ &\Psi_{ij} \prec 0, \quad i, j \in \{1,2\} \end{aligned} \tag{158}$$

With:

$$\Psi_{ij} = \begin{bmatrix} -H - H^T + P & (*) & 0 & (*) \\ \begin{bmatrix} A_{rBF} & 0 \\ A_{ij} - E_i E_r^{-1} A_{rBF} & A_{ij} \end{bmatrix} H + \begin{bmatrix} 0 \\ B \end{bmatrix} \begin{bmatrix} F_{ij} & G_{ij} \end{bmatrix} & -\begin{bmatrix} E_r & 0 \\ 0 & E_i \end{bmatrix} J_j - (*) + \begin{bmatrix} 0 & 0 & 0 \\ 0 & m^2 S_{ij} & 0 \\ 0 & 0 & 0 \end{bmatrix} & (*) & (*) \\ 0 & J_j & -P & 0 \\ \begin{bmatrix} \Omega_{ij} - \Upsilon_i E_r^{-1} A_{rBF} & \Omega_{ij} \end{bmatrix} H & -\begin{bmatrix} 0 & \Upsilon_i \end{bmatrix} J_j & 0 & -S_{ij} \end{bmatrix}$$

4.3.2 Discrete Simulation

The controller will be designed for a person with $M = 95.5\,kg$ and the following identified parameters for the simulations, where $M_b = M + M_{b_{frame}}$. $M_b = 112.64\,kg$, $M_w = 4.68\,kg$, $J_b = 11.99\,kg \cdot m^2$, $J_w = 0.36\,kg \cdot m^2$ $\mu_m = 0.85\;kg/s$, $\mu_{wg} = 1.79\,kg/s$, $r = 0.3\,m$, $l = 0.295\,m$, $K_t = 2.22\,Nm/A$. Matrices from reference model (141) are:

$$E_r = \begin{bmatrix} 130.05 & 33.22 & 0 \\ 33.22 & 21.79 & 0 \\ 0 & 0 & 1 \end{bmatrix} \; A_r = \begin{bmatrix} 129.01 & 33.50 & 0 \\ 33.50 & 21.70 & 16.30 \\ 0 & 0.05 & 1 \end{bmatrix} \; B_r = \begin{bmatrix} 0.37 \\ -0.11 \\ 0 \end{bmatrix}$$

First of all, the definition of the reference trajectories has to be done, that resumes to finding the linear gain F_r for the control law (142). A pole placement has been used corresponding to

a smooth trajectory. The corresponding gain is $F_r = \begin{bmatrix} 22.58 & 37.52 & 168.79 \end{bmatrix}$ and it fixes the closed-loop reference trajectory matrices $\left(E_r, A_{rBF}\right)$ in (158).

Then the uncertain description of the descriptor model is set with the bounds $\bar{\psi} = 0.4\,rd$, $\dot{\bar{\psi}} = 4\,rd/s$, and $\max\left(\Delta M_b\right) = 20\,kg$, thus $M_b \in \begin{bmatrix} 92.64 & 132.64 \end{bmatrix} kg$ and mass of the person is $M \in \begin{bmatrix} 75.5 & 115.5 \end{bmatrix} kg$. The resulting matrices of the model are:

$$E_0 = \begin{bmatrix} 187.96 & 30.60 & 0 \\ 30.60 & 21.79 & 0 \\ 0 & 0 & 1 \end{bmatrix}, E_1 = \begin{bmatrix} 187.96 & 33.22 & 0 \\ 33.22 & 21.79 & 0 \\ 0 & 0 & 1 \end{bmatrix}$$

$$A_{00} = \begin{bmatrix} 186.93 & 30.88 & 0 \\ 30.88 & 21.70 & 15.01 \\ 0 & 0.05 & 1 \end{bmatrix}, A_{10} = \begin{bmatrix} 186.93 & 33.51 & 0 \\ 33.51 & 21.70 & 16.30 \\ 0 & 0.05 & 1 \end{bmatrix},$$

$$A_{01} = \begin{bmatrix} 186.93 & 30.88 & 22.1 \\ 30.88 & 21.70 & 15.01 \\ 0 & 0.05 & 1 \end{bmatrix}, A_{11} = \begin{bmatrix} 186.93 & 33.51 & 26.58 \\ 33.51 & 21.70 & 16.30 \\ 0 & 0.05 & 1 \end{bmatrix}$$

$$\Omega_{00} = \begin{bmatrix} 1.0 & 0.27 & 0 \\ 0.27 & 0.09 & 0.13 \end{bmatrix}, \Omega_{10} = \begin{bmatrix} 1.0 & 0.29 & 0 \\ 0.29 & 0.09 & 0.14 \end{bmatrix},$$

$$\Omega_{01} = \begin{bmatrix} 1.0 & 0.27 & 0.22 \\ 0.27 & 0.09 & 0.13 \end{bmatrix}, \Omega_{11} = \begin{bmatrix} 1 & 0.29 & 0.24 \\ 0.29 & 0.09 & 0.14 \end{bmatrix}$$

$$\Upsilon_0 = \begin{bmatrix} 1.0 & 0.27 & 0 \\ 0.27 & 0.09 & 0 \end{bmatrix}, \Upsilon_1 = \begin{bmatrix} 1.0 & 0.29 & 0 \\ 0.29 & 0.09 & 0 \end{bmatrix}$$

At last, the robust quasi-LPV controller is designed using the *LMI Quadratic Discrete Descriptor T-S Robust Stabilization Problem* (158) with $\lambda = 230$ set after several trials. The resulting matrices of the control law (147), i.e. $u_k = \begin{bmatrix} F_{vw} & G_{vw} \end{bmatrix} H^{-1} \begin{bmatrix} x_{rk} \\ e_k \end{bmatrix}$ are:

$$H = \begin{bmatrix} 1.59 & -5.12 & 0.98 & -1.22 & 4.14 & -0.78 \\ -5.18 & 20.70 & -4.30 & 4.48 & -17.41 & 3.59 \\ 0.99 & -4.33 & 0.97 & -0.87 & 3.71 & -0.83 \\ -1.22 & 4.42 & -0.85 & 1.42 & -4.20 & 0.76 \\ 4.15 & -17.25 & 3.66 & -4.21 & 17.36 & -3.68 \\ -0.79 & 3.58 & -0.82 & 0.77 & -3.69 & 0.86 \end{bmatrix}$$

$$F_{00} = \begin{bmatrix} 1.40 & -5.72 & 1.42 \end{bmatrix},\ F_{10} = \begin{bmatrix} -1.48 & 2.00 & 0.32 \end{bmatrix},$$

$$F_{01} = \begin{bmatrix} -1.11 & 2.59 & -0.04 \end{bmatrix},\ F_{11} = \begin{bmatrix} -4.05 & 11.59 & -1.47 \end{bmatrix},$$

$$G_{00} = \begin{bmatrix} -4.21 & 6.66 & 0.15 \end{bmatrix},\ G_{10} = \begin{bmatrix} -1.07 & -4.01 & 1.92 \end{bmatrix},$$

$$G_{01} = \begin{bmatrix} -2.63 & 4.61 & 0.15 \end{bmatrix},\ G_{11} = \begin{bmatrix} 0.64 & -3.82 & 1.38 \end{bmatrix}.$$

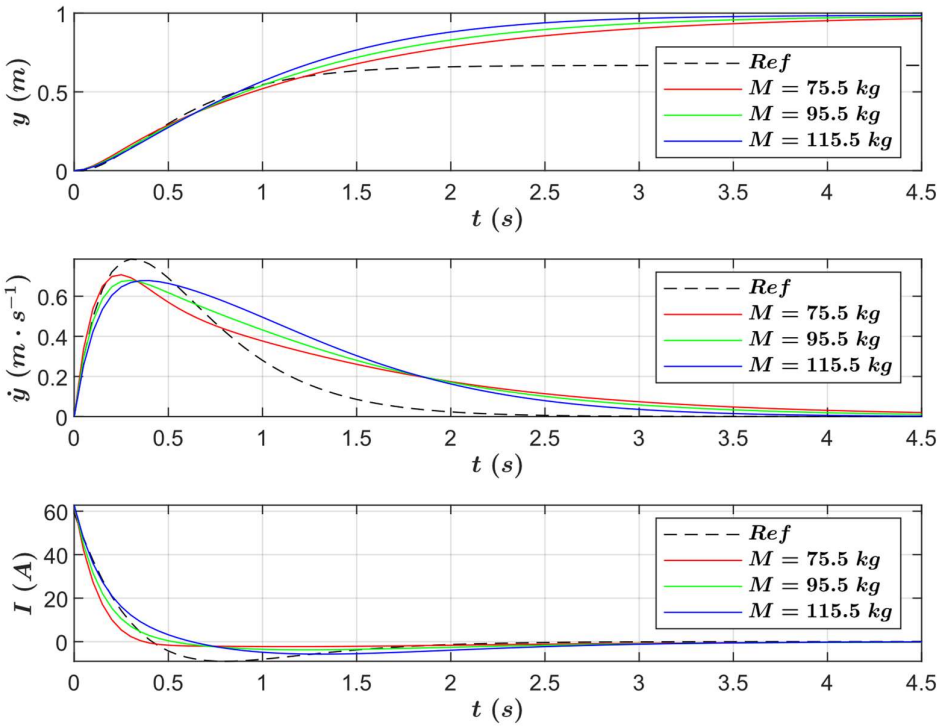

Fig. 52. Simulation discrete swing-up trajectories $y, \dot{y}$

Fig. 52 and Fig. 53 present 3 swing-up trials in simulation according to the nominal mass 95.5 *kg* and the two extreme human masses 75.5 *kg* and 115.5 *kg*. Of course, the model considered for simulations is the full nonlinear model in continuous. The reference trajectory is the dotted dark curve. As it is a state reference trajectory based on a linearization of the model,

none of the simulation signals match exactly the state reference trajectory. Nevertheless, the approach guaranteeing stability, robustness and performances, even though the reference model cannot be followed exactly, the controller capabilities of the control to swing-up the system with $\pm 20\,kg$ mass variations are clearly demonstrated.

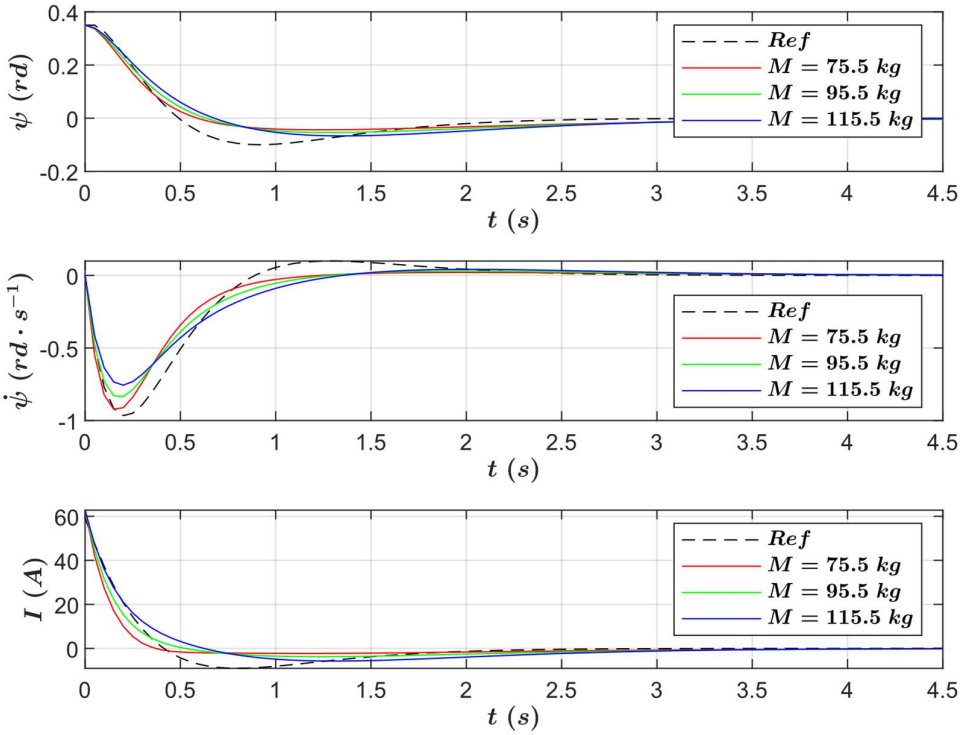

Fig. 53. Simulation discrete swing-up trajectories $\psi, \dot{\psi}$

Following the same way-of-doing of the previous chapter for the trials, to enhance the simulation validity, a nonlinear continuous model closer to "reality" is used. It includes the quantization error from the encoders and the gyroscopes measurement noise (previously recorded on hardware). Results are depicted in Fig. 54, Fig. 55 and corresponds to the swing-up of the wheelchair: the black curves represent the reference trajectory and the other colors, 2 different users weighting respectively $80\,kg$ and $100\,kg$. These masses are used because the results can be compared with real-time tests with such users, Fig. 56 and Fig. 57.

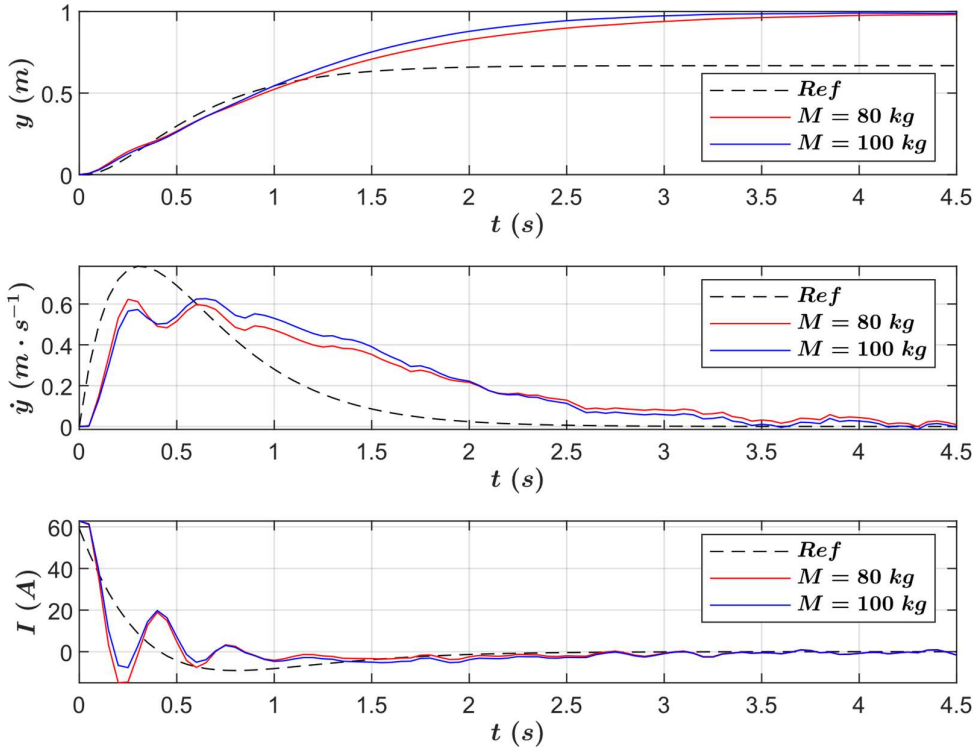

Fig. 54. Simulation discrete swing-up with noise for trajectories $y, \dot{y}$

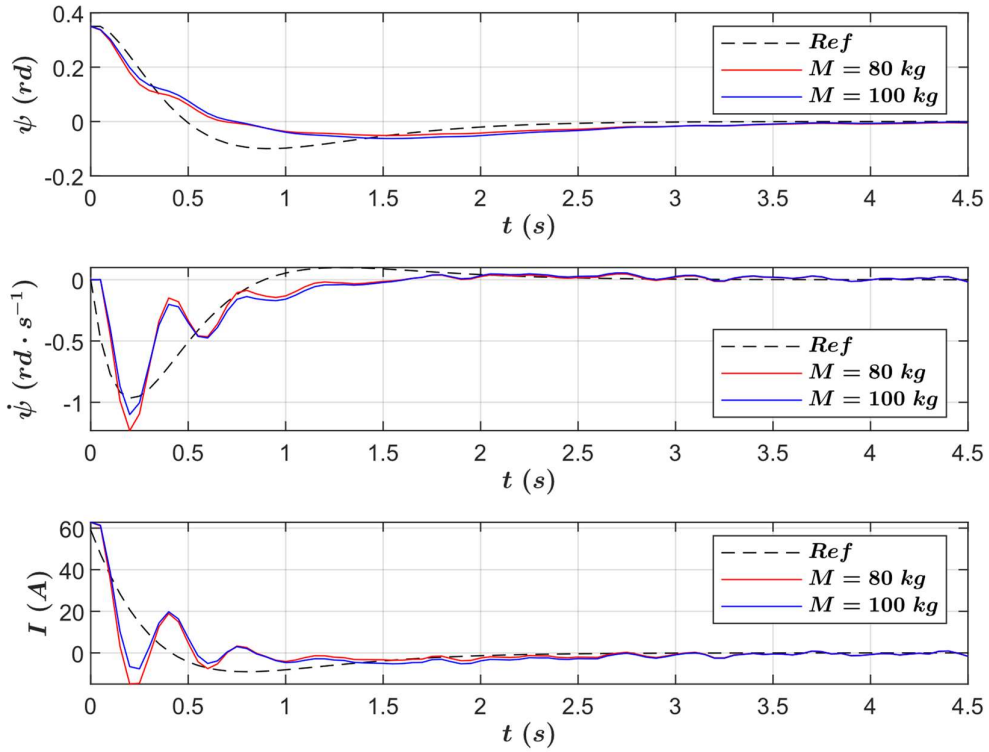

Fig. 55. Simulation discrete swing-up with noise for trajectories $\psi, \dot{\psi}$

4.3.3 Discrete real-time

The real-time tests were performed with the experimental systems of Autonomad-Mobility. A video showing a set of real-time trials can be found at the following address:

https://pod.uphf.fr/video/1583-discrete-reference-tracking-control-to-swing-up-an-electric-wheelchair/.

The unique robust controller was designed for a nominal mass of $M = 95.5\,kg$ and then tested with users' masses $M = \{80, 100\}\,kg$ or model parameter $M_b = \{97.14, 117.14\}\,kg$ where $M_b = M + M_{b_{frame}}$. Fig. 56 and Fig. 57 show the swing-ups for both users. $\dot{y}$, $\dot{\psi}$, ψ trajectories are presented as well as the control u obtained from (147). The dashed black curves are the reference trajectories and the solid red and blue curves correspond to the 2 trials.

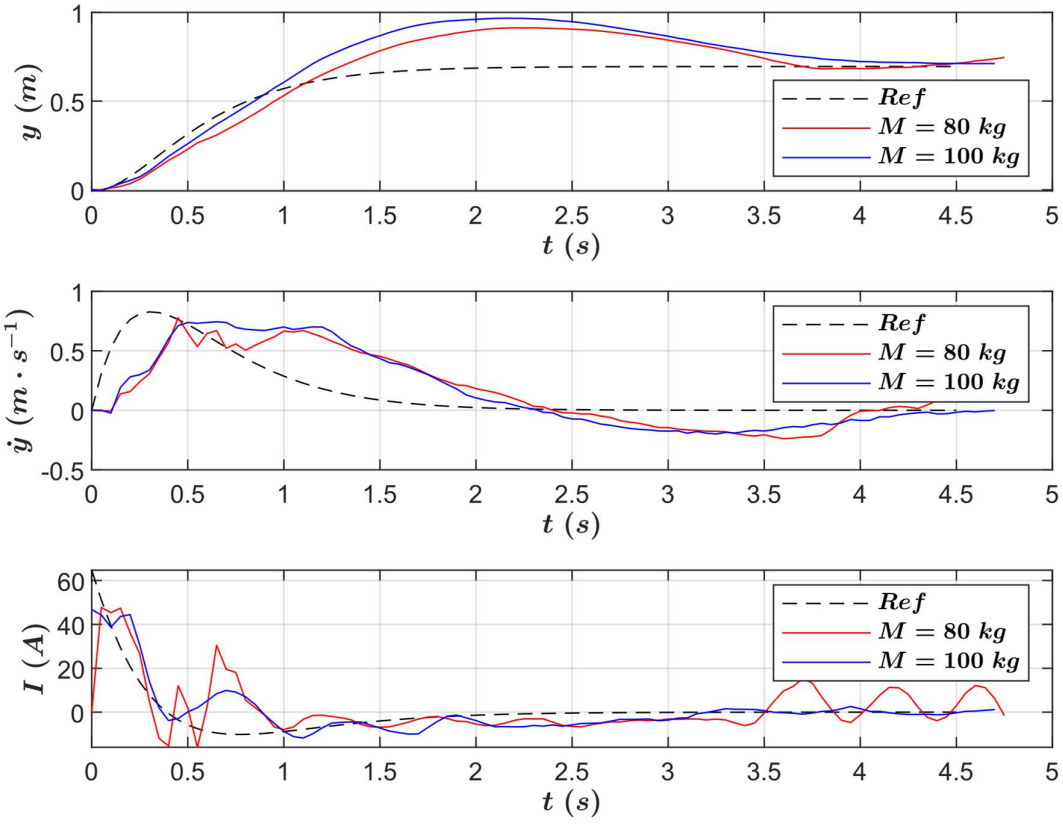

Fig. 56. Discrete swing-up real-time results for trajectories $y, \dot{y}$

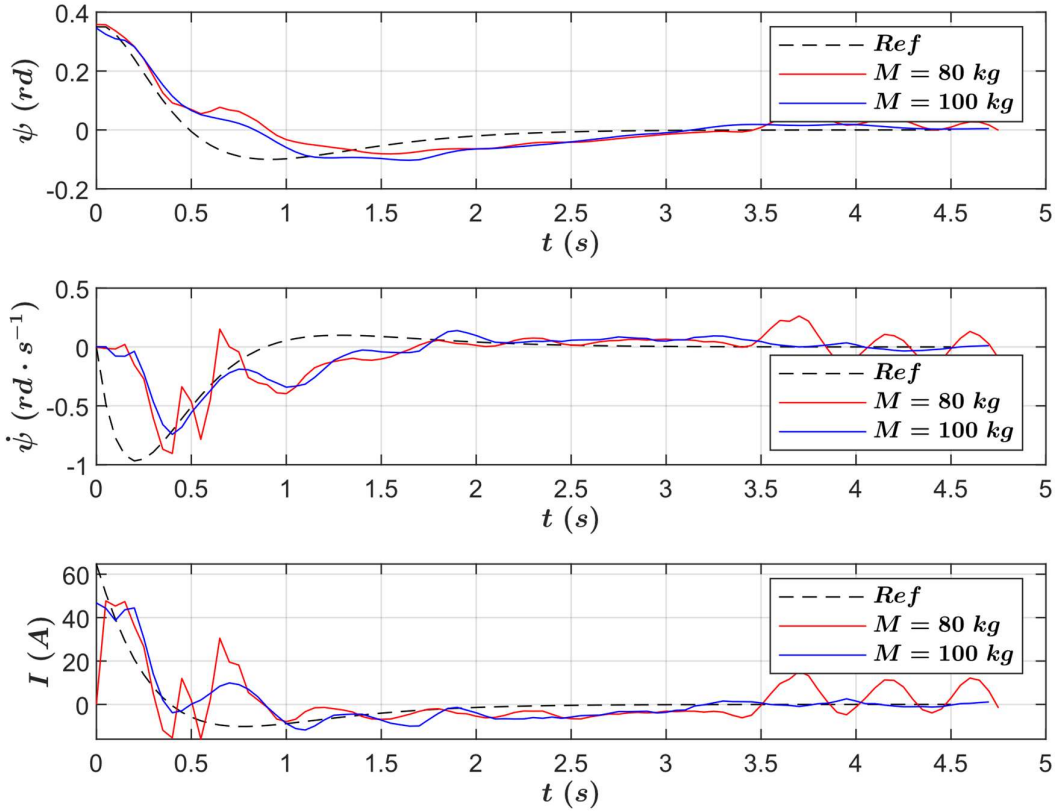

Fig. 57. Discrete swing-up real-time results for trajectories $\psi, \dot{\psi}$

These experiments show that the controller can bring the wheelchair from the standard mode to gyroscopic mode in a smooth and safe manner. The reader can also see on the video the robustness obtained when the user is voluntarily rocking in the wheelchair. This effect can be seen partly on Fig. 57 right part for the $80\,kg$ user (red curve), the shaking start after about $t = 3.5\,s$. The other smaller oscillations, as expected, are caused both by the encoder quantization error present on $\dot{y}$ and the gyroscopic measurement $\dot{\psi}$ noise.

This control law can swing-up and stabilize safely the system even for unmeasured uncertainties like as the user and/or wheelchair masses. The robustness performances around the unstable equilibrium point are excellent when looking to the movements made by the users in the video, independently from the weight. For now, to gain more performances, the quantization error should be decreased and the possible sampling period increased. This would lead to be able, potentially, to use higher gains that would reduce the time to swing-up and moreover, to reduce the oscillations seen during the swing-ups, for example, Fig. 56, Fig. 57 at about $t = 0.5\,s$. Simulations study has been done and show the relevance of these remarks.

4.4 Conclusion

The objective was to discretize the model to find a control law that would automate the process of transitioning safely a wheelchair from standard mode to gyroscopic mode in a smooth manner while being robust to different wheelchair + user masses. Differently from the previous chapter the choice was to use a unique formulation and control synthesis, the LMI constraints framework. In order to propose such a solution, the idea of coupling tracking reference (acting as a feedforward part) and uncertainty description in a quasi-LPV framework was used. The adequate LMI constraints problems were derived with the possibility of having design parameters to settle a safe and performant strategy. Intensive simulations and experiments were conducted, some of them presented or available at the given previous video address in the previous section.

Chapter 5 Conclusion and Future Research

The objective was to find a control algorithm that could safely and comfortably swing-up a power-assisted electrical wheelchair. This project was proposed by the company Autonomad-Mobility in the context of a CIFRE convention with the LAMIH UMR 8201 at Université Polytechnique Hauts-de-France.

5.1 Prototype

Since Autonomad-Mobility already designed and sold the electrical assistance kit so-called NOMAD (self-balancing wheelchair), the focus of this part was to design a new control box including an embedded system compatible with actual software such as MATLAB / Simulink. The control box is the housing for the joystick, the electronic card, and the IMU (gyroscopic and accelerometer). With the new electronic card Simulink programs can be uploaded directly into the card without any coding in C and Simulink as well as log data and display it in real-time. The control box was designed in Solidworks and 3D printed in the shop. The wheelchair prototype included two brushless wheels embedded in the push-wheels, a socket for the battery, and the battery.

5.2 Modeling & Identification

Since we were mainly concerned with the swing-up of the wheelchair we did not need a model that moved in 3D space. The 2D model has 2 degrees of freedom; a translation of the base in y and a rotation of the body in ψ. In order to derive the equations of motion the classical Euler-Lagrange method was used.

Then, identification of the main parameters have to be done, taking into account that there was no need to get a precise modeling but a model that would be compatible with robustness of the control laws to be designed. Moreover, as we wanted to operate on a 2-Wheels mode, identification was a little more complicated than usual due to the unstable behavior of the system around its equilibrium point. Nevertheless, the proposition of a 3-steps procedure was made to end with the adequate parameters and the results were validated through real-time experiments.

5.3 Continuous swing-up

The mechanical system being naturally in a descriptor form, this form was kept into its exact representation using quasi-LPV or so-called T-S fuzzy descriptor model. From the model designed a continuous time controller was designed to track reference trajectories to swing-up with a two-step process.

First the reference trajectories were computed by using the optimal control framework. The objective is to find the trajectories that are smooth and comfortable for the user while still minimizing the distance needed to perform the swing-up. The tradeoff between comfort and minimizing the distance was decided by comparing the optimal trajectories to the trajectories generated by a professional user doing the swing-up manually.

Once the reference trajectories set up, a robust controller is designed to compensate for the state space error between the system outputs and the references. The design uses first the Differential Mean Value theorem to derive asymptotic convergence of the error. From classical uncertain model framework, a classical Lyapunov 2^{nd} method allowed to design a LMI constraints problem, the solution of which ensures stability and performances.

Lastly, the controller was extensively tested in simulation and in real-time.

5.4 Discrete swing-up

The goal of this chapter was to propose a unique framework to solve the swing-up problem taking into account non-modelled uncertainties such as the masses of the user and the wheelchair. The discrete space was chosen and therefore, the continuous fuzzy descriptor model discretized. Forward Euler's method was chosen as it keeps the same the signification of the state space vector.

From this model, the idea was to build potentially "feasible" state space trajectories using a linearization of the model. Therefore, as for the continuous law, the feedback part has only to compensate for state trajectory errors. A robust design using LMI constraints problem was made accounting for masses variations and including performances requirements.

Lastly, the controller was extensively tested in simulation and in real-time.

5.5 Future work

This was an exciting project from my point-of-view with a realization that goes from specifications to a final prototype intensively tested. Robustness and performances were the first goals, in order for the company to have a control that is at most “user and wheelchairs independent”.

Next steps would be to introduce, for the discrete framework, the position of the basis wheelchair y, in order to act (more than control) on the distance for swing-up. The idea here is that y is not the main variable to be controlled, it is just an added performance to swing-up on the smallest distance the wheelchair. Another important reflection is the interest of getting more flexibility on the sampling period and reducing the quantization effects, both things should require another hardware to design. Nevertheless, it would help to attain larger feasible solutions to the LMI constraints problems. Increasing the set of solutions would allow increasing the performances and robustness issues.

Two other points can be of high importance, taking into account the motor saturations into the theoretical framework and to introduce also the ground uncertainties. Both extensions are feasible in a reasonable time. The latter one corresponds to increase the uncertainty matrices such as $\Xi(\cdot)$, equation (154). The former, concerning the input saturations, can be held including LMI constraints such as (Tingshu and Zongli 2001)

Of course writing the LMI constraints is one thing, getting solutions and, even more, getting solutions of “quality” (robustness and performances) another, and the fact of adding constraints leads to reduce the set of admissible solutions. These points will have to be explored.

Even if the swing-down phase is less crucial, in the sense that the wheelchair goes from the unstable 2-Wheels equilibrium to its stable 4-Wheels position, making a smooth and user-friendly transition is also important. A solution can be provided with identical tools. After that, swing-up and swing-down can be challenged if the ground is not horizontal, the slope being “far” from $0°$, swinging-up in a climb (positive slope) or swinging-down in a descent have to be thought with strong safety issues. At last, maximum height and/or form of the obstacles could be also taken into account. What could be the maximum security / safety levels that could be attained and guaranteed, function of some parameters such as the mass of user + wheelchair,

ground conditions etc. Of course, robustness of the control laws should certainly be adapted, and extensive campaign tests realized.

On a much larger and long-time horizon, several improvements can be thought. A “balancing” chair for example, in order that whatever is the position of the body of the wheelchair, the user keeps a horizontal position. This would imply mechanical developments and would end with a supplementary degree of freedom to control, but a real plus for the user’s comfort and security feeling. Taking into account the journey, if a long trip is planned could also be added. Navigation could be thought not only in time or minimum path but also in a way the wheelchair minimizes the number of swing-up and down, minimizes the energy consumption, or more generally increases the global user’s comfort. As the wheelchair as an excellent capability of mobility (rough terrains, small obstacles crossing), a connection with cell phone apps could come at hand (GPS, interactive maps, for example) for solving these optimization problems.

References

Ahmad, S, and M O Tokhi. 2008. "Forward and backward motion control of wheelchair two wheels." *3rd IEEE Conf. on Indust. Elect. and App.* 461-466.

Barfield, J, et L Malone. 2013. «Perceived exercise benefits and barriers among power wheelchair soccer players.» *Jour. of rehab. research and develop.* 50: 231-8.

Bouarar, T, K Guelton, et N Manamanni. 2010. «Robust fuzzy Lyapunov stabilization for uncertain and disturbed Takagi–Sugeno descriptors.» *ISA Transactions* 49 (4): 447-461.

Boyd, S P, and L Vandenberghe. 2018. *Introduction to applied linear algebra: vectors, matrices, and least squares.* Cambridge; New York: Cambridge University Press.

Boyd, S, L El-Ghaoui, E Feron, et V Balakrishnan. 1994. *Linear Matrix Inequalities in System and Control Theory.* Philadelphia: Society for Industrial and Applied Mathematics.

Chadli, M, and M Darouach. 2012. "Novel bounded real lemma for discrete-time descriptor systems: Application to H∞ control design." *Automatica* 48 (2): 449-453.

Cline, D, et M Sarkis. 2017. *Variational principles in classical mechanics.* NewYork: University of Rochester River Campus Libraries.

Estrada_Manzo, V, T M Guerra, Z Lendek, and M Bernal. 2013 . "Improvements on non-quadratic stabilization of continuous-time Takagi-Sugeno descriptor models." *IEEE Inter. Conf. on Fuzzy Syst.* 1-6.

Estrada-Manzo, V, Z Lendek, T M Guerra, et P Pudlo. 2015. «Controller Design for Discrete-Time Descriptor Models: A Systematic LMI Approach.» *IEEE T. on Fuzzy Sys.* 23 (5): 1608-1621.

Geering, H P. 2007. *Optimal Control with Engineering Applications.* Berlin: Springer-Verlag Berlin Heidelberg.

Gray, M, T M Guerra, S Delprat, et S Mohammad. 2020. «Control of an automated wheelchair.» *Presented at IFAC World Congress 2020 Berlin.*

Guelton, K, S Delprat, et T M Guerra. 2008. «An alternative to inverse dynamics joint torques estimation in human stance based on a Takagi-Sugeno unknown inputs observer in the descriptor form.» *Control Engineering Practice* 16 (12): 1414-1426.

Guerra, T M, M Bernal, A Kruszewski, and M Afroun. 2007 . "A way to improve results for the stabilization of continuous-time fuzzy descriptor models." *46th IEEE Conf. on Decision and Cont.* 5960-5964.

Guerra, T M, M Bernal, et M Blandeau. 2018. «Reducing the number of vertices in some Takagi-Sugeno models: example in the mechanical field.» *IFAC-PapersOnLine* 51 (10): 133-138.

Guerra, T M, R Márquez, A Kruszewski, and M Bernal. 2018. "Hinf LMI Based Observer Design for Nonlinear Systems via Takagi–Sugeno Models With Unmeasured Premise Variables." *IEEE Trans. on Fuzzy Syst.* 26 (3): 1498-1509.

Ichalal, D, and S Mammar. 2015. "On Unknown Input Observers for LPV Systems." *IEEE Trans. on Indust. Elect.* 62 (9): 5870-5880.

Ichalal, D, and T M Guerra. 2019. "Decoupling Unknown Input Observer for nonlinear quasi-LPV systems." *58th Conf. on Decision and Cont.* 3799-3804.

Jaekook, A, et S Jung. 2008. «Swing-up fuzzy control of an inverted pendulum system for control education with an experimental kit.» *Int. Conf. on Control, Auto. and Sys.* 1709-1714.

Johansen, T A, R Shorten, and R Murray-Smith. 2000. "On the interpretation and identification of dynamic Takagi-Sugeno fuzzy models." *IEEE Trans. on Fuzzy Sys.* 8 (3): 297-313.

Kaye, H S, T Kang, and M P LaPlante. 2000. *Mobility Device Use in the United States.* Washington D.C.: Department of Education, National Institute on Disability. Accessed Oct. 19, 2020.

Kierzenka, J, and L F Shampine. 2001. "A BVP solver based on residual control and the Maltab PSE." *ACM Trans. Math. Softw.* 27 (3): 299–316.

Kirk, D E. 2004. *Optimal control theory: an introduction.* Mineola: Dover Publications.

Kloosterman, M, G Snoek, L Woude, J Burrke, et J Rietman. 2012. «A systematic review on the pros and cons of using a pushrim-activated power-assisted wheelchair.» *Clinical rehabilitation* 27.

Lendek, Z, T M Guerra, R Babuška, and B De Schutter. 2010. *Stability Analysis and Nonlinear Observer Design Using Takagi-Sugeno Fuzzy Models.* Germany: Springer.

Lendek, Z, Z Nagy, and J Lauber. 2018. "Local stabilization of discrete-time TS descriptor systems." *Engineer. App. of Artificial Intel.* 67: 409-418.

Li, J, S Zhou, et S Xu. 2008. «Fuzzy Control System Design via Fuzzy Lyapunov Functions.» *IEEE Trans. on Sys, Man, and Cybernetics Part B* 38 (6): 1657-1661.

Lofberg, J. 2004 . "YALMIP : a toolbox for modeling and optimization in MATLAB." *IEEE Inter. Conf. on Robo. and Automat.* 284-289.

Lopez Estrada, F R, J C Ponsart, D Theilliol, et C M Astorga-Zaragoza. 2015. «Robust H−/H∞ fault detection observer design for descriptor-LPV systems with unmeasurable gain scheduling functions.» *Int. Journal of Control* 88 (11): 2380-2391.

Mercer, J L, M Boninger, A Koontz, D Ren, T Dyson-Hudson, et Cooper R. 2006. «Shoulder joint kinetics and pathology in manual wheelchair users.» *Clinical Biomechanics* 21 (8): 781-789.

Mohammad, S, and T M Guerra. 2019. Wheelchair propulsion method, kit, and wheelchair implementing such a method. France Patent US10252638B2. Apr 9.

Naidu, D S. 2003. *Optimal control systems.* Boca Raton: CRC Press.

Ohtake, H, K Tanaka, et H O Wang. 2001. «Fuzzy modeling via sector nonlinearity concept.» *Proc. Joint 9th IFSA WC and 20th NAFIPS Int. Conf.* 1: 127-132.

Okoro, A, N D Hollis, A C Cyrus, and S Griffin-Blake. 2018. "Prevalence of Disabilities and Health Care Access by Disability Status and Type Among Adults — United States, 2016." *Morbidity and Mortality Weekly Report* 67 (32): 882-887.

Pridemobility. n.d. *Jazzy-passport.* Accessed 11 03, 2020. https://www.pridemobility.com/jazzy-power-chairs/jazzy-passport/.

Rothenberg, A, G Gasbarro, J Chlebeck, et L Albert. 2017. «The Coracoacromial Ligament: Anatomy, Function, and Clinical Significance:.» *Orthopaedic Jour. of Sports Med.* 5 (4).

Sala, A, et C Arino. 2007. «Relaxed Stability and Performance Conditions for Takagi–Sugeno Fuzzy Systems With Knowledge on Membership Function Overlap.» *IEEE Trans. on Sys., Man, and Cybernetics B, Cybern.* 37 (3): 727-732.

Scherer, C, et S Weiland. 2004. *Linear Matrix Inequalities in Control.* Delft: Dutch Inst. syst. control, Delft Univ.

Schoukens, J, and L Ljung. 2019. "Nonlinear System Identification: A User-Oriented Road Map." *IEEE Control Sys. Mag.* 39 (6): 28-99.

Skelton, R E, T Iwasaki, et K Grigoriadis. 1998. *A Unified Algebraic Approach to Linear Control Design.* London: Taylor & Francis.

Takahashi, Y, et O Tsubouchi. 2005. «Modern control approach for robotic wheelchair with inverse pendulum control.» *5th Int. Conf. on Intel. Sys. Design and App.* 364-369.

Takahashi, Y, N Ishikawa, and T Hagiwara. 2003. "Soft raising and lowering of front wheels for inverse pendulum control wheel chair robot." *Proc. IEEE Int. Conf. on Intel. Robots and Sys.* 3: 3618-3623.

Tanaka, K, et O H Wang. 2001. *Fuzzy Control Systems Design and Analysis: A Linear Matrix Inequality Approach.* New York: Wiley.

Taniguchi, T, K Tanaka, and H O Wang. 2000. "Fuzzy descriptor systems and nonlinear model following control." *IEEE Trans. on Fuzzy Sys.* 8 (4): 442-452.

Taniguchi, T, K Tanaka, H Ohtake, et H O Wang. 2001. «Model construction, rule reduction, and robust compensation for generalized form of Takagi-Sugeno fuzzy systems.» *IEEE T. on Fuzzy Sys.* 9 (4): 525-538.

Tingshu, Hu, and L Zongli. 2001. *Control Systems with Actuator Saturation.* Boston: Birkhäuser Basel.

Torkia, C, D Reid, N Korner-Bitensky, D Kairy, P W Rushton, L Demers, and P S Archambault. 2015. "Power wheelchair driving challenges in the community: a users' perspective." *Disability & rehab. Assitive tech.* 10 (3): 211-215.

Tuan, H D, P Apkarian, T Narikiyo, and Y Yamamoto. 2001. "Parameterized linear matrix inequality techniques in fuzzy control system design." *IEEE Trans. on Fuzzy Sys.* 9 (2): 324-332.

Wang, H O, K Tanaka, and M Griffin. 1995. "Proceedings of 1995 IEEE International Conference on Fuzzy Systems." *Proc. of 1995 IEEE Int. Conf. on Fuzzy Sys.* 2: 531-538.

Watson, N, and B Woods. 2015. "History of the wheelchair." Febuary 11. Accessed October 21, 2020. https://www.britannica.com/topic/history-of-the-wheelchair-1971423.

Wikipedia contributors. 2020. *IBOT.* Accessed Nov. 3, 2020. https://en.wikipedia.org/w/index.php?title=IBOT&oldid=983937456.

—. 2020. *Stephan Farfler.* Accessed October 21, 2002. https://en.wikipedia.org/wiki/Stephan_Farffler.

World Health Organization. 2011. *World report on disability.* Geneva: World Health Organization. Accessed 1 20, 2020. https://www.merriam-webster.com.

Zemouche, A, B Mohamed, and L Bara. 2008. "Observers for a class of Lipschitz systems with extension to H-infinity performance analysis." *Systems and Control Letters* 57 (1): 18-27.

Zhang, G, Y Xia, et P She. 2008. «New bounded real lemma for discrete-time singular systems.» *Automatica* 44 (3): 886-890.

Zill, D G, and W S Write. 2011. *Calculus: early transcendentals.* Sudbury: Jones and Bartlett.

Abstract

According to the World Health Organization, more than 70 million disabled people in the world need a wheelchair to aid their daily mobility needs. In order to mitigate the physical effects of the repeated efforts on the push rims, the Autonomad Mobility developed an electrification kit. In this thesis, different control laws are proposed to swing-up the wheelchair from the grounded position to the unstable equilibrium position (gyroscopic mode). The system is modeled as a continuous Takagi-Sugeno descriptor model and a reference trajectory tracking problem is proposed. The closed loop Lyapunov stability is formulated as a set on Linear Matrix Inequalities to be solved. The reference control and state trajectories are computed as a solution to an optimal control problem. A second control law is formulated in discrete time and account for model uncertainties. Both simulation and experimental results are discussed.

Résumé

D'après l'Organisation Mondiale de la santé, plus de 70 millions de personnes à mobilité réduite ont besoin d'un fauteuil roulant pour assurer leurs déplacements quotidiens. Pour limiter les troubles musculaires liés aux appuis répétés sur les roues, la société Autonomad Mobility propose un kit d'électrification. Dans cette thèse, plusieurs lois de commande sont proposées pour assurer le passage du mode stable (avec les 4 roues posées sur le sol) à la position en équilibre instable du mode gyroscopique. Un modèle mathématique à temps continu du fauteuil et de l'utilisateur est construit en utilisant les lois de la mécanique. Le passage à la position d'équilibre instable est formulé comme un problème de suivi de trajectoire. Le système est écrit sous la forme d'un descripteur flou de type Takagi Sugeno et la stabilité de la boucle fermée est formulée comme un ensemble d'inégalités linéaires matricielles. Une deuxième loi de commande, formulée en temps discret, est également proposée et permet de prendre en compte les incertitudes sur les paramètres du modèle. Les résultats obtenus en simulation et lors des expérimentations avec les deux lois de commandes sont discutées.